Neuro-fuzzy Modeling of Multi-field Surface Neuroprostheses for Hand Grasp

PhD Thesis - 2016

Eukene Imatz Ojanguren

Supervised by

Eloy Irigoyen Gordo and Thierry Keller

Neuro-fuzzy Modeling of Multi-field Surface Neuroprostheses for Hand Grasp

PhD Thesis - 2016

Eukene Imatz Ojanguren

Supervised by

Eloy Irigoyen Gordo and Thierry Keller

PUBLISHED BY BUBOK
First printing, March 2016

Zuri.

Abstract

Neuroprostheses are systems based on FES, which is a technique that applies electrical pulses to peripheral nerves in order to substitute lost sensory/motor functions. Neuroprostheses are aimed at people with neurological disorders that present motor dysfunctions. Indeed, they have been found to positively influence motor recovery in neurologically impaired people, supporting the restoration of lost motor functions. Surface neuroprostheses are not invasive and they are easy to don/doff, which makes them preferred for therapeutic applications. However, their main disadvantage is the reduced capacity of selectively activating target nerve fibers. Selective activation with surface neuroprostheses requires well-directed and local currents with rather high density. This can lead to discomfort and difficulties for achieving fine movements. The latter is an issue in upper-limb applications as forearm and hand are comprised of several small overlapped muscle layers. In fact, the complex neuroanatomy of the forearm and hand, its dimensionality, the diverse non-cyclic tasks and the inter-subject variability of movements, have resulted in few available neuroprostheses for grasping. The increase in selectivity enabled by multi-field electrodes together with knowledge on FES-induced discomfort and FES-induced hand movements could thus move grasping neuroprostheses a step forward.

In this thesis I analyzed the discomfort differences of two stimulation techniques applied with multi-field electrodes in 15 healthy subjects. Additionally, I represented the spatial distribution of discomfort rates of different upper-limb areas in form of pain-maps, which were obtained from 11 chronic stroke subjects. Regarding modeling, I carried out a feasibility study to check the possibility of using neuro-fuzzy structures for modeling hand movements induced by a surface FES system based on multi-field electrodes. Finally, I tested and compared different neuro-fuzzy structures trained with data collected from 3 able-bodied and 3 brain injured hemiplegic subjects.

The discomfort analysis showed that asynchronous stimulation was preferred over synchronous stimulation in terms of discomfort. Regarding the spatial distribution of discomfort on the arm, no significantly painful spots were found along the forearm, whereas most proximal fields of the upper-arm were found to be significantly more painful. With respect to modeling, the recurrent fuzzy neural network was found successful for predicting wrist and finger flexion/extension behavior with stimulation parameters and application site as inputs. Different structure parameters and learning strategies showed a high inter-subject variability in the model performance. In any case, these models showed the capacity of successfully approximating the FES-induced hand kinematics for both able-bodied and neurologically impaired subjects.

Both the discomfort analysis and the neuro-fuzzy models presented in this thesis pretend to support the design and development of advanced surface neuroprostheses for grasping. The generated knowledge on FES-induced discomfort can be used as a guide for developing more comfortable FES based upper-limb applications. Analogously, the presented models can be used to support the design and development of successful neuroprostheses and control techniques for advanced grasping.

Laburpena

Neuroprotesiak estimulazio elektriko funtzional (FES ingeleseko siglen arabera) teknikan oinarritutako sistemak dira, eta FES teknika nerbio periferikoetan pultsu elektrikoak igortzean datza, galdutako funtzio motor/sentsorialak ordezkatzeko asmoz. Gorputz-adarretako neuroprotesiak disfuntzio motoreak dituzten pertsonei bideratuta daude, gaitz neurologikoak pairatzen dituzten pertsonei, hain zuzen. Funtzio motorea ordezkatzeaz gain, neuroprotesiek ondorio onuragarriak eragiten dituzte gaitz neurologikoak pairatzen dituzten gaixoengan, galdutako funtzioen errehabilitazioa bermatuz. Gainazal-neuroprotesiak ez dira inbaditzaileak, azalaren gainetik jartzen baitira. Jarri eta kentzeko errazak direnez aplikazio terapeutikoetarako egokienak dira. Dena dela, hauen desabantaila nabarmenena nerbio-zuntzak era selektiboan aktibatzeko ahalmen murriztua da. Ezaugarri honek erabiltzailearengan sentsazio deserosoa eta mugimendu finak eragiteko zailtasunak gauzatu ditzake. Azkenengo hau arazo bihurtzen da besaurrea eta eskuko aplikazioetan, biak bata bestearen gainean kokatutako gihar txiki ugariz osatuta daudelako. Izan ere, eskurako neuroprotesi erabilgarri gutxi existitzen dira eta hauek oraindik nahiko mugatuak dira. Arrazoiak, besteak beste, beasurre eta eskuko neuroanatomia konplexua, eskuaren dimentsionalitatea, mugimendu ez-zikliko ugariak eta erabiltzaileen arteko desberdintasunak dira. Beraz, multi-zelai elektrodoen selektibitatea hobetzeko ahalmenak, eta FES-ek eragindako deserosotasunaren eta mugimenduen gaineko jakintzak, eskurako neuroprotesien garapenean narbarmen lagundu dezake.

Tesi honetan multi-zelai elektrodoen bidez igorritako bi estimulazio tekniken arteko deserosotasun desberdintasuna aztertu dut 15 pertsona osasuntsurengan. Bestalde, goiko gorputz-adarreko atal desberdinetako deserosotasun distribuzio espaziala aztertu dut gaitz neurologikodun 11 gaixorengan eta deserosotasun mapen bidez adierazi dut. Ereduei dagokienez, neuro-fuzzy egitura motako ereduak neuroprotesiak eragindako esku mugimenduak aurreikusteko gai diren jakiteko bideragarritasun analisi bat egin dut. Bukatzeko, neuro-fuzzy egitura desberdinak probatu eta alderatu ditut 3 pertsona osasuntsu eta 3 gaixo hemiplegikorengandik jasotako datuekin.

Deserosotasun analisiaren emaitzek estimulazio asinkronoa sinkronoa baino erosoagoa dela erakutsi dute. Distribuzio espazialari dagokionez, besaurrean ez da gune mingarri esanguratsurik aurkitu, baina besoko gune proximalenak mingarriagoak direla aurkitu da. Ereduei dagokienez, Recurrent Fuzzy Neural Network izeneko ereduak eskumutur eta atzamarren flexio/extensio jokaera aurreikusteko gaitasuna erakutsi du, estimulazio parametroak eta estimulazio tokia sarrerako informazio bezala hartuta. Eredu egitura eta ikasketa

algoritmo desberdinek emaitza desberdinak eman dituzte pertsonaren arabera. Dena dela, proposatutako ereduek neuroprotesiek eragindako esku kinematika aurreikusteko gaitasuna erakutsi dute bai pertsona osasuntsuengan bai gaitz neurologikoak dituzten gaixoengan.

Tesi honetan aurkeztutako deserosotasun analisiaren eta proposatutako neuro-fuzzy ereduen asmoa gain-azaleko eskurako neuroprotesi berrien diseinu eta garapenean laguntzea da. Deserosotasunari buruz sortutako ezagutza baliogarria da goiko gorputz-adarretara bideraturako neuroprotesi erosoagoak diseinatzeko. Era berean, proposatutako ereduak eskurako neuroprotesi eta kontrol teknika berriak diseinatu eta garatzeko lagungarriak dira.

Resumen

Las neuroprótesis son sistemas basados en la estimulación eléctrica funcional (FES por sus siglas en inglés), la cual consiste en aplicar pulsos eléctricos a los nervios periféricos con el objetivo de sustituir funciones motrices/sensoriales perdidas. Las neuroprótesis para miembros superiores o inferiores dan asistencia a personas con disfunciones motrices causadas por trastornos neurológicos. Además, estas neuroprótesis han mostrado una influencia positiva en la rehabilitación motriz, reforzando la reeducación de funciones perdidas en pacientes con trastornos neurológicos. Las neuroprótesis superficiales no son invasivas y son de fácil colocación, por lo que son preferidas para aplicaciones terapéuticas. Aun así, su mayor desventaja es su reducida capacidad de estimular de manera selectiva los nervios objetivo. Este hecho puede causar sensaciones incómodas y dificultades para conseguir movimientos finos. Esto puede ser problemático especialmente en aplicaciones de miembro superior, debido a que el antebrazo y la mano están compuestos por numerosos y pequeños músculos superpuestos. La complejidad de la neuroanatomía del antebrazo y la mano, su dimensionalidad, las diversas tareas no-cíclicas y la variabilidad de movimientos entre sujetos, ha dado lugar al diseño de un número reducido de neuroprótesis orientadas a agarres básicos. La posibilidad de hacer más selectiva la estimulación mediante los electrodos multi-campo, junto con el conocimiento sobre la incomodidad y los movimientos que genera la aplicación de FES en miembro superior, podrían ser base fundamental para el desarrollo de neuroprótesis de agarre más avanzadas.

En esta tesis se analizan las diferencias existentes en relación a la incomodidad generada por dos técnicas de estimulación aplicadas con electrodos multi-campo en 15 sujetos sanos. Además, se presentan mapas de dolor que describen la distribución de incomodidad para distintas zonas del miembro superior obtenidas de las puntuaciones de 11 pacientes que han sufrido un accidente cerebrovascular. En cuanto a la modelización, se ha llevado a cabo un estudio de viabilidad para comprobar la posibilidad de utilizar estructuras neuro-difusas para modelizar los movimientos de la mano inducidos por un sistema FES basado en electrodos multi-campo. Finalmente, se ha evaluado y comparado distintas estructuras neuro-difusas que han sido entrenadas con datos obtenidos de 3 sujetos sanos y 3 pacientes con daño cerebral adquirido.

El análisis de incomodidad ha demostrado que la estimulación asíncrona es preferida respecto a la síncrona. En cuanto a la distribución espacial de la incomodidad, no se han encontrado puntos significativamente más dolorosos que otros en el antebrazo. Por el contrario, los campos proximales del brazo han resultado ser significativamente más dolorosos que otros campos del brazo.

Respecto a la modelización, la red neuro-difusa recurrente ha mostrado ser capaz de predecir la flexión/extensión de la muñeca y los dedos, tomando los parámetros de estimulación y la zona de aplicación de la estimulación como información de entrada. Los resultados de las distintas estructuras y estrategias de aprendizaje han mostrado una gran variabilidad entre pacientes. En cualquier caso, estos modelos han demostrado su capacidad de aproximar satisfactoriamente la cinemática de la mano inducida por la aplicación de FES tanto para sujetos sanos como para sujetos con trastornos neurológicos.

Tanto el análisis de incomodidad como los modelos neuro-difusos propuestos en esta tesis pretenden servir como apoyo para el diseño y desarrollo de neuroprótesis superficiales avanzadas para la función de agarre. El conocimiento generado respecto a la incomodidad puede ser utilizado como guía para desarrollar aplicaciones de FES de miembro superior más cómodas. Del mismo modo, los modelos propuestos en esta tesis pueden ser utilizados para apoyar el diseño y la validación de sistemas de control avanzados en neuroprótesis dirigidas a la función de agarre.

Acknowledgements

First and foremost I would like to thank my supervisors Thierry Keller and Eloy Irigoyen for your invaluable advice throughout the duration of the PhD, it was both a pleasure and a honor to have you as supervisors. Thank you Thierry for showing me that there is always room for improvement and thank you Eloy for showing me that there is no room for frustration, I learned a lot from both of you. You introduced me to this research field, which I am really proud to belong to, and I hope we will keep jointly contributing to it.

I would also like to thank to all my colleagues from Tecnalia, and I mean each of you with which I had the pleasure to at least have a chat, but specially the M1 team, including those of you that left some time ago but left your memories in M1 and I will not forget. Each of you have contributed to this thesis with your advice, help, support (this thesis would not exist without the FES team!), and friendship, which were present at any time and any day, but specially at those inspiring brainstorming-coffee-breaks, lunch times, *pintxopote*s, barbecues, and a long list of events. Thank you all.

Although I have met the people from the automatics department of UPV/EHU later on time and spent less time with you, I am glad that I met you. I want to thank you for sharing with me those funny coffe-breaks in which transcendental topics were seriously discussed in the university canteen, and for providing me valuable insight into the academic world while surrounded by microwaves at lunch time.

Amaitzeko, euskeraz eskertu nahi dodaz doktoretza luze honetan zehar hurbil izan dodazan pertsona guztiak. Eskerrik asko kuadrila eta lagunei, doktoretzako gora-beherak ahaztarazteko ahalmena dekozuelako, eta zuekaz egoteak edo berba egiteak efektu terapeutikoak dekozelako, eskerrik asko. Tesien detailetxueri buruz zuen iritzie emoteagaitik be mile esker kuadri! Amaitzeko, azkenengo txanpan desagertute egon arren, whatsapp-etik jaso dodazan animo guztiengatik eskerrik asko danori.

Eskerrik sakonenak be, zelan ez, Imanol, ama eta aitari. Beti egon zarie hor laguntzeko prest, eta doktoretzan zehar ez da gitxiago izan. Eskerrik asko doktoretzako egun txarrenetan be nire umore txarra jasateagatik eta zuen pazientziagatik. Datorrena datorrela, batera mantendu gara beti eta holan jarraitu daiela. Eskerrik asko benetan familia.

Eta azkenengo eskerrak zuretzako doaz Iurgi. Zu barik tesi hau ezan posible izango, eskerrik asko zure pazientziagatik, uneoro hor egoteagatik, prozesu luzea izan arren aurrera jarraitzeko indarra emoteagatik, lan egiteko denpora emoteagatik, zure laguntzagatik, etab. luze bat. Sentitzen dodan beste eskertzeko hitzik ez dagoen arren, bihotz-bihotzez dinotsut: ESKERRIK ASKO.

Contents

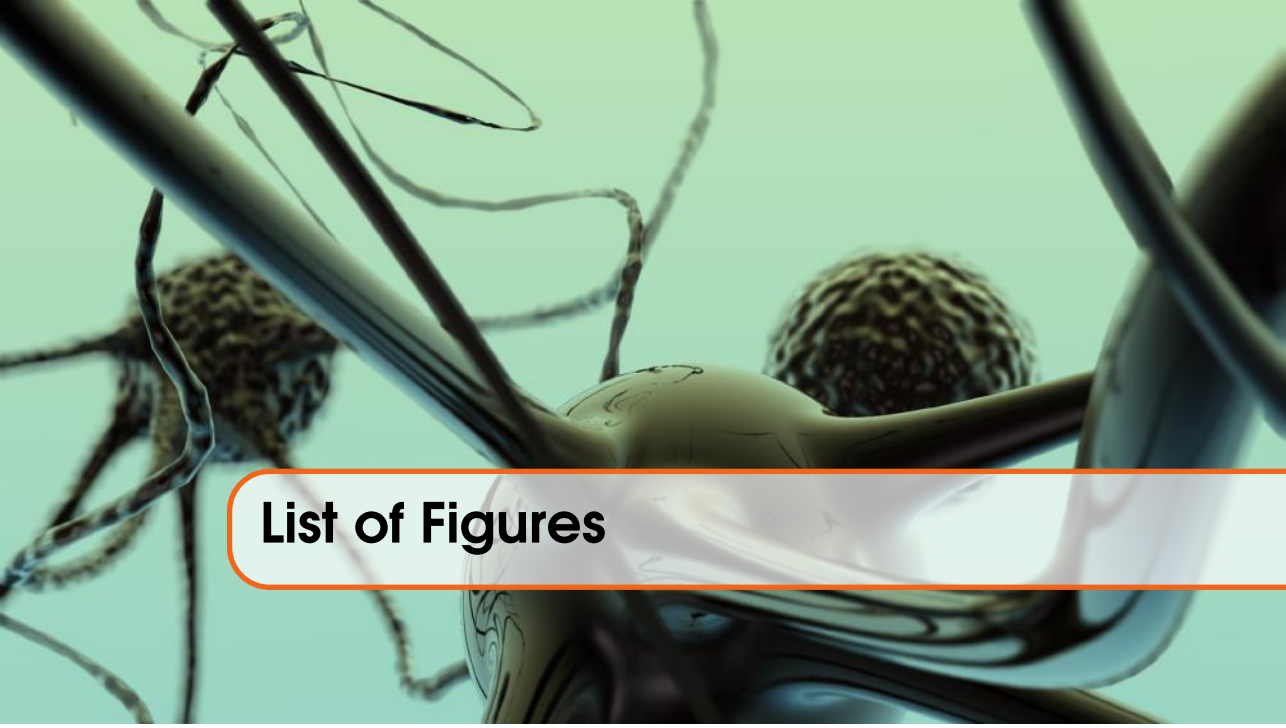

List of Figures

List of Tables

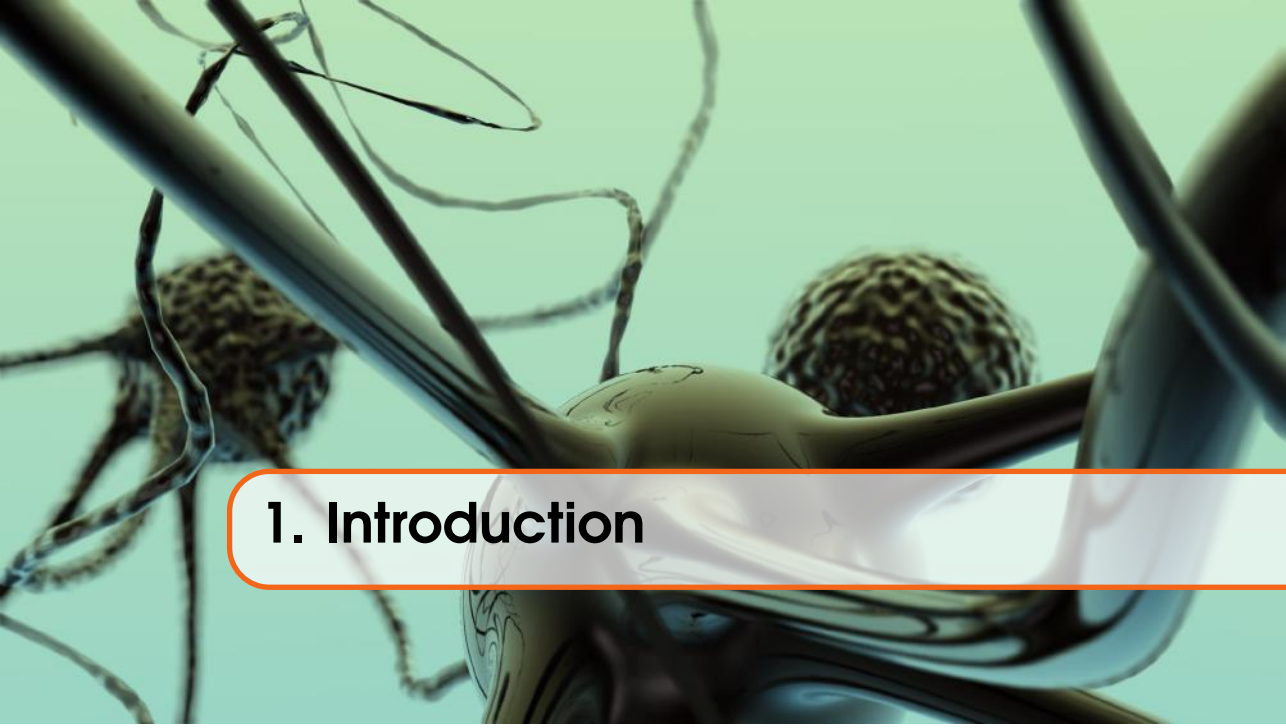

1. Introduction

Neuroprostheses are devices that aim at replacing lost sensory/motor functions in people suffering from neural disorders. These are based on Functional Electrical Stimulation (FES), which applies electrical pulses in order to artificially excite target nerve fibers [8, 14]. Neuroprostheses can replace both sensory and motor functions, e.g. cochlear implants provide the sense of sound, and pacemakers ensure heart muscle contractions. However, this thesis focuses on their application for restoring limb motor functions, more specifically, upper-limb grasping function. People who benefit most from limb function neuroprostheses include people with neurological disorders such as Spinal Cord Injury (SCI), stroke, multiple sclerosis (MS) or cerebral palsy (CP) [33, 34, 35, 36]. Although they differ greatly in the cause of origin and pathology, all present interrupted pathways in some sensory-motor nerve structures of the nervous system, which can lead to limb dysfunctions or paralysis [40]. In these cases, neuroprostheses can provide assistance for functions such as standing, walking, reaching or grasping [44, 46, 47]. Additionaly, neuroprostheses have been found to provide therapeutic effects by positively influencing motor recovery [35, 49, 54].

Regarding technology, neuroprostheses include two main components, which are the stimulator and the electrodes. The stimulator generates the electrical pulses that the electrodes transmit to the peripheral nerves. There are three types of neuroprosthesis grouped by invasiveness level [7]: implanted, percutaneous and surface systems. In implanted systems both the stimulator and the electrodes are placed under the skin by means of surgery, and the latter are either attached to the target nerves or close to them [18, 20, 21]. In percuta-

neous systems the electrodes are placed under the skin by a minimally invasive technique but wires come out from the skin to connect to an external stimulator [23]. Finally, surface systems are completely external, where most electrodes include a hydrogel layer that acts like the interface between the electrode and the skin and permits attaching them on top of the skin [26]. Implanted systems permit a selective stimulation of target nerve fibers, therefore, they are usually preferred for long-term assistive applications. On the contrary, due to the ease of donning/doffing them, surface systems are preferred for short-term therapeutic applications. However, the main disadvantage of surface neuroprostheses rely on their reduced capacity of selectively exciting the target nerve fibers without acting in neihboring tissues, which can also result in discomfort caused by the excitation of nerve fibers corresponding to cutaneous receptors. This selectivity issue is critical in upper-limb applications, specially in grasping applications, due to the complex neuroanatomy of the forearm and hand, where small muscles are overlapped and located at different depths [4, 6]. Nevertheless, multi-field electrodes, which consist on a group of several tiny conductive fields that can be activated or deactivated independently, have shown selectivity improvements with respect to conventional surface electrodes [28, 29].

Upper-limb neuroprostheses should face additional challenges when compared to lower-limb applications. Most important of these are the complex neuroanatomy of the arm, high amount of degrees of freedom (DOF), non-cyclic type of tasks and inter-subject variability of movements [103, 169]. If disadvantages inherent to surface FES, such as reduced selectivity and discomfort, are added, the design and development of grasping neuroprostheses turns out to be a complex problem to solve. Therefore, few surface neuroprostheses for generating hand grasp are available at present. The available ones provide basic grasps and are not so broadly accepted in clinics because of technological and functional limitations [48].

Hence, in this thesis we aim at contributing to the grasping neuroprostheses field by providing an upper-limb discomfort analysis followed by the proposal of a novel FES model based on intelligent computing techniques. The discomfort caused by surface FES can limit the performance of neuroprostheses in sensitive users. Thus, this analysis aims at finding more comfortable stimulation techniques and describe spatial distribution of discomfort induced by FES on different areas of the arm. Like this, new surface neuroprostheses can be built avoiding potentially painful spots and using more comfortable stimulation techniques. Analogously, the models proposed on this thesis aim at supporting the design of new surface neuroprostheses and new control techniques. The models of FES-induced movements presented in this thesis are neuro-fuzzy models that are able to predict wrist and finger flexion/extension behavior from stimulation

parameters and application site, and have been trained and tested with data collected from both healthy and neurologically impaired subjects. The use of these models could speed up the design of successful grasping neuroprostheses by allowing to test different simulation techniques without compromising the safety of neurologically impaired subjects. In brief, the objective of the present thesis is to provide knowledge and tools for the design and development of more comfortable and successful neuroprostheses for advanced hand grasps.

This thesis is divided in two main parts, which describe the discomfort analysis and the FES-induced hand movement modeling respectively. In the first part, Chapter 2 describes the basic neurophysiology concepts necessary to understand the underlying processes in the application of FES, from the nerve cells to the neuroanatomy of the arm. Then, Chapter 3 describes the functioning principles of FES including a brief description of the main parameters, the technology and its main applications. Afterwards, Chapter 4 presents the experiments carried out to compare different stimulation techniques in terms of discomfort. The materials and methods used in the experiments followed by the obtained results and a brief discussion are described. Finally, Chapter 5 presents the experiments and pain-maps obtained from neurologically impaired subjects following a similar structure as the previous chapter.

Regarding the second part, Chapter 6 gives an overview of the background of FES modeling, where analytic models previously proposed for different subsystems are presented, and complete models for upper-limb applications are then briefly described. Chapter 7 describes main concepts of Computational Intelligence (CI) such as artificial neural networks, fuzzy systems or evolutionary algorithms, followed by some of their applications in already proposed FES systems. Afterwards, Chapter 8 describes the experiments carried out to check the feasibility of using a neuro-fuzzy approach for modeling FES-induced hand movements. Then, in Chapter 9 a deeper analysis is presented, where different neuro-fuzzy structures are tested and compared with data collected from both healthy and neurologically impaired subjects.

Finally, Chapter 10 aims at summarizing main conclusions that can be drawn from the presented work, including its limitations and future research work.

Part One

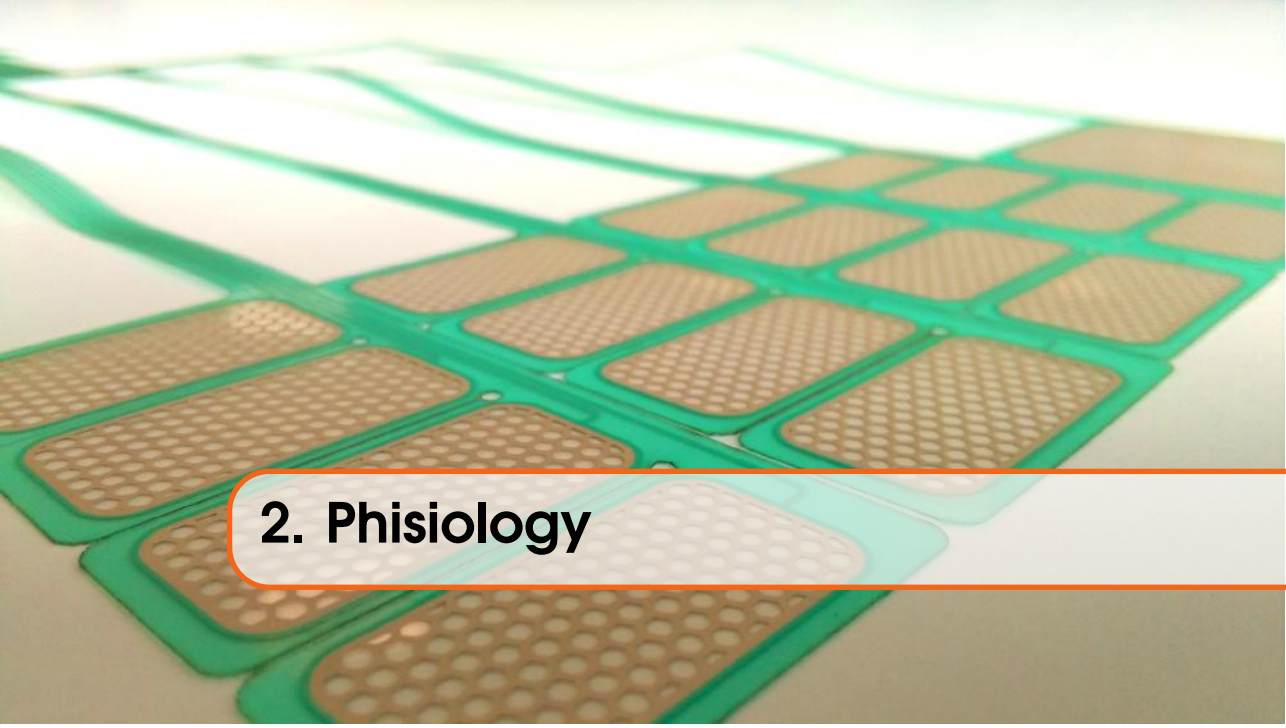

2. Phisiology

In this chapter, a brief description of physiological processes needed to understand the functioning principles of neuroprostheses is given. Basic aspects of the nervous system are firstly explained, followed by a description of the anatomical terminology and the neuromuscular anatomy of the arm.

2.1 Nervous System

The human nervous system is one of the most complex biological systems on Earth, composed by hundreds of billions of neurons that communicate with each other in a highly structured manner and, as a result, allows us to interact with our environment. Although some aspects of the most complex neural networks of the nervous system are still being unraveled, there is great knowledge of most of the elements and processes that conform it.

The human nervous system is divided in two main parts, which are the central nervous system (CNS) and the peripheral nervous system (PNS). The CNS is composed by the brain and the spinal cord, while the peripheral system includes the spinal, cranial and autonomic nerves and their branches. In this section we will focus on the PNS as it is the part that concerns us.

2.1.1 Nerve cells

The nervous system is composed of two types of cells: nerve cells (also called neurons) and glial cells. The latter are not directly involved in information processing but they play other vital roles such as supporting neurons, producing

myelin, or removing debris, among others [1]. Nerve cells, on the contrary, are the main signaling units of the nervous system and can process, generate and transmit information through electrical and chemical signals.

Nerve cells have different morphological regions, as shown in Figure 2.1, for specific functions. Main parts of a typical neuron are the following [2]:

- Dendrites: they are the connection regions where the neuron receives information from other neurons.
- The cell body (or soma): it is the metabolic center of the cell, which contains the nucleus and other organelles.
- Axon: it is a key component of the neuron, over which information is transmitted to the terminal parts of the neuron.
- Synaptic terminal: it is the region where the neuron forms a connection with another neuron and transmits the information by means of a synaptic transmission.

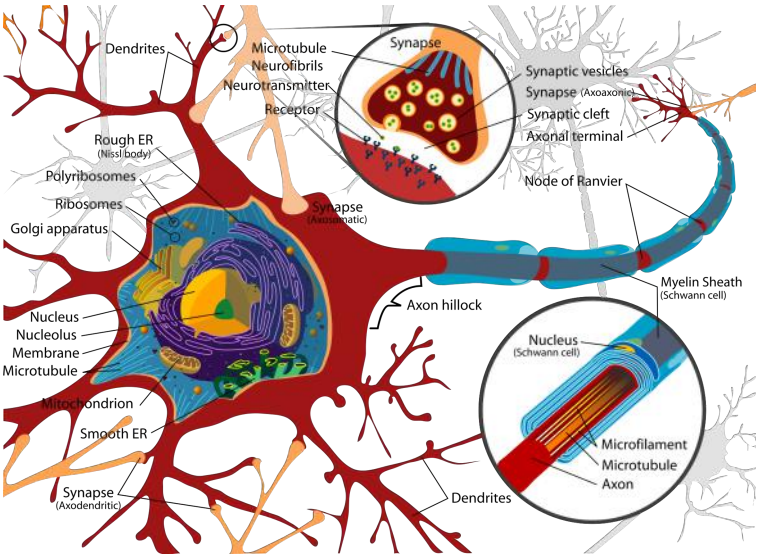

Figure 2.1: Nerve cell [3].

Nerve cells are electrically excitable, and this is the property that makes them able to process and transmit information. The information travels along the nervous system by means of electrical signals, called action potentials (AP). AP are short electrical spikes or impulses (around 1 ms) elicited in an all-or-nothing fashion. It is the AP firing rate which determines the stimulus intensity, not the amplitude of the AP spikes, which are independent of stimulus intensity (usually around 100 mV) [1, 2].

The generation of an AP happens in the nerve cells in an all-or-nothing manner as described next. At rest, neurons maintain a difference in the electrical potential on either side of the external membrane, which is called the resting membrane potential (around $-65\,\text{mV}$) caused by the unequal distribution of electrically charged ions, in particular, the positively charged Na+ and K+ ions and the negatively charged amino acids and proteins on either side of the cell membrane. This resting potential can be disturbed by a synapse with another neuron, or by electrochemical receptor terminals, which lead to a reduction of the negative membrane potential called depolarization that happens at the axon. If this depolarization reaches a determined membrane potential, called threshold, then an AP is triggered, as a result of the Na+ and K+ ion flow through the voltage-sensitive channels in the cell membrane [1, 2]. The shape of an AP is shown in Figure 2.2.

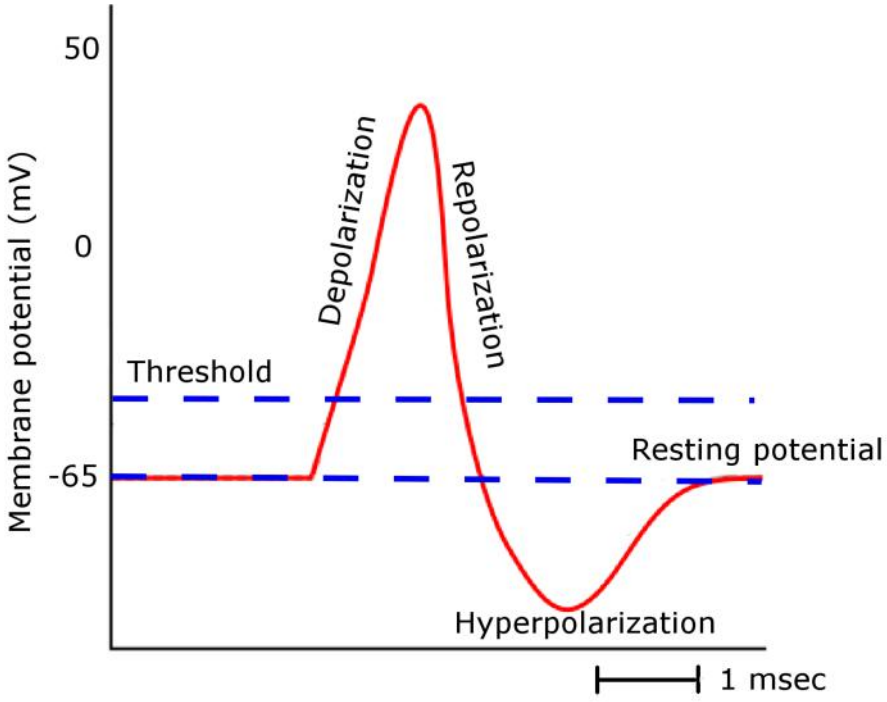

Figure 2.2: Action Potential.

The triggering of an AP causes a current flowing inwards at the point where it was generated, which depolarizes adjacent sections of its membrane. If sufficiently strong, this depolarization provokes a similar AP at the neighboring membrane areas, propagating the AP along the axon as a wave until reaching

the synaptic terminals. However, some axons are wrapped by an insulating myelin sheath that has regular interruptions called nodes of Ranvier and behave in a different manner. On these axons ion flow does not happen within the myelinated segments, but only at the nodes of Ranvier. This property makes current flow through the cytoplasm (external to the cell membrane), which, if sufficient, will depolarize the subsequent node of Ranvier generating a new AP. This fact enables a fast and efficient transduction of AP along the axon known as saltatory conduction. In many types of neurons the dendrites have voltage-sensitive Ca2+, K+, and Na+ ion channels. Thus, in those cases where AP are propagated backwards to the dendrites, the passive, electrotonic conduction of synaptic potentials is modified, which can influence the excitability of involved neurons [1, 2].

2.1.2 Somatosensory system

The somatosensory system is one of the sensory systems of the PNS, and it is responsible for informing about the external environment through discriminative touch, proprioception, temperature and pain sensing. The different receptor organs of the somatosensory system perceive environmental changes and transform the information into electrical signals, which are carried to the CNS through an extensive neural network. These neural pathways carrying information from sensory receptors to the CNS are called afferent nerve fibers, whereas the neural pathways carrying information in the opposite direction are called efferent nerve fibers [1].

Sensory receptors present in the somatosensory system can be classified as cutaneous receptors or proprioceptive receptors. In any case, the location and the structure of a sensory receptor will determine its specific sensing modality. Regarding cutaneous receptors, their terminals can be either encapsulated or not, depending on the receptor type. Figure 2.3 shows an illustration of cutaneous receptors present in the skin. The skin sensitivity of different areas of the body differ depending on the amount, distribution and type of cutaneous receptors present in each of them [1].

Properties of cutaneous receptors are briefly described next [1, 2]:

- Meissner corpuscles: they are found only in glabrous skin (hairless skin) and they are able to sense flutter and movement.
- Pacinian corpuscles: they are found in subcutaneous tissue beneath the dermis and they are able to sense vibration or tickle.
- Ruffini corpuscles: they are found deep in the skin and are sensitive to skin stretch.
- Hair follicles: they are non-encapsulated receptors and are able to sense hair movements.

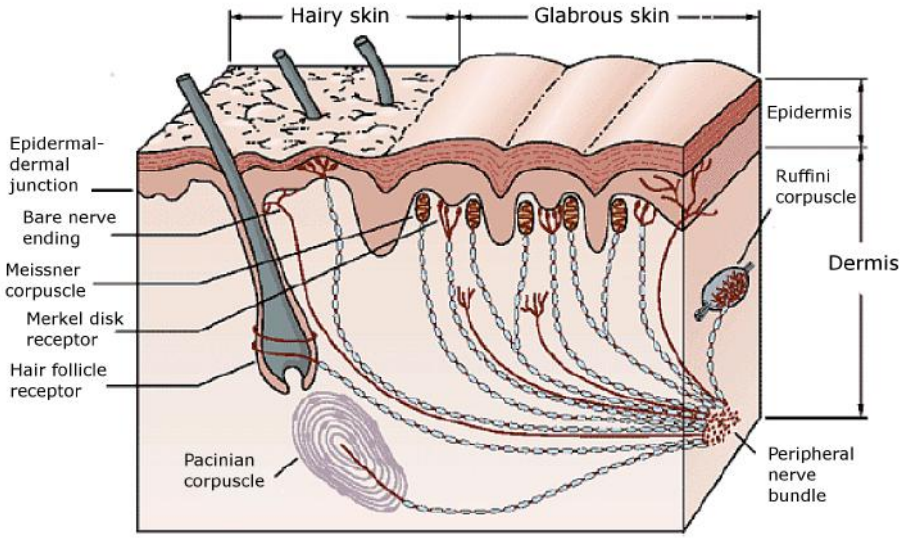

Figure 2.3: Cutaneous receptors [1].

- Merkel disks: they are non-encapsulated receptors found in both hairy and non-hairy skin, more concretely, in the basal layer of the epidermis. Merkel disks are considered to be the fine tactile receptors that make us able to sense pressure, localize tactile stimuli and to perceive the edges of objects.
- Bare (or free) nerve endings: they are free nerve endings found throughout the body and different functional types of them can sense nociceptive or tissue-damaging stimuli (pain), skin cooling, skin warming or touch. Bare nerve endings are considered to be the somatosensory receptors for pain, temperature and crude touch.

Should be noted that thermal receptors and nociceptors have small-diameter axons that are either unmyelinated or thinly myelinated, so AP are propagated slower in these nerves than in the ones corresponding to the rest of described receptors [1].

Finally, regarding proprioception, two main receptors should be mentioned: the Golgi tendon and the muscle spindle. Both are encapsulated proprioceptors, but their location is different within the muscles as shown in Figure 2.4. The Golgi tendon organ is located at the junction of muscle and tendon, and monitors and signals muscle contraction against a force (muscle tension). On the other

hand, the muscle spindle is located in the muscle and monitors and signals muscle stretch (muscle length) [2].

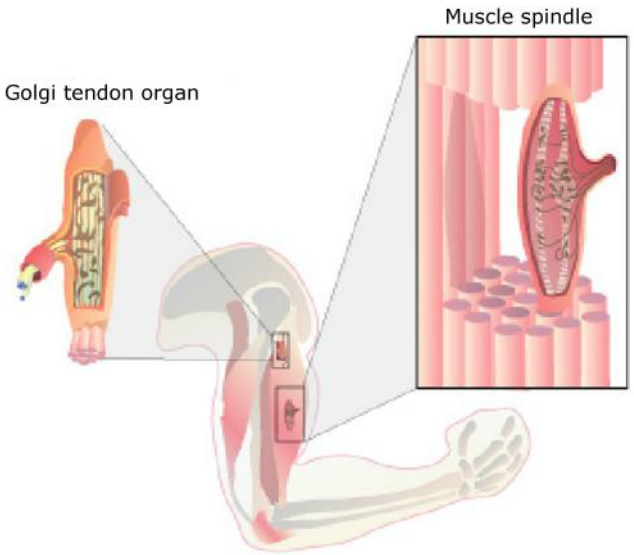

Figure 2.4: Proprioceptive receptors [2].

2.1.3 Motor system

Finally, the nervous system also enables us to act upon our environment by generating movements. Although the autonomous system also includes movements, in this section we will only refer to movements caused by skeletal muscles.

A typical muscle is controlled by hundreds of motor neurons, whose axons enter the muscle and branch into a number of terminals that form neuromuscular synapses with muscle fibers. A single skeletal muscle can consist of hundreds of thousands of muscle fibers, which are parallel contractile elements grouped forming fascicles. Those motor neurons that control limb and body movements are located in the anterior horn of the spinal cord. A motor unit is then comprised of a motor neuron and the muscle fibers it innervates. Muscle fibers corresponding to a single motor unit are spread throughout the whole muscle, like this, when an AP is triggered by a single motor neuron, a weak uniform contraction over the entire muscle will be produced. Small motor units are present on muscles that require a fine degree of control, whereas large motor units are common in muscles that need more strength than fine control [1, 4, 5]. An illustration of the described concepts is shown in Figure 2.5.

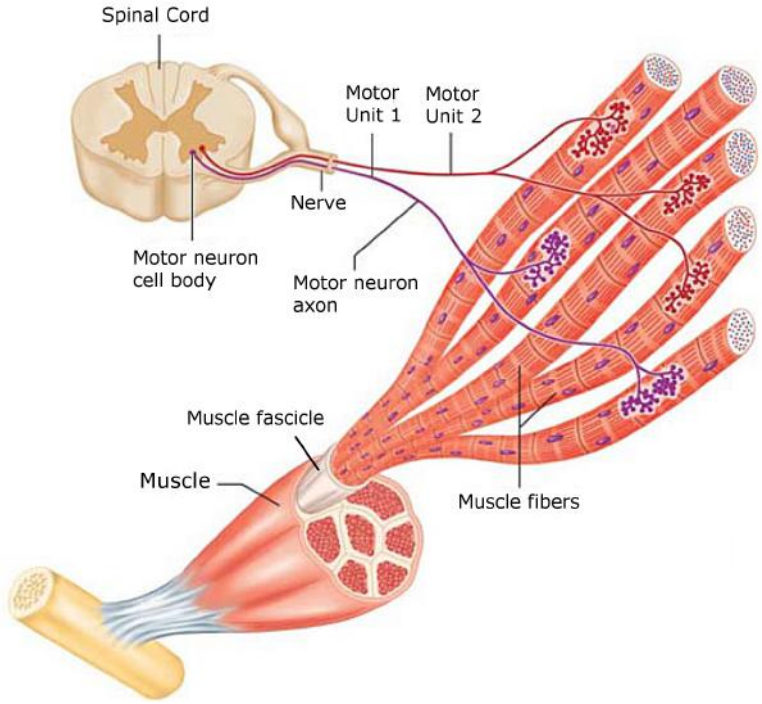

Figure 2.5: Motor Unit [4].

There are three types of muscle fibers, classified upon the speed of response and their resistance to fatigue. Although most muscles contain fibers of the three types, fibers corresponding to the same motor unit are all the same type. Fiber types [1, 5]:

- Type I (slow-twitch): muscle response (contraction and relaxation) following an AP is slow, but they can last long periods of time producing small forces without fatiguing. Small motor neurons innervate these type of fibers.
- Type IIA (fast-twitch fatigue-resistant): muscle response is fast, they produce larger forces than type I fibers but they are not able to maintain these for very long periods.
- Type IIB (fast-twitch fatigable): muscle response is fast and they produce large amounts of force that last very little because they fatigue very quickly. Large motor neurons innervate these types of fibers.

The muscle force is controlled by motor neurons and it is determined by two main factors: the AP rate and the motor neuron recruitment order. As described earlier, the AP carry information, and the intensity of the stimulus

is coded by the rate at which the AP are generated. Therefore, an increase in the rate of AP fired by a motor neuron results in an increase on the amount of force of the corresponding motor unit. With low rates only muscle twitches are achieved, but with higher rates a summation of force is produced because a new AP is delivered before muscle is relaxed back to baseline. This summation increases with higher AP rates, but above a certain rate, the muscle has no time to relax at all between stimuli, and the twitches fuse into a smooth contraction called tetanic contraction [2, 5]. Figure 2.6 shows the tetany and the summation effect caused by AP rates.

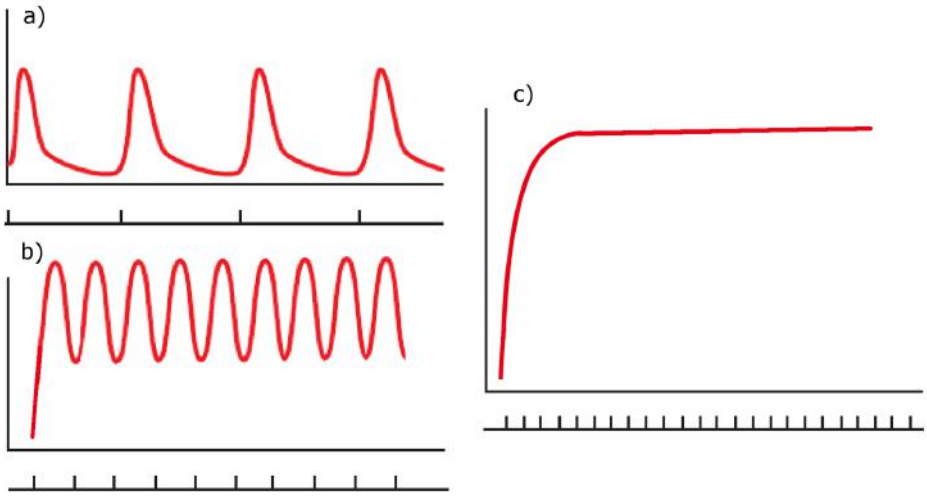

Figure 2.6: AP rates and force summation. Vertical axis represents muscle tension. a) lowest AP rates generate single muscle twitches. b) intermediate AP rates show summation effect. c) high AP rates generate tetanic contractions.

The motor neuron recruitment order is determined by the motor neuron size principle, which dictates the order at which motor neurons are recruited to execute a movement. If the input to motor neurons coming from the CNS is weak because a slight contraction is needed, then only small motor neurons will be recruited, as these have a smaller membrane surface area and lower synaptic current is sufficient to generate an AP. As the strength of the signal coming from the CNS increases, bigger motor neurons will be recruited, causing an increased number of muscle fiber contractions and increased muscle force. If we associate the size of the motor neurons with the fiber types they innervate, it turns out that the slow fatigue-resistant fibers are recruited first, which produce lower forces. If more muscle force is needed then fast fatigue-resistant fibers are recruited, and in the very last position, fast fatigable fibers are recruited.

This recruitment order delays fatigue and permits a fine control of the force produced by muscles [2].

2.2 Anatomy

This section defines some basic anatomical terms and describes briefly the neuroanatomy of the arm, which will be useful for a better understanding of the work presented in the following chapters.

2.2.1 Orientation and terminology

The most important reason for using anatomical terminology remains in the fact that "up/down" or "right/left" terms can become confusing when we are talking about human body parts.

The anatomical position shown in Figure 2.7 provides a standard frame of reference for anatomical description and dissection. It consists on a standing position, with feet flat on the floor, arms at the sides of the trunk and palms, face and eyes facing forward. Anatomical planes, which are standard imaginary planes that pass through the body also serve as a guide for anatomical description [5]. Major anatomical planes include sagittal, frontal and transverse planes, which are shown in Figure 2.7.

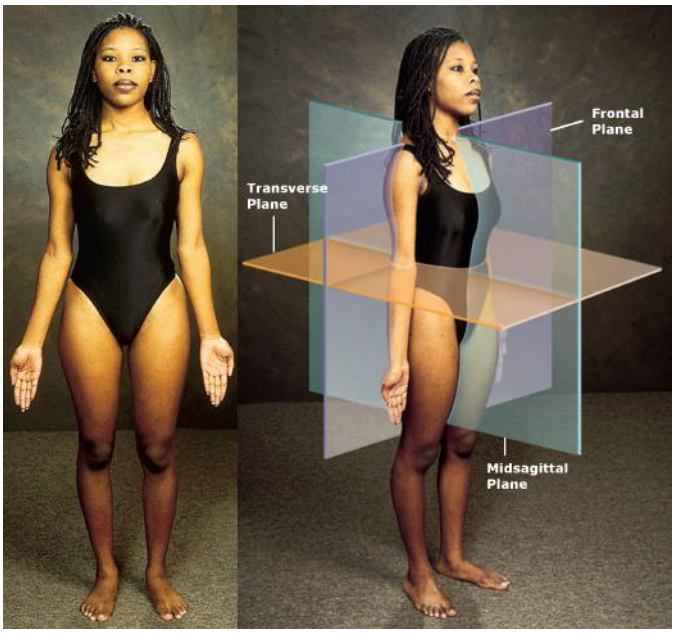

Figure 2.7: Anatomical position and anatomical planes [5].

Finally, directional terms that describe the position of a structure relative to another can be defined taking the anatomical position and anatomical planes as a reference [4, 5]:

Anterior Toward the front (in front)
Posterior Toward the back (behind)
Ventral Same as anterior in humans
Dorsal Same as posterior in humans
Superior Toward the head (above)
Inferior Away from the head (below)
Medial Toward the midsagittal plane
Lateral Away from the midsagittal plane
Proximal Closer to the point of origin (closer to the point of attachment to the body trunk)
Distal Farther from the point of origin (farther from the point of attachment to the body trunk)
Superficial Toward the body surface
Deep Away from the body surface

2.2.2 Arm neuroanatomy

Musculoskeletal muscles are attached to bones and are responsible of their movements, which happen at different bone joints or articulations on the body and can be of different forms depending on the joint structure. In the following list, the main movements happening at arm and hand joints are briefly described [5]:

Flexion Movement that decreases the angle of a joint, usually in a sagittal plane.
Extension Movement that straightens a joint and generally returns a body part to the anatomical position. Some joints like the wrist can extend over 180^{o} or over the anatomical position, which is also called hyperextension.
Abduction Movement away from the midsagittal line. Abduction of fingers is to spread them apart.
Adduction Movement toward the midsagittal line or, for fingers, toward the median axis of the middle digit, in other words, returning to the anatomical position.
Supination In the case of the forearm, it consists on its rotation to place the palm facing forward (anatomical position) or upward.
Pronation In the case of the forearm, it consists on its rotation to place the palm facing backward or downward.
Opposition Movement of the thumb to approach or touch the fingertips.

The upper limb includes the brachium (arm), antebrachium (forearm), carpus (wrist), manus (hand), and digits (fingers) and it is composed by around 50 muscles innervated by different branches of different motor nerves corresponding to the PNS. Figure 2.8 shows the superficial view of the muscles involved in the upper arm, which enable us to generate some of the previously explained movements at shoulder and elbow joints [4].

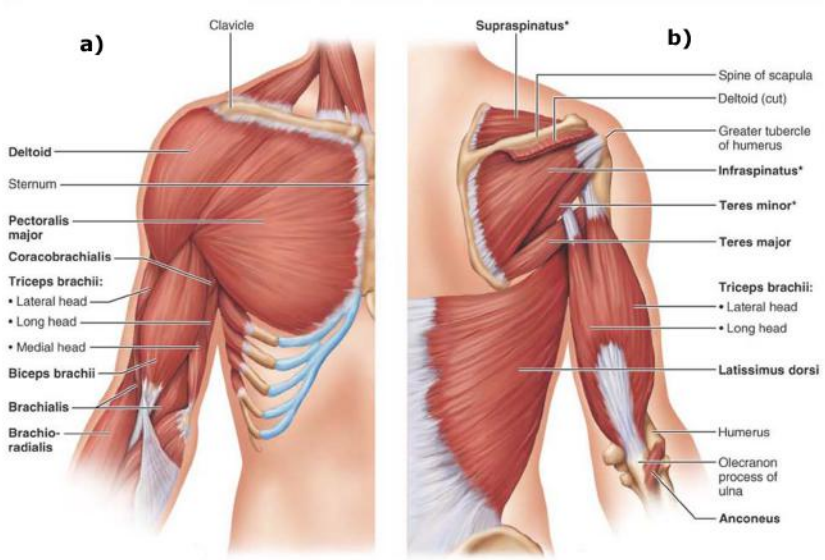

Figure 2.8: Upper arm superficial muscles [4]. a) Anterior view. b) Posterior view.

Most important muscles of the upper arm include the deltoid, triceps, biceps and brachialis. Deltoid is responsible for shoulder abduction, flexion and extension and it is innervated by the axillary nerve. Biceps and brachialis are prime movers of elbow flexion and they are inervated by the musculocutaneous nerve. The brachioradialis, which is located on the forearm, also contributes significantly to elbow flexion. Finally, triceps muscle is the prime mover of elbow extension and it is innervated by the radial nerve [4].

Regarding forearm, most muscles act at wrist, finger or thumb joints. The forearm muscles that generate finger and thumb movements are known as the extrinsic muscles of the hand, which arise in the forearm and insert into the digits via long tendons crossing the wrist. The intrinsic muscles of the hand, which arise and insert within the hand, are involved in finer finger and thumb movements. These are beyond our scope as the surface FES system used for

the present work is not applied on them. The anterior and posterior views of different layers of forearm muscles are shown in Figures 2.9 and 2.10 [4].

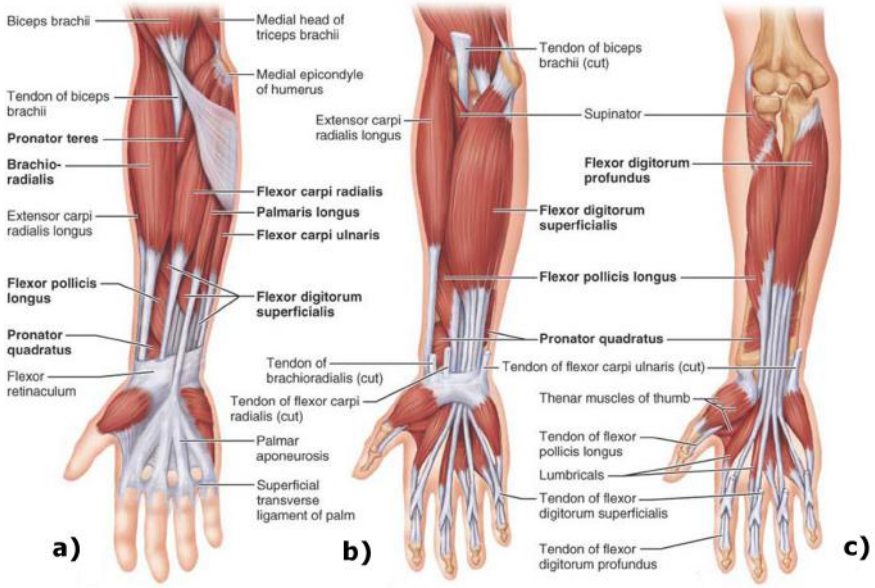

Figure 2.9: Forearm anterior muscles [4]. a) Superficial view. b) Intermediate view. c) Deep view.

As it can be seen in the figures, forearm muscles compound a complex structure of small overlapped muscles located at different depths. Most muscles located on the anterior part of the forearm generate flexion movements at the wrist and fingers and are mainly innervated by the median or ulnar nerve. Conversely, muscles located on the posterior part of the forearm generate extension movements at the wrist and fingers and are innervated by the radial nerve and its branches. Although there are forearm muscles that act on the thumb, the intrinsic thenar muscles are the prime movers of thumb abduction and opposition, which are innervated by the median or the ulnar nerve [4, 6]. In Figure 2.11 we can see an illustration of how the radial, median and ulnar nerves innervate forearm muscles and their corresponding cutaneous innervation areas.

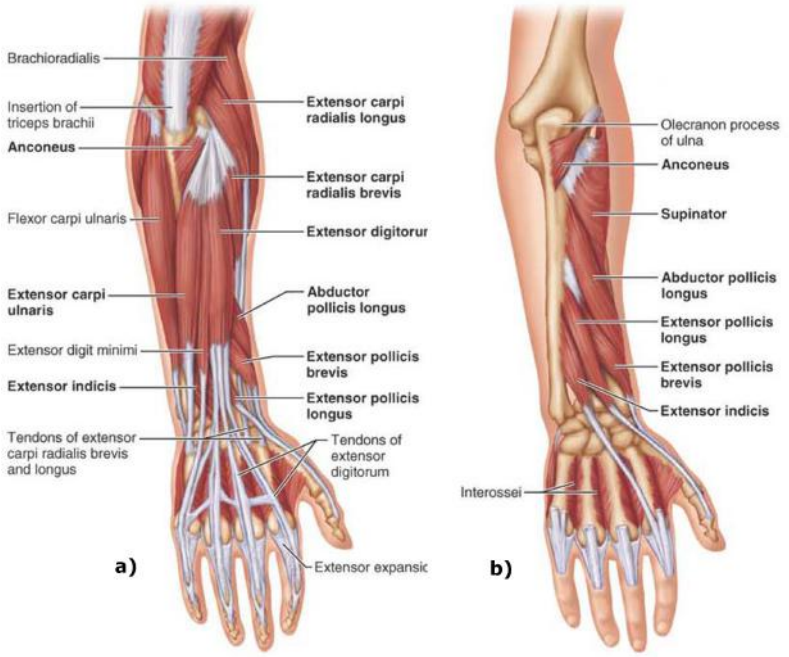

Figure 2.10: Forearm posterior muscles [4]. a) Superficial view. b) Deep view.

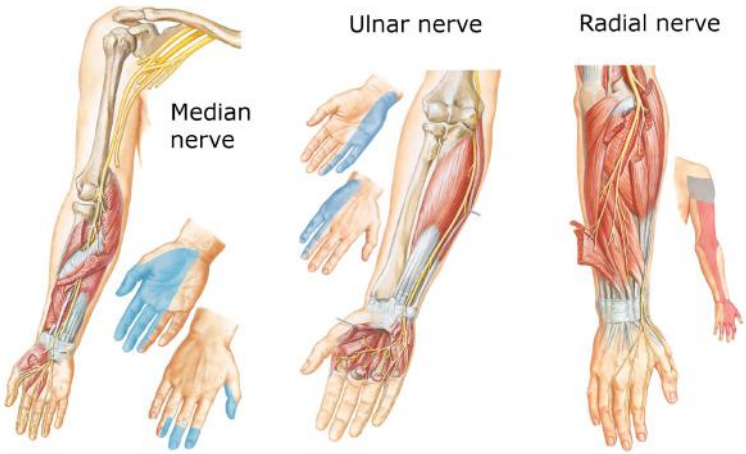

Figure 2.11: Nerves innervating forearm muscles [6]. Colored areas indicate cutaneous innervation of the corresponding nerve.

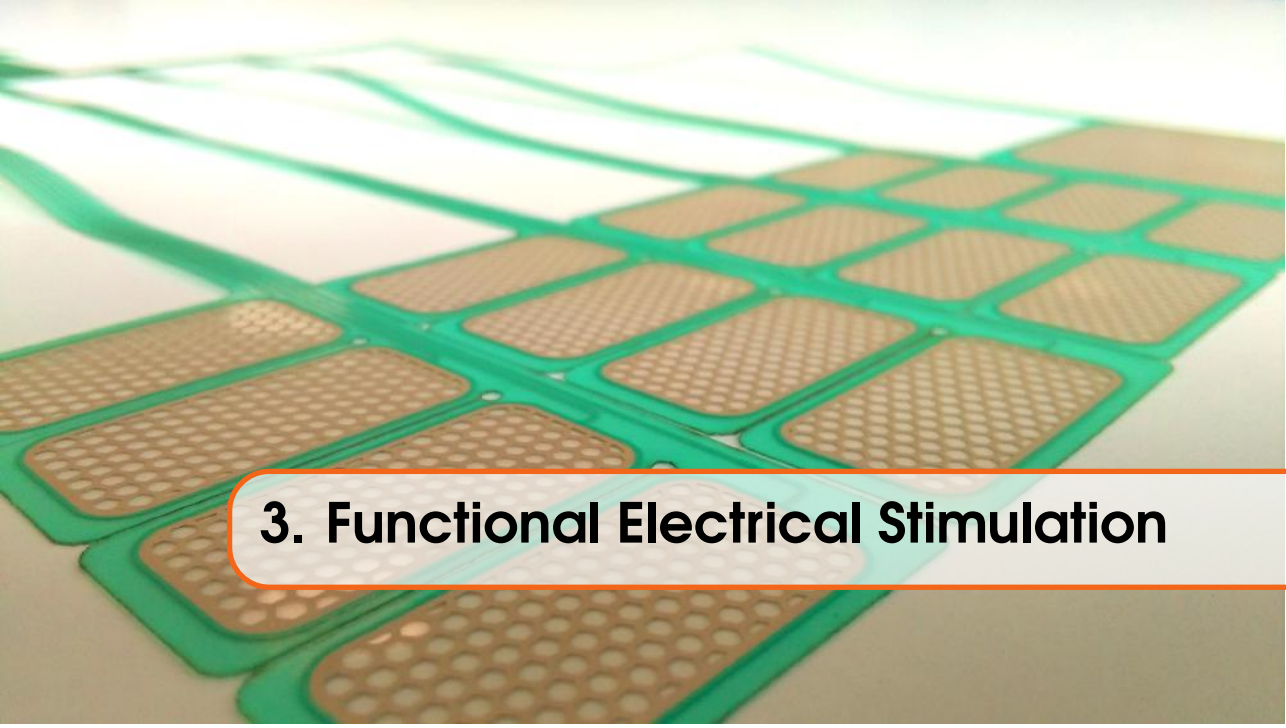

3. Functional Electrical Stimulation

Neuromuscular Electrical Stimulation (NMES) consists on applying electrical pulses to peripheral motor nerve fibers in order to generate muscle contractions. If these muscle contractions are generated in a coordinated manner aiming at achieving a specific function, it is called Functional Electrical Stimulation (FES). Although FES also includes sensory functions, in this chapter only basics of FES applied to muscles will be described, since sensory FES does not concern to the thesis topic. Thus, the basic functioning principles are the same for NMES and FES in this case.

3.1 Principles

In NMES applications, electrical pulses are delivered by means of at least a pair of electrodes located close to the targeted nerve or nerves. The flow of ions between the electrodes causes the depolarization of the cell membrane of nearby neurons, where if the threshold value is exceeded, an AP is triggered. As described in the previous chapter, this AP is then propagated along the neural pathway until it reaches the terminal neuromuscular synapses. As a result, the muscle fibers innervated by the artificially excited neurons will contract [7].

3.1.1 Waveforms

As the aim of NMES is to produce a muscle contraction by artificially exciting nerves, the electrical signals applied to them should be able to generate AP. Therefore, the most common electrical signal used in NMES consists of bursts of

pulses, where each pulse aims to depolarize the nerve cell membrane and elicit an AP. Voltage-regulated or current-regulated pulses can be applied, although the voltage-regulated approach presents some disadvantages over the current-regulated approach: 1) maximum stimulation happens only at the beginning of each pulse, 2) an increase in the resistance of the conduction path causes an additional voltage drop, and 3) injected charge and driven current cannot be controlled. Therefore, current-regulated approach is generally preferred [8]. Regarding pulse waveform, different shapes, number of pulses and monopolar and biphasic approaches have been tested in terms of performance, discomfort, charge-efficiency and tissue damage, and so far, biphasic square-shaped pulses have shown best acceptation [8, 9, 10, 11, 12]. However, there are differences in terms of performance, tissue damage and electrode corrosion between different square-shaped approaches, as Figure 3.1 illustrates.

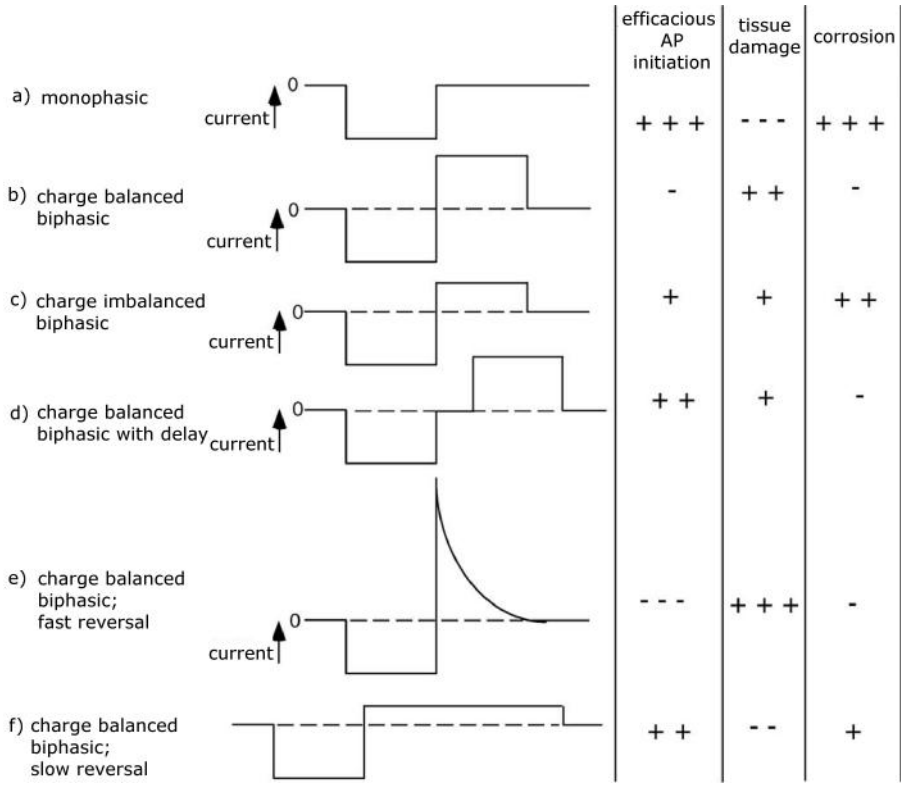

Figure 3.1: Waveform effect on AP initiation, tissue damage and electrode corrosion [9]."+ + +" meaning best and "- - -" worst.

The first phase of the waveform elicits an initiation of an AP, however, a compensatory phase is used to reverse the direction of the electrochemical

processes happening within the skin tissues. As it can be seen in Figure 3.1a, the absence of this charge balance can lead to a tissue damage and, thus, biphasic waveforms with a reversal phase are preferred for NMES applications. However, high current reversal phases may inhibit the AP generation, whereas slow charge reversal phases can result in skin tissue damage due to the slow reversal of the electrochemical processes happening within the skin tissues [9].

3.1.2 Stimulation parameters

The square-shaped-pulse waveforms are the most used in NMES and are characterized by three parameters: amplitude, pulse-width and frequency. The strength of muscle contraction is controlled by manipulating these parameters.

Amplitude determines the height of each pulse (usually defined in current units - A) and pulse-width determines the duration of each pulse. Both parameters control the amount of recruited motor units. As the amplitude or pulse-width increase, the injected electric charge increases, resulting in a larger electric field and a broader activation region, where more nerve fibers will be reached. This is represented in Figure 3.2 and it is called spatial summation. Thus, increasing either of both parameters will result in an increase of muscle contraction strength [7, 8].

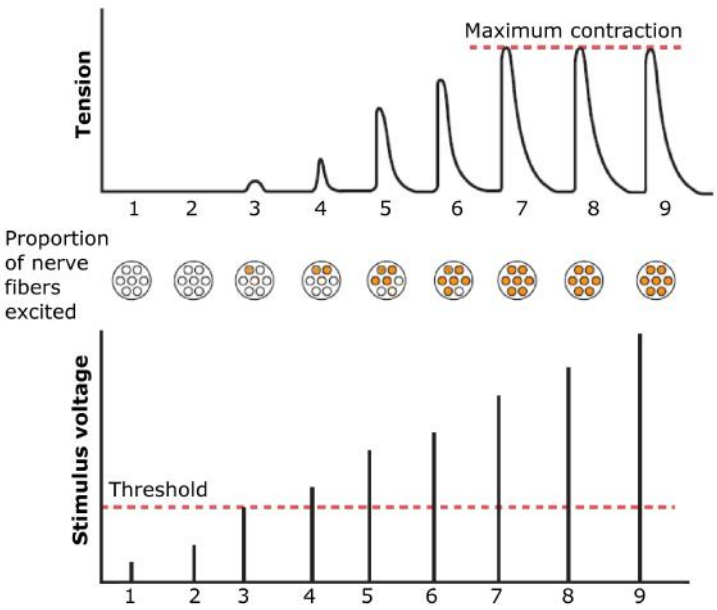

Figure 3.2: Amplitude effect on fiber recruitment [5].

In Figure 3.3, the amplitude vs. pulse-width relation is shown, where the curve represents the combination of parameter values that correspond to an AP initiation. It can be seen that as pulse-width decreases, amplitude needs to be increased to compensate, and viceversa. However, as pulse-width increases amplitude only decreases down to a certain minimum value. There is no AP generation if amplitude is below that value, even with widest pulse-width values. This amplitude value is called Rheobase, and the time point that belongs to double of Rheobase value is called Chronaxie time [8, 13] . Thus, in order to be energy-efficient and charge-efficient, for FES applications pulse-width values are usually set between 100μs and 300μs.

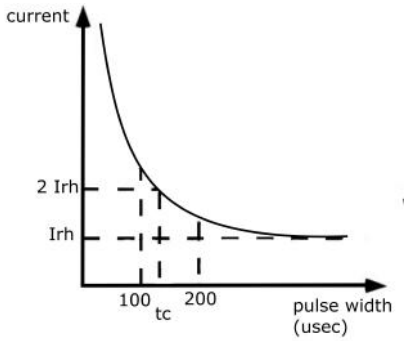

Figure 3.3: Amplitude vs. Pulse-width, where the curve represents combinations that lead to an AP initiation [9]. Irh=Rheobase intensity, tc=Chronaxie time.

The last stimulation parameter is the frequency and determines the rate at which square pulses are delivered. As it was described in the previous chapter, AP rate has an influence in the generation of muscle force due to the summation effect. Thus, electric pulse frequency influences the same way. Low frequencies generate single muscle twitches, whereas high frequencies generate tetanic contractions [7, 8, 13]. Figure 3.4 shows the effect of different frequencies in muscle tension. Since FES aims at generating functional movements, smooth tetanic contractions are preferred, and accordingly frequencies above 20 Hz are usually applied.

As previously explained, physiological control of muscle contraction force is carried out through two mechanisms: the AP rate and the motor unit recruitment. This can be mimicked in NMES by controlling the frequency (AP rate) and pulse-width and amplitude (motor unit recruitment). However, there is a big difference between naturally and artificially generated muscle contractions, which is the recruitment order. Actually, the motor unit recruitment order is just the opposite when applying NMES. This is because in the natural process AP

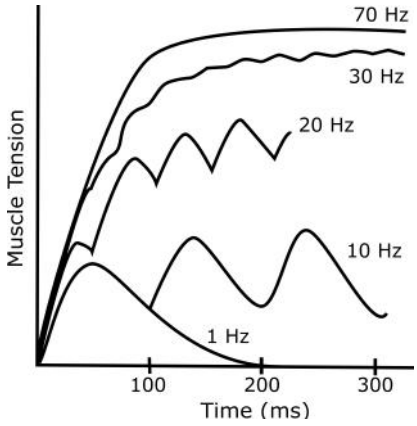

Figure 3.4: Frequency effect on muscle tension. Adapted from [8].

are generated at CNS level, whereas in NMES the stimulation is applied to the PNS at the axon level. In the NMES case, the AP are triggered by electrodes that generate a potential difference on the extracellular environment between at least two adjacent nodes of Ranvier. The distance between these nodes of Ranvier are larger on nerve fibers with larger diameters, hence, it is easier to generate an AP in larger motor neurons than in smaller ones. These differences on excitability results in an earlier recruitment of largest motor units. As amplitude or pulse-width is increased, the activation region increases and other smaller nerve fibers are also excited. Therefore, unlike in the natural muscle contraction process, first, large motor units that correspond to fast-fatigable motor fibers are recruited, followed by smaller motor units as the stimulation signal gets stronger. This fact causes a premature fatigue, which is an important drawback of FES systems, specially in applications where big muscles are involved. In these cases, fatigue impedes performing FES-induced tasks for prolonged periods [8, 13, 14].

As the recruitment order is reversed and fast-fatigable muscle fibers are always recruited when using NMES, high frequencies lead to stronger contractions of those fibers, and as a result fatigue is earlier achieved. In order to avoid this effect and delay fatigue, in FES applications it is common to set frequency constant at low values (20 Hz to 50 Hz) and to control muscle force by modulating amplitude or pulse-width [8, 9, 13, 15].

3.1.3 Electrode configuration and size

This section refers to transcutaneous or surface NMES, which is applied by electrodes located on the skin. As it has already been explained, the ions flowing between at least a pair of electrodes cause a membrane depolarization at nerve

fibers that are under the activation area of the generated electric field. However, different electrode configurations and size have different effects on performance or discomfort.

In case of using two electrodes (most typical approach), these are usually arranged in a monopolar or bipolar configuration. In the monopolar case, one of the electrodes (active electrode) is placed near the target peripheral nerve, whereas the other electrode (return electrode) is placed in a remote area over less excitable tissue, such as tendon or fascia. This configuration works well on small muscle applications, as it is preferable to excite a small area under the active electrode without exciting other nerves underneath the return electrode. On the other hand, in the bipolar case, the return electrode is placed close to the active electrode over excitable tissue. The bipolar configuration is often used in applications involving big muscles, as the fact of having two electrodes over the targeted muscle may enhance the stimulation and produce higher forces. Distance between both electrodes affects performance of stimulation as well, since distance gets smaller the current tends to pass through the most superficial layers of the skin because they are less resistive. On the contrary, if distance between them increases then current can spread deeper on the skin layer [7, 8, 14].

Regarding the electrode size, it affects mainly the current density, which is the amount of current flow per unit area. A low current density implies a small amount of ion movement in a particular area of the tissue, and it may not be sufficient for membrane depolarization. If same current is passed through a big electrode and a small electrode, the latter one will imply a higher current density, which is desirable near target nerve fibers. On the other hand, a big electrode will tend to distribute the current into a broader area, resulting in a lower current density. Thereby, small electrodes are desirable to be placed close to the target nerves because the excitation is more localized and lower current is needed to elicit an AP. However, deep target nerves require higher amplitudes, which in the case of very small electrodes can result in high current densities that produce discomfort. Conversely, large electrodes are preferable in those areas where no selective excitation is desired or target nerves are deep from the surface, because the current distributes over a broader area. Therefore, electrode size balance should be found for every FES application. [16, 17].

3.2 Electrode types

The electrical pulses are generated by a stimulator, which usually includes waveform and parameter control options. Then, via wires, electrical pulses are transmitted to the electrodes, being themselves responsible of transmitting these to the peripheral nerves. Hence, the main objective of the electrodes is to deliver

electrical pulses to target nerve fibers minimally exciting additional nerve fibers and without damaging any tissue at the stimulation site. Electrode types can be classified by the level of invasiveness in three main groups: implanted, percutaneous and transcutaneous (surface) electrodes [7, 14].

3.2.1 Implanted electrodes

Implanted electrodes are placed attached or close to the nerves and they are connected by leads under the skin to an implanted stimulator. Such stimulator is usually controlled by an external device by means of a radio-frequency link. There are many types of implanted electrodes, but main electrodes include: epimysial electrodes, which are implanted on the muscle surface [18]; intramuscular electrodes, which are placed inside the muscle [19]; epineural electrodes, which are placed close to the nerve [20]; and cuff electrodes, which wrap around the nerve [21].

Implanted electrodes are invasive because they require surgery for placement or removal. Some have shown success in long-term use and chronic applications [22].

3.2.2 Percutaneous electrodes

Percutaneous electrodes are inserted into the muscles (intramuscular) through the skin by means of a minimum invasive technique using a hypodermic needle [23]. Although they are less invasive than implanted electrodes, common electrode lead fracture or infection risks make them less preferred than implanted electrodes for chronic applications [24]. Nevertheless, they are commonly used as precursors for fully implanted systems [25].

3.2.3 Transcutaneous (surface) electrodes

Transcutaneous electrodes are placed on the skin surface and so, they are non-invasive. These are usually placed over motor points of the target muscles, which are defined as stimulation sites that produce an isolated contraction of the target muscle at the lowest stimulation level. Usually, a motor point corresponds to an area on the skin where a nerve branch passes most superficial and so, it is easier to excite with lower stimulation levels. The main advantages of surface electrodes are that they are very simple to don/doff, they can be reused, they are available in many shapes and sizes by diverse manufacturers, and that their prize is very low. This make them preferred in clinics for short-term and therapeutic applications [26].

Different materials have been used for transcutaneous electrodes in the last decades, such as metal electrodes covered by a spongy tissue or rubber electrodes. However, the self-adhesive hydrogel electrodes have shown to be

the ones producing less discomfort and they are easier to attach/detach [16, 26]. Therefore, except for special applications almost exclusively self-adhesive hydrogel electrodes are used for transcutaneous electrical stimulation. These electrodes use a gel to contact a conductive member with the subject's skin. The electrode is built in a multi-layer configuration with first hydrogel layer acting as a skin interface and the second hydrogel layer connecting the substrate with the previous layer [26].

Although widely used, still surface electrodes face some disadvantages compared to percutaneous or implanted electrodes. One of them is that afferent fibers corresponding to cutaneous receptors are usually excited together with motor nerve fibers when surface stimulation is applied, which can cause discomfort to the user. Indeed, the discomfort can become worse due to the skin inhomogeneities or electrode edge effect, which can cause painful localized high current densities. In order to avoid this happening, high resistivity hydrogels are suggested [27]. Yet, the main problem of surface electrodes lies in the selectivity. This is the capacity of exciting the targeted nerve fibers without exciting the surrounding ones that can result in unwanted muscle contractions. As electrodes are attached to the skin, some deep nerves become almost inaccessible, and on the contrary, superficial nerves located next to the electrode are too easily excited. This is an issue specially in applications that involve the stimulation of small muscles. Besides, high resistive skins and thick fat layers under the skin may also force to apply higher amplitudes to reach deeper nerves, compromising comfort and selectivity [17].

Nevertheless, research on surface multi-field electrodes seeks to overcome with some of these disadvantages. A multi-field electrode consists on a group of several tiny conductive fields, which can be activated or deactivated independently, distributed along a big area. This configuration adds a new dimension to surface electrical stimulation methods, as it brings new stimulation possibilities and combinations that should be tested. So far, surface multi-field electrodes have shown selectivity improvements [28, 29] and delay of fatigue effect [30] with respect to pairs of conventional single electrodes. Moreover, the tedious work of manual search of motor points can be avoided by automated search implemented with multi-field electrodes [31, 32].

3.3 Applications

Although FES has many clinical applications, only the ones involving limb functions and its benefits are briefly described, as other applications are not relevant for understanding the current work.

3.3.1 Neurological disorders

Main benefits of FES have been found within the neurorehabilitation field, where the target population includes patients suffering from neural disorders such as spinal cord injury (SCI), stroke, multiple sclerosis (MS) or cerebral palsy (CP) among others [33, 34, 35, 36].

Although the mentioned diseases differ greatly in the cause of origin and pathology, they all present interrupted pathways in some sensory-motor nerve structures of the nervous system, which can lead to motor dysfunctions. In any case, disorders with the cause of origin either at the brain (stroke and CP), spinal cord (SCI) or nerve (MS), result in interrupted neural pathways, causing weakness or paralysis of limbs. Moreover, long-periods of inactivation of muscles lead to loss of muscle mass and strength, often worsening the symptoms [37, 38, 39, 40]. Another frequent symptom found in patients suffering from neurological disorders is spasticity. Spasticity is associated with an increase in muscle tone and exaggerated tendon reflexes. It is defined as a velocity-dependent resistance of the muscle to stretch caused by the activation of tonic stretch reflexes. Predominantly, anti-gravity muscles are affected (arm flexors or leg extensors) [40].

Consequently, movement patterns of patients suffering from neural disorders are different to the healthy ones, and they are different for each disease and pathology. In the stroke case, patients usually present a hemiparesia or hemiplegia (partial paralysis of muscles half side of the body), combined with spasticity on flexors of the affected limb. This results in a limb weakness, loss of volitional control and muscle spasticity known as upper motor neuron syndrome. If the spasticity is severe it can cause deformities in resting position of the limbs. In the upper limb case, it commonly consists of shoulder adduction and internal rotation, forearm pronation, and elbow, wrist, digit and thumb flexion [39, 41]. In order to compensate functional disabilities, movement patterns are modified, e.g., in the case stroke patients performing reaching tasks, an increased involvement of the trunk is appreciated due to the inability of properly flexing the shoulder or/and extending the elbow [42].

It is important to point out that independent of the pathology, in order to apply FES successfully, subjects should have excitable peripheral nerves and healthy neuromuscular synapses at stimulation sites, i.e. intact lower motor neurons. This is inherent to FES working principles described in previous sections.

3.3.2 Assistive and therapeutic effects

Some of the disorders mentioned above can be improved or reduced by the application of FES. Actually, in its origin FES applications aimed at substituting

lost motor functions on people with limb dysfunctions or paralysis caused by neural disorders. These complete FES systems that act as a bridge to damaged neural pathways and substitute lost motor functions are called neuroprostheses. Main neuroprostheses developed for lower limbs include drop-foot (inability of making voluntary dorsiflexion of the foot) correction devices for stroke patients [43, 44] and standing and walking neuroprostheses for incomplete SCI patients (partial paralysis of lower limbs) [45, 46]. Regarding upper-limb, fewer neuroprostheses are available for generating grasping function and these are not so broadly accepted, specially systems based on surface electrodes, because of technological and functional limitations [47, 48].

In addition to providing assistance for achieving certain motor functions, neuroprostheses have been found to provide therapeutic effects in different studies, where motor function has been improved in incomplete SCI and stroke patients after following FES based therapy [35, 49, 50, 51, 52, 53, 54]. Not only movement patterns can improve with FES, but some studies found that spasticity can also improve with FES application [55, 56]. Besides, different studies have shown diverse additional benefits of applying FES such as muscle strengthening, increase of muscle mass, improvement of edemas, increase of bone-mass or increase of blood-flow, among others [33, 57]. Although not all patients are able to rehabilitate to the same extent, some patients may recover enough function after following FES based therapy, and may not need to use an assistive neuroprosthesis any longer. For this reason, transcutaneous or surface FES systems are highly recommended over implanted systems for therapeutic applications in neurorehabilitation.

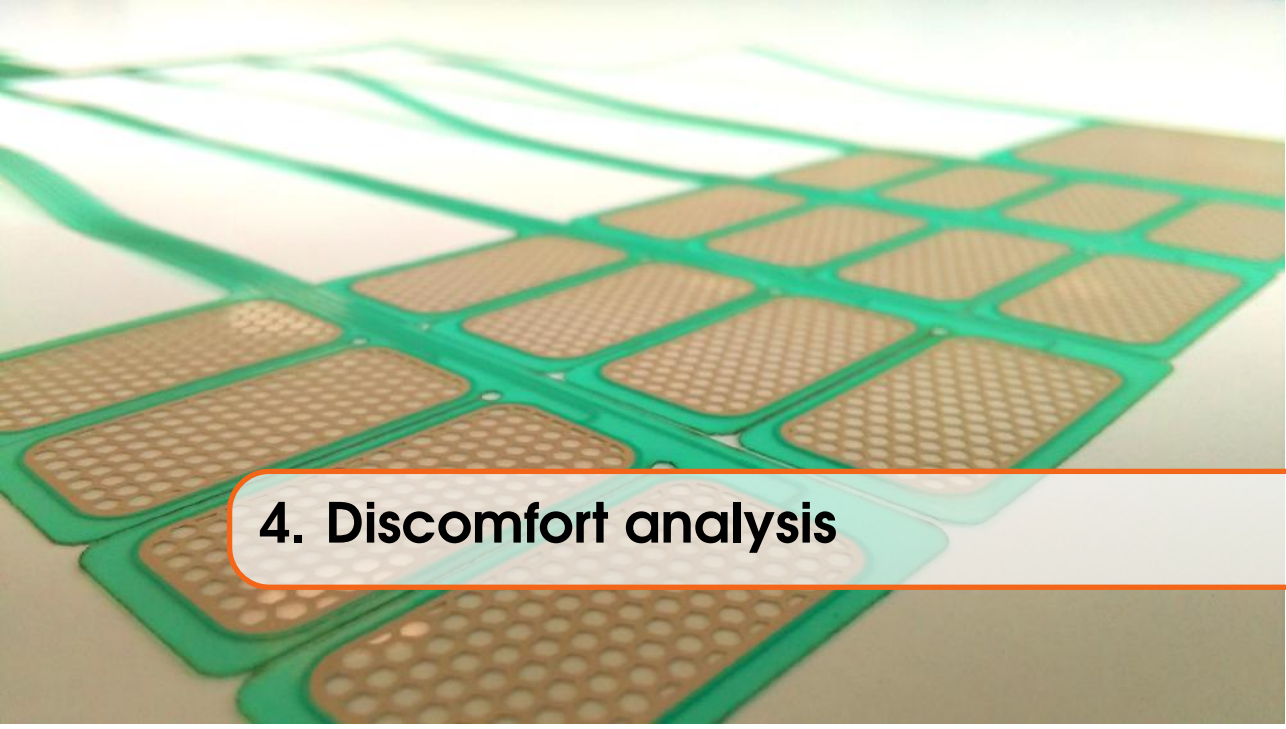

4. Discomfort analysis

The main motivation to carry out these experiments was the lack of studies regarding discomfort caused by different stimulation techniques that new multi-field electrodes make possible. Although asynchronous stimulation has been mainly used in latest research with multi-field electrodes [30, 32], synchronous stimulation is an alternative stimulation method that can be also applied with multi-field electrodes. The reason why these experiments were focused on sensation was that surface FES activates afferent nerve fibers corresponding to cutaneous receptors that can result in discomfort, limiting performance and use of FES in some cases. Therefore, different stimulation techniques should be tested and compared in order to find methods that can ensure good performance producing as low discomfort as possible. The goal of this study was to provide new knowledge regarding discomfort with two different stimulation methods.

4.1 Materials

The materials used in these experiments consisted of a FES system and a custom-built set-up for measuring wrist torque. Both systems were fully controlled by a custom-made Graphical User Interface (GUI) built on Matlab Software.

4.1.1 FES system

The FES device that we used in these experiments was the IntFES stimulator device shown in Figure 4.1, which was designed for functional electrical therapy (FET) [58]. It was a single channel electronic stimulator that provided current-

regulated biphasic stimulation. It could provide an output current ranging from 0 mA to 50 mA, an output frequency ranging from 1 Hz to 50 Hz, and an output pulse-width ranging from 50 µs to 1000 µs. The setup of the stimulation parameters was carried out remotely via Bluetooth.

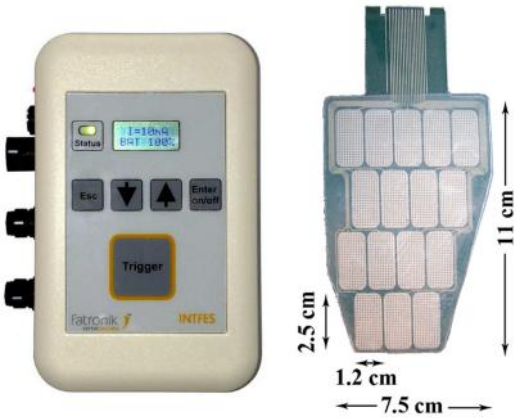

Figure 4.1: IntFES stimulator [58] and multi-field electrode[59] .

Although it only had one channel, the IntFES stimulator was designed to control up to two 16-field IntFES electrodes (32 fields in total). The IntFES electrodes were multi-field electrodes divided into 16 fields that could be activated independently and with different current amplitudes. For our experiments we used a single 16 field electrode matrix specially designed for the dorsal forearm stimulation [59] shown in Figure 4.1. The hydrogel of the electrode was the AG803 type from AmGel Technologies, which had a volume resistivity of 15000 ohm-cm minimum and 30000 ohm-cm maximum. The return electrode was a conventional single hydrogel electrode of size 50x50 mm.

4.1.2 Wrist torque measuring set-up

Measuring the hand dynamics or kinematics could be done in several ways, but we decided to go for a dynamic approach by measuring wrist torque because our main focus was not movements but discomfort, and because isometric wrist-torque measurements permits comparing performance between methods and among individuals easier than with other approaches.

For these experiments a custom wrist torque measuring set-up was designed and built. The set up was based on a JR3 force sensor 45E15A-I63-AF, with a load rating of 1000 N and 6 Degrees Of Freedom (DOF), which provided force and torque measurements on three axes (X,Y,Z). The X and Y axes were in the plane of the sensor body, and the Z axis perpendicular to the X and Y

axes. The reference point for all load data was the geometric center of the sensor. The analog outputs produced by the force sensor were collected by a National Instrument NI-USB 6218 Data Acquisition Card and connected via Universal Serial Bus (USB) to the computer. Our solution consisted of an aluminum structure where the force sensor was integrated as shown in Figure 4.2. The force sensor was screw-mounted between two aluminum plates that were supported at a certain height from the base. The aluminum plate on the front had holes distributed along a circumference of 10 cm radius, with a separation of 10 ° between each hole from $-50°$ to $90°$. The aim of these holes was to hold a bar that fixed the position where the isometric torque measurement was carried out. On top of this bar, located in any of the holes of the aluminum plate, a plastic plate was supported, where the hand rested. The torque measured in Z edge was directly the torque generated on the wrist on an isometric contraction in a determined position. In order to achieve a proper alignment with the Z axis of the sensor, the components of the structure that supported the forearm and hand could be adapted to different hand and arm sizes.

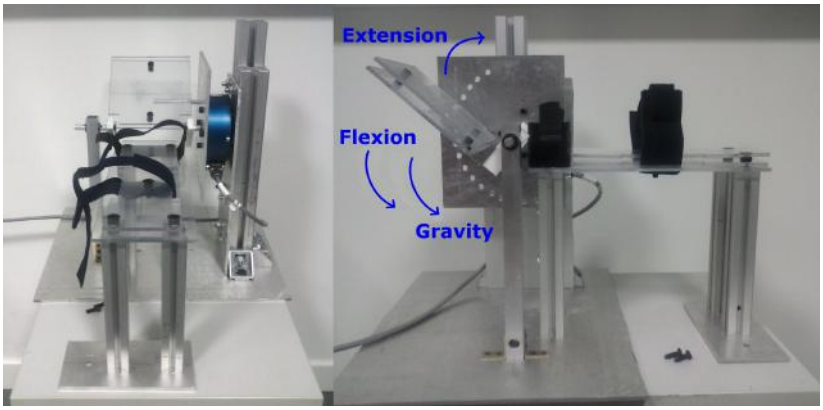

Figure 4.2: Frontal and lateral views of the custom-built wrist torque measuring set-up. Arrows indicate the direction of the corresponding torques.

The hand was placed facing down fixed to the plastic plates with velcro straps, so this way torque in both directions could be measured. If the force was applied to the bar that was located underneath the plastic plate, then the measured torque corresponded to the sum of both torque generated by gravity forces and torque generated in the wrist by flexor muscles (torques in same direction). On the contrary, if the force was applied to the bar that was located on top of the plate, then the measured torque represented the sum of both the torque generated on the wrist by muscle extensors and torque generated by

gravity forces (torques in opposite direction). The direction of the mentioned torques are illustrated in Figure 4.2.

To validate the whole set-up, error estimation and gage repeatability and reproducibility (Gage R&R) study were carried out [60]. Torques produced around the Z axis by a 256 gr. weight located on the plastic plate were measured for the full range (-50° to 90°) several times. Then, obtained measurements were compared to theoretical torque at each position as shown in Figure 4.3. The maximum Mean Square Error (MSE) value found was of 0.0001 N m and corresponded to the -20 $^\circ$ position.

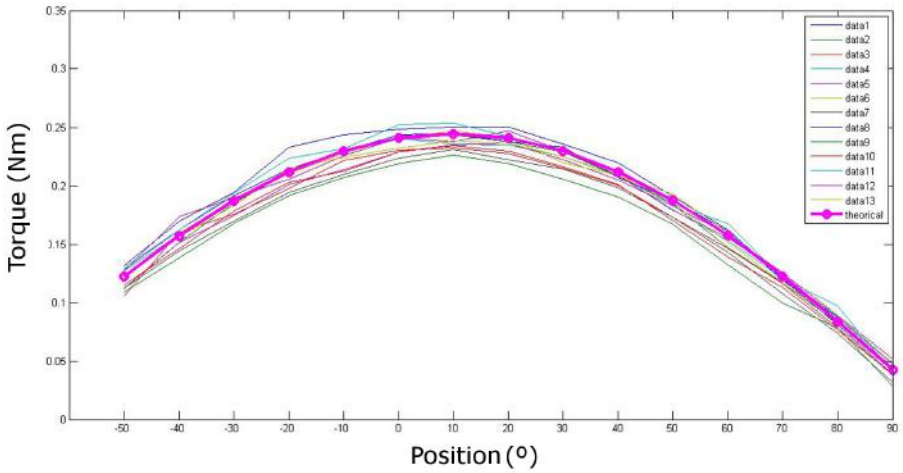

Figure 4.3: Error of torque-measuring set-up. Pink line represents theoretical torques generated by a 256 gr. weight at different positions and rest of lines represent measurement values.

Afterwards, the Gage R&R analysis was applied to the data with Minitab statistical software. Results shown in Figure 4.4 proved that the set-up was able to differentiate slight torque differences caused by position changes. First graph shows that the variability in measurements across different positions was much bigger (98,97%) than variability caused by repeatability issues (14,34%). Second graph shows that deviations in all positions were within the control limits and the average standard deviation for all data was 0.0087 N m. The third graph shows all the measurements with data distributed in boxplots for different positions and mean values for each position. Finally, the fourth graph presents measurements and control limits, where it is shown that variations between means in different positions are higher than tolerance limits. Summing up, the results showed that the precision and repeatability of the wrist torque-sensor set up was appropriate to carry out the following experiments.

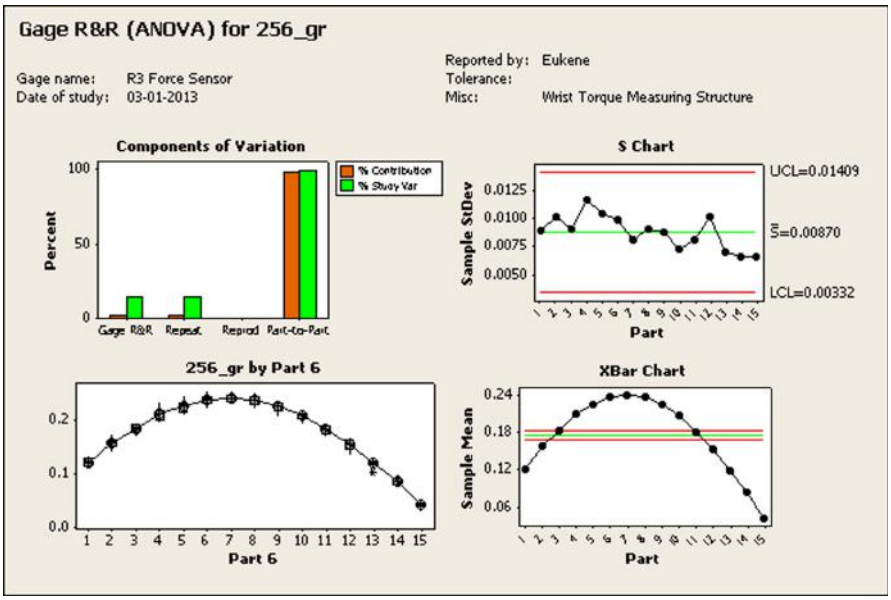

Figure 4.4: Gage R&R results.

4.2 Methods

In these experiments, discomfort caused by two different stimulation methods applied with multi-field electrodes on 15 healthy subjects was compared and analyzed. The experiments were carried out in TECNALIA and all the participants signed an informed consent.

4.2.1 Stimulation methods

Two stimulation methods were compared: synchronous stimulation and asynchronous stimulation.

Synchronous stimulation consists of the simultaneous activation of fields as shown in Figure 4.5. The current is distributed among all the activated fields at the same time, hence, the activated fields act like a big single electrode covering the area of the active fields [61].

Asynchronous activation method activates different electrode fields one right after the other as shown in Figure 4.6. Some research suggest that superposition principle is applicable to asynchronous stimulation as far as time between pulses of different fields is small enough [32]. This means that asynchronous activation of multiple fields would produce a movement equal to the sum of the movements produced by each single field.

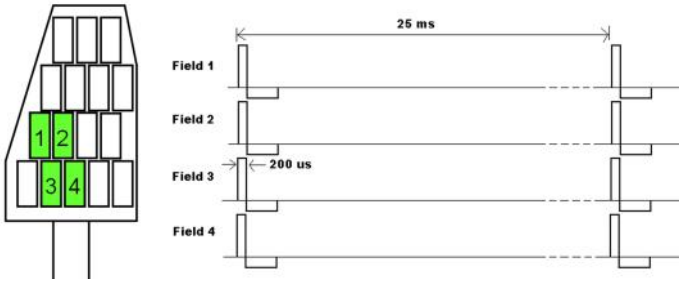

Figure 4.5: Synchronous stimulation.

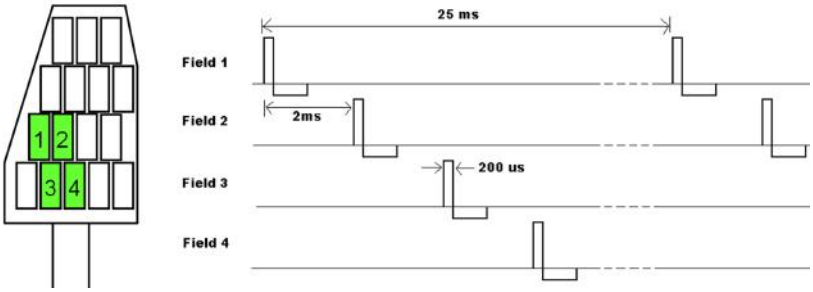

Figure 4.6: Asynchronous stimulation.

In both cases, charge-balanced biphasic stimulation was used, with the frequency fixed at 40 Hz and the pulse-width fixed at 200 µs.

4.2.2 Experiment design

The aim of the experiments was to see if any difference in sensation could be perceived between asynchronous and synchronous stimulation when applied to a population of 15 healthy subjects. However, because the objective of FES is to produce functional movements, a balance between discomfort and performance should be found. It would be useless to find a stimulation method that does not cause discomfort if it does not produce any torque. Therefore, although the main objective was to compare discomfort, we decided to measure isometric torque (torque generated at constant muscle length or no movement) generated by wrist extensors as well as to see if there were evident differences in performance between both methods. Isometric torque was measured when a target bar located at 45 ° of extension was achieved. Like this, the wrist was forced to make a little excursion (from 0° to 45°) before starting the isometric contraction. At this position we could measure isometric wrist torque with less gravitational influence, but also visually detect evident differences during the

short wrist extension excursion. An example of the hand at rest (0°) and the hand producing isometric forces at the target position (45°) is shown in Figure 4.7.

Figure 4.7: Experiment set-up target position. Hand at rest and hand reaching the target position.

Regarding discomfort, a simplified version of the Transcutaneous Electrical Stimulation Comfort Questionnaire [16] rating method was designed. It consisted in two descriptors, which were deep and superficial discomfort. These could be rated in a scale from 1 to 5, where 1 meant no discomfort and 5 meant pain.

Finally, we thought that the number of active fields or the location of these could also affect discomfort, since current density and activation regions of the skin change. Therefore, we decided to test the effect on discomfort of 4 different cases: two neighbor fields activated, three neighbor fields activated, two distant fields activated and three distant fields activated. Distant fields were defined as fields which had at least one other field between them, as it is shown in Figure 4.8. Thus, four cases were tested with each of the two stimulation methods. These cases were randomly ordered for each subject so fatigue or getting used to the FES feeling would not affect the results.

4.2.3 Adaptation sessions

During two days before the experiments, adaptation sessions were carried out with each subject. These sessions consisted in two sessions of 20 minutes of interrupted stimulation where amplitude was increased gradually. The aim of the adaptation sessions was to get subjects familiarized with sensations produced by FES before the main session was performed.

4.2.4 Main session

After the adaptation sessions a main session was carried out. This lasted about 1h and 30 minutes including donning, calibration, tests and doffing. All the

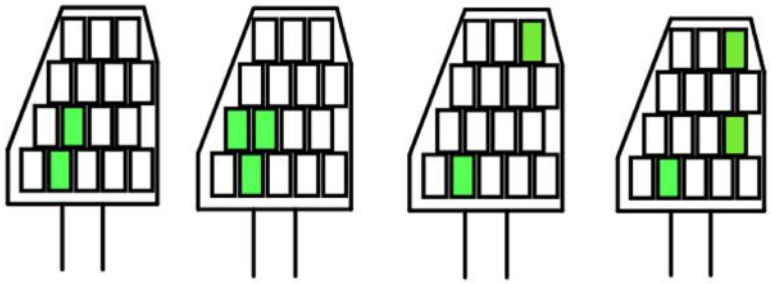

Figure 4.8: Example of neighbor and distant cases. From left to right: 2 neighbor fields, 3 neighbor fields, 2 distant fields and 3 distant fields.

tests were carried out with a biphasic compensated pulse at 40 Hz frequency and 200 µs pulse width.

First stage was donning, which consisted on putting the multi-field electrode covering the extensor muscles of the forearm, the return electrode on the wrist, correctly sitting the subject on the chair and aligning the wrist with the force sensor as shown in Figure 4.9. In addition, elastic bands were wrapped around the forearm to ensure good skin-electrode contact. Subjects were asked to remain seated and to leave their arm relaxed throughout the experiment.

Figure 4.9: Discomfort analysis experiment set-up.

Once donning was done, a manual calibration stage was carried out. The aim of this stage was to define the reference amplitude and optimum fields for each of the four cases described previously. For this, the amplitude was

increased gradually until the target of 45 ° wrist extension was achieved with a single field (randomly selected from the bottom row of the electrode, located proximally on the forearm). After the target was reached, each of the 16 fields was activated with this amplitude. Then four possible configurations for the four cases were defined, selecting those fields that reached the target producing higher torque. Finally, the reference amplitude was defined as the amplitude with which the subject reached the target when activating independently each of the selected fields. Sometimes the initial amplitude had to be increased to reach the target with each of the selected fields for the four cases.

Once the reference amplitude and the fields for the four cases were selected, the tests were carried out. In this stage, comparison between methods was performed and the following sequence was followed for each of the four cases. First of all, the selected fields were separately activated with the reference amplitude defined in the calibration stage. The reference torque was then defined as the maximum torque reached by any of the separately activated fields. The reference torque was used as a target torque and for normalizing the torque of each subject and each case. Once the reference torque was obtained, previously selected fields were activated with one of the methods in random order. Initially low amplitude was used, 6 mA lower than the reference amplitude, and it was increased 1 mA at a time. Each of the stimulation periods consisted of a starting ramp of 500 ms, 6 s of stimulation and a descending ramp of 500 ms, followed by 7 s of rest before next stimulation period started. When 45° extension was reached and reference torque was reached or exceeded, the stimulation was stopped. At this point, the subjects were asked to rate their discomfort. If any subject felt high discomfort or pain and did not want to go higher in amplitude before the target was reached we considered it an unsuccessful test, but the subject was equally asked to rate his feeling. These last steps (starting at 6 mA) were repeated with the remaining method and then the whole sequence was repeated with each of the four cases.

When all the tests were finished we proceeded to loosen the straps and remove the electrodes from the subject's forearm.

4.3 Results

4.3.1 Success rates

We considered that a test was successful if the 45° extension was achieved and the reference torque was exceeded. If the subject felt pain or a very uncomfortable feeling and decided to stop increasing amplitude before he reached the target, we considered it an unsuccessful test. In Figure 4.10 we can see the amount of people that achieved a success with each method and for each case.

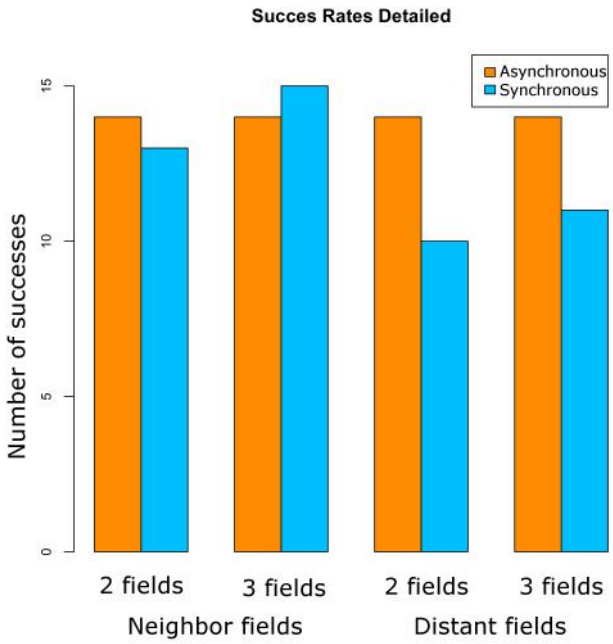

Figure 4.10: Success rates for different cases.

14 subjects reached the goal with asynchronous method independent of the case, whereas synchronous method showed differences depending on the case, resulting worse in distant field cases, where the amount of subjects that achieved a success was smaller. 5 subjects with two distant fields and 4 subjects with three distant fields did not achieve the target when fields were synchronously activated. It is important to point out that the subjects that failed to succeed with synchronous stimulation described high discomfort or pain at the wrist, where the return electrode was located. It also has to be mentioned that one of the 15 subjects turned out to be very sensitive to electrical stimulation and only reached the target in one case, which was synchronous activation of three neighbor fields.

4.3.2 Discomfort

As mentioned before, discomfort was separated into two descriptors: superficial and deep discomfort. Each of them was rated from 1 to 5 either when the subject reached the target or when the subject wanted to stop increasing amplitude due to a very uncomfortable feeling. Figure 4.11 shows medians and interquartiles for each method, each case and each descriptor. Differences in the median

values are seen for asynchronous and synchronous methods, especially in superficial discomfort ratings for neighbor field cases and deep discomfort ratings for distant field cases. However, the variability in the discomfort ratings was considerably high due to the large inter-subject variability in sensitivity to electrical stimulation.

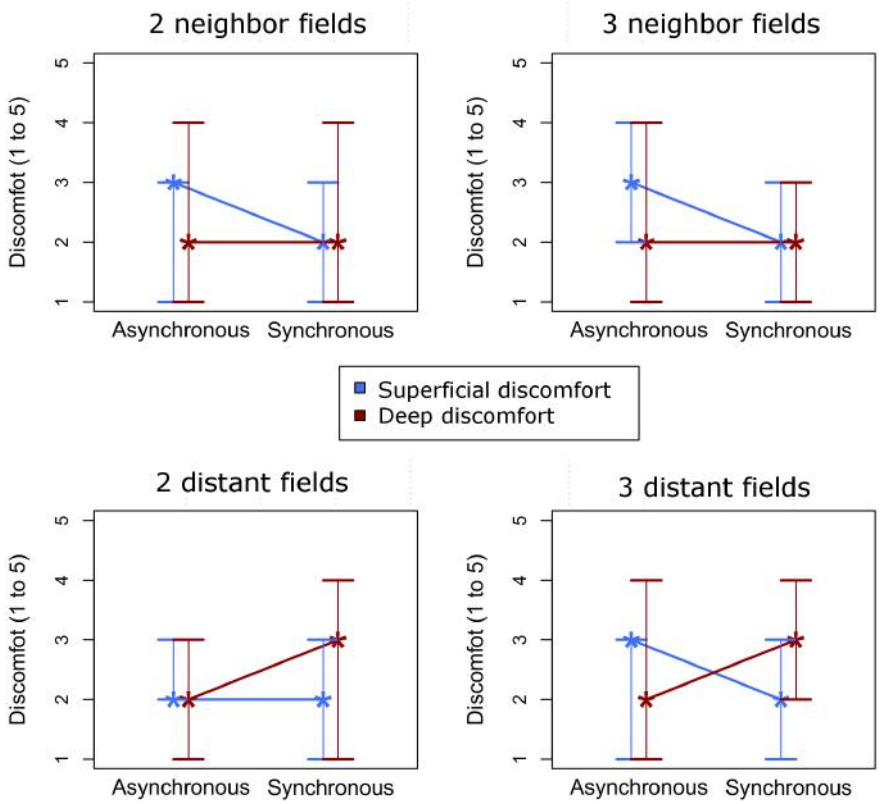

Figure 4.11: Discomfort median and interquartiles.

Aditionally, paired Wilcoxon statistical tests were carried out. First, each of the four cases was separately analyzed but no significant differences were found due to the small size of the samples. Thus, these four cases were grouped into two cases, which were neighbor field and distant field cases. Deep and superficial discomfort rating differences were again analyzed by Wilcoxon paired tests. Results, summarized in Table 4.1, only showed significant difference between synchronous and asynchronous methods for deep discomfort descriptor and for the distant field cases. No significant differences were found in superficial discomfort or in deep discomfort in neighbor field cases between asynchronous and synchronous methods.

Table 4.1: Wilcoxon paired test results

	Neighbor fields	Distant fields
Superficial discomfort	p=0.1677	p=0.1155
Deep discomfort	p=0.4644	p=0.0156*

* Significant differences (p<0.05) between synchronous and asynchronous methods were found in this case

4.4 Discussion

The results showed that synchronous stimulation produced significantly higher deep discomfort than asynchronous stimulation when distant fields were activated with the proposed multi-field electrode configuration. Indeed, subjects pointed out that they felt deep discomfort around the wrist, where the return electrode was located. This discomfort caused by synchronous stimulation limited its effectiveness in distant fields cases, as 5 people with two and 4 people with three activated fields failed to succeed reaching the target due to pain or big discomfort. This effect could be caused by higher current densities present on the return electrode with synchronous stimulation than with asynchronous stimulation, which could result in the activation of a larger amount of afferent fibers corresponding to deep cutaneous receptors. However, this effect was not a problem in neighbor field cases, since lower amplitudes were needed in general to achieve the target and therefore the current density was smaller. This last fact supports the suggested hypothesis that stated that synchronously activated neighbor fields might act like a bigger electrode.

Regarding activation of neighboring fields, no significant differences were found between both methods in terms of discomfort. In fact, asynchronous stimulation showed stable discomfort rates and successful attempts for all the cases. Thus, considering that a stimulation method should give the possibility of successfully using the widest variety of field activation patterns as possible, asynchronous stimulation has shown to be the best option between both methods in terms of discomfort. Taking into account the presented results, and the previously reported benefits on fatigue and selectivity of asynchronous stimulation [29, 30], we conclude that it is the best method tested so far with multi-field electrodes. Therefore, for the rest of the experiments presented in this work, asynchronous stimulation has been used.

The most significant results of the work described in this chapter were presented in the 18th Annual Conference of the International Functional Electrical Stimulation Society [62].

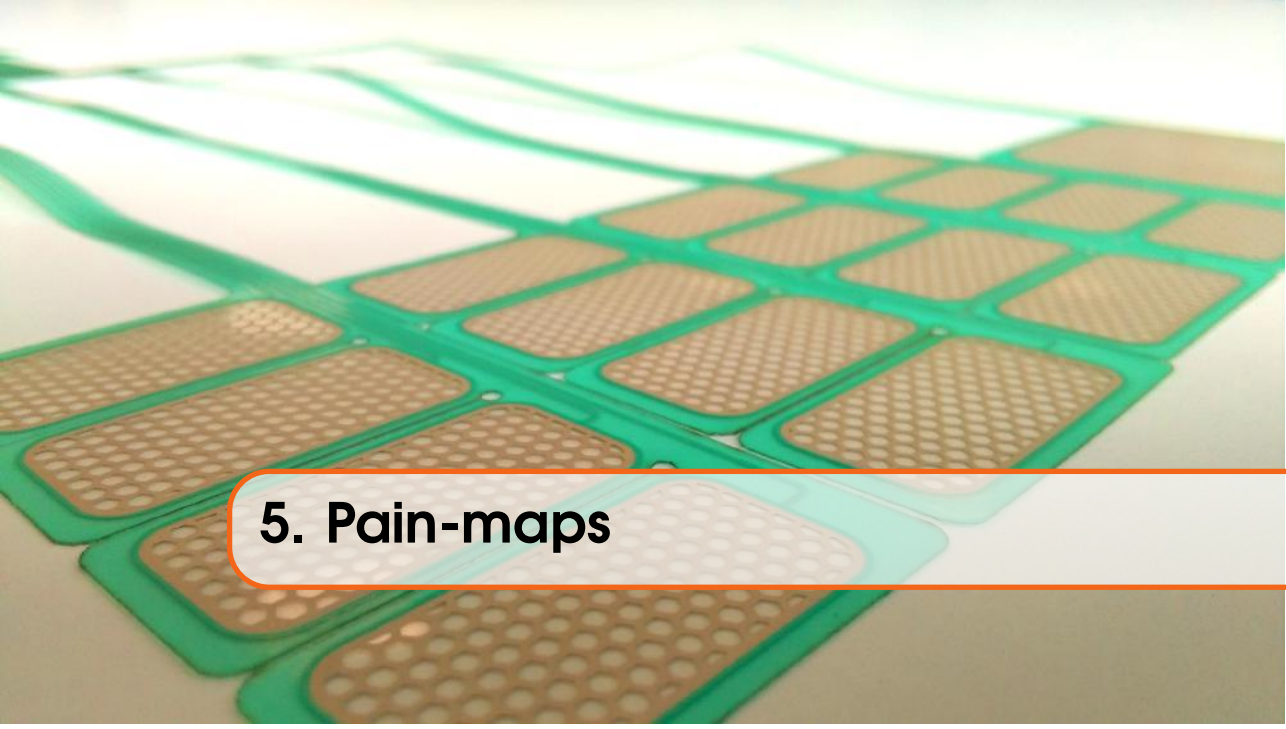

5. Pain-maps

Tactile sensitivity of the upper limb has been intensively studied, determining the tactile spatial acuity of different sites of the arm and the effect of different factors influencing it [63, 64, 65, 66]. Sensitivity to electrotactile stimulus has also been studied, showing the effect of different stimulation parameters and stimulation sites of the body [67, 68]. However, there is a lack of studies focused on spatial distribution of pain or discomfort caused by transcutaneous FES on the arm, which is essential for designing more comfortable neuroprostheses for this part of the body. Therefore, this study aimed at creating pilot pain-maps, defined as graphical representations of pain ratings of different sites of the arm. These could point out painful spots on the arm that should be avoided or less painful spots that should be preferred for applying FES, which could be used as a reference for the design of more comfortable neuroprostheses.

5.1 Materials

The FES device that we used in these experiments was the IntFESV2 device shown in Figure 5.1, a second version of the IntFES stimulator described in the previous chapter [58]. As the previous version, it was a single channel electronic stimulator that provided current-regulated biphasic stimulation. Similarly, the output ranges went from 0 mA to 50 mA for the amplitude, from 1 Hz to 400 Hz for the frequency, and from 50 µs to 1000 µs for the pulse-width. This new version was provided with an embedded touchscreen that permitted

controlling all the stimulation parameters locally. Additionally, it could be remotely controlled via Bluetooth and CAN communication.

Figure 5.1: IntFESV2 stimulator.

The IntFESV2 stimulator was designed to control up to four 16-field IntFES electrodes (64 fields in total), and not only amplitude, but pulse-width of each field could also be controlled independently on this new version. For these experiments a regular matrix, shown in Figure 5.2, was designed to be used in four areas on the upper limb: anterior forearm, posterior forearm, anterior upper-arm and posterior upper-arm. The multi-field electrode size and configuration were designed in order to: a) be flexible to adapt to different arm sizes and shapes and b) cover the maximum area to obtain complete pain maps. A common return electrode of size 50x50mm was used, and the size of each field was 30x15mm.

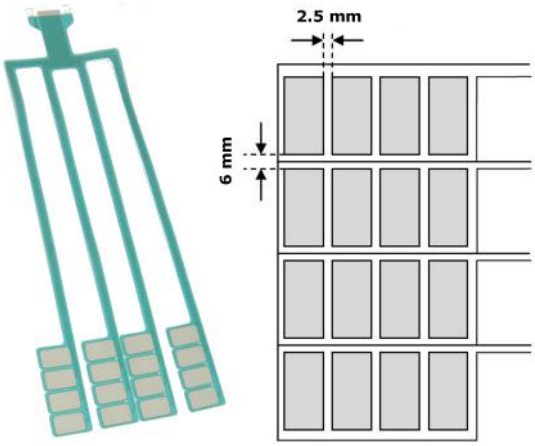

Figure 5.2: IntFES multi-field electrode matrix.

5.2 Methods

The objective of this study was to check if there was a common pattern within subjects regarding discomfort in different areas of the upper limb. Subjects suffering from neural disorders such as stroke usually suffer from sensory deficits and their discomfort or pain thresholds are different to healthy subjects [39]. Therefore, the experiments were carried out with stroke subjects. The study was carried out in collaboration with LAMBECOM lab at Universidad Rey Juan Carlos. The protocol was approved by the ethical committee of Universidad Rey Juan Carlos and all the participants signed an informed consent.

5.2.1 Subjects

12 chronic stroke patients were recruited for these experiments. However, before starting the program one of them had to leave because of health issues unrelated to this study, so in the end the experiments were carried out with 11 chronic stroke patients. The subject group included 10 males and one female, whose mean age was 62.73 +/-6.78 years. Time from injury was over one year for all of them and none of them suffered from aphasia, so they had the cognitive ability to understand, follow and participate in the study without any difficulties. They were evaluated with the upper extremity Fugl-Meyer assessment [69, 70] before starting the study. Fugl-Meyer overall scores were 65.82 +/-17.98 (out of 126) and scores corresponding to the sensation section were 8.64 +/-3.32 (out of 12).

5.2.2 Experiment design

Unlike other sensitivity studies [63, 64, 66], we wanted to build discomfort maps useful for transcutaneous neuroprostheses design. Therefore, it was important to build these discomfort maps based somehow on the motor response to the application of electrical stimulation. For this reason, the procedure was designed to obtain pain ratings related to the motor threshold (MT), which is the minimum amplitude where a motor response is perceived. As it was previously explained, higher amplitudes lead to an increased current density and the recruitment of a bigger amount of efferent and afferent nerve fibers, usually resulting in higher discomfort. Thus, rating pain at MT values would result in pain maps that pointed out painful spots that could be due to a high amount of superficial afferent nerve fibers or due to a high MT value. On the contrary, less painful spots could be the result of less amount of superficial afferent nerves or lower MT values. In any case, the resulting pain maps would show spots that should be avoided or preferred in FES applications.

5.2.3 Adaptation sessions

The aim of these sessions was to make the subjects familiar to the feeling of transcutaneous electrical stimulation before carrying out the main session. Standard commercial neuromuscular stimulators (Cefar Rehab X2) were delivered to patients and they were instructed to run the program twice a day in the four areas (posterior/anterior forearm, posterior/anterior upper-arm) during the week before the main session. Patients only needed to place the standard single electrodes on top of the four different areas, adjust the amplitudes and run the predefined program of 30 minutes of duration described next:

- Phase 1: frequency 8 Hz, pulse-width 200 µs, initial ramp 0.5 s, low amplitude (above sensory threshold but below motor threshold), 7.5 s stimulation and 7.5 s rest periods. (5 minutes)

- Phase 2: frequency 50 Hz, pulse-width 200 µs, initial ramp 0.5 s, high amplitude (as high as tolerated), 7.5 s stimulation and 7.5 s rest periods. (20 minutes)

- Phase 3: frequency 3 Hz, pulse-width 200 µs, initial ramp 0.5 s, low amplitude (above sensory threshold but below motor threshold), 7.5 s stimulation and 7.5 s rest periods. (5 minutes)

5.2.4 Main session

This session was held in the LAMBECOM lab. Parameters during the whole session were set to 25 Hz frequency and 200 µs pulse-width. The whole session took around 90 minutes.

First of all, the subject was seated in a comfortable chair resting his forearm on top of a table. Then, the matrix multi-field electrodes and the return electrodes were placed over the four different areas of his affected arm, which were posterior forearm, anterior forearm, posterior upper-arm and anterior upper-arm, with medial and lateral epycondiles taken as a reference as shown in Figure 5.3. Next, the following procedure was carried out for each of the 16 fields on each arm area:

- Randomly select a field and set it with 0 mA.

- Increase amplitude in steps of 1 mA until visually perceiving a weak contraction (MT).

- If no contraction was obtained at 25 mA or the subject could not tolerate an amplitude of two times MT, next steps were skipped.

- Apply an amplitude of double MT and stimulate during 5 s.

- Ask the subject to rate the felt pain on a visual analog scale (VAS) [71, 72].

- Note down the MT amplitude and the rated pain for the selected field.

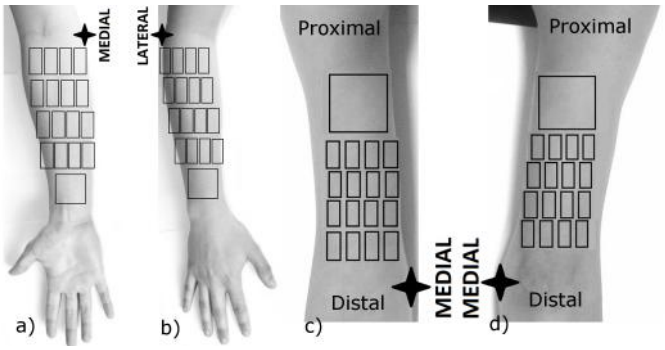

Figure 5.3: Matrix multi-field position. a) anterior forearm, b) posterior forearm, c) anterior upper-arm and d) posterior upper-arm.

5.3 Results

5.3.1 Individual pain-maps

After collecting all pain ratings, data of each patient and each of the four stimulation areas were normalized. To enable comparing and visualizing pain ratings of patients with left and right affected sides, data from patients with left arm affected was mirrored, so all the graphs shown in this section represent data for the right arm. Individual pain ratings of the 11 patients are shown in Figures 5.4, 5.5, 5.6 and 5.7, where each graph represents the area covered by the multi-field electrodes as shown in Figure 5.3. The color of each square represents the pain rating corresponding to the field on that position. Darker colors (red) represent fields that got higher pain ratings, and accordingly, lighter colors (white-yellow) represent less painful fields. As explained in the previous section, if no MT was achieved for a specific field or its amplitude value was considered too high to double it and be tolerated by the patient, then the amplitude was not doubled and pain rating was not collected. In order to remark this fact, the pain rating was assumed to be as high as the highest value given by the patient in any field of that area. If one patient presented more than 4 cases like this in a certain area of the arm, the whole dataset for that patient in this area was discarded.

5.3.2 Average pain-maps

After analyzing individual data, averages were obtained for each of the fields of the four areas. These are shown in Figures 5.8, 5.9, 5.10 and 5.11 where each graph represents the area covered by the multi-field electrodes. As before, darker colours (red) represent fields that got higher pain ratings, and accordingly, lighter colours (white-yellow) represent less painful fields.

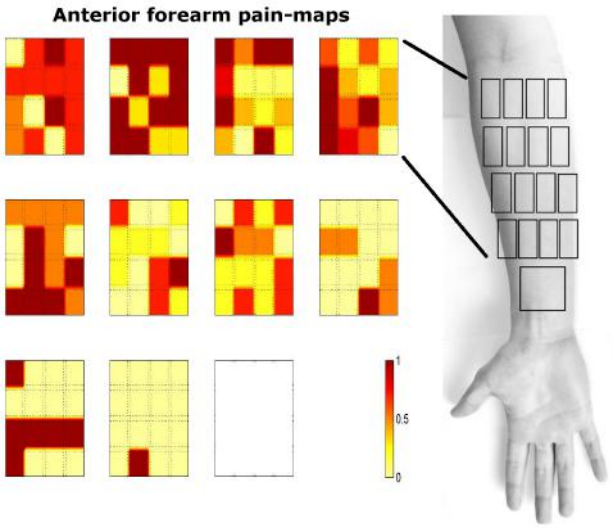

Figure 5.4: Normalized pain ratings of 11 patients for the anterior forearm. Each square represents one field of the multi-field electrode when placed as shown in Figure 5.3 a). The empty graph corresponds to a subject where MT amplitude was not doubled for discomfort reasons in more than 4 fields.

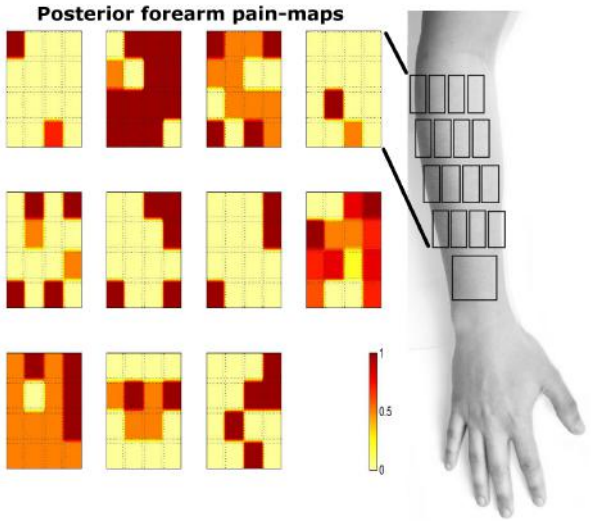

Figure 5.5: Normalized pain ratings of 11 patients for the posterior forearm. Each square represents one field of the multi-field electrode when placed as shown in Figure 5.3 b).

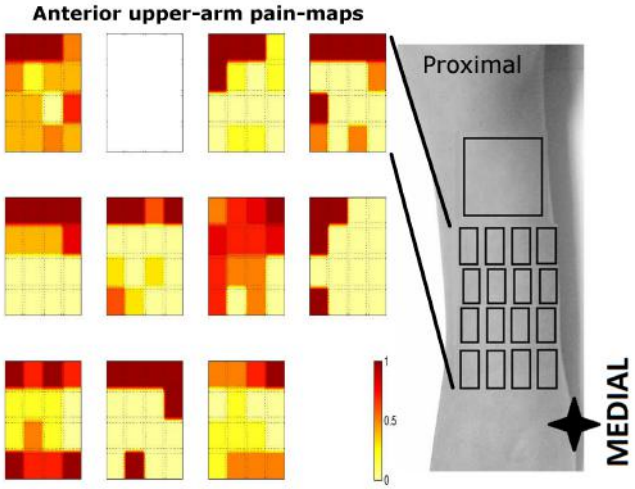

Figure 5.6: Normalized pain ratings of 11 patients for the anterior upper-arm. Each square represents one field of the multi-field electrode when placed as shown in Figure 5.3 c). The empty graph corresponds to a subject where MT amplitude was not doubled for discomfort reasons in more than 4 fields.

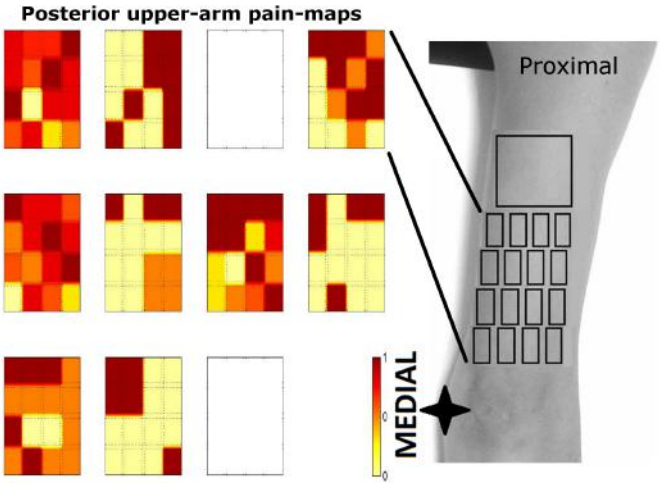

Figure 5.7: Normalized pain ratings of 11 patients for the posterior upper-arm. Each square represents one field of the multi-field electrode when placed as shown in Figure 5.3 d). The empty graphs corresponds to subjects where MT amplitude was not doubled for discomfort reasons in more than 4 fields.

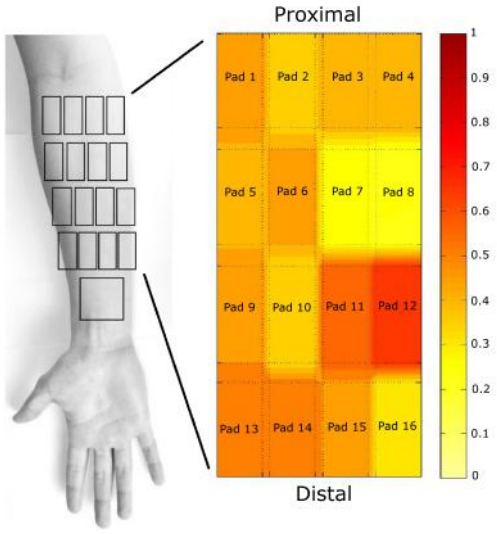

Figure 5.8: Average normalized pain ratings of 11 subjects for anterior forearm. Each square represents one field of the multi-field electrode when placed as shown on the left.

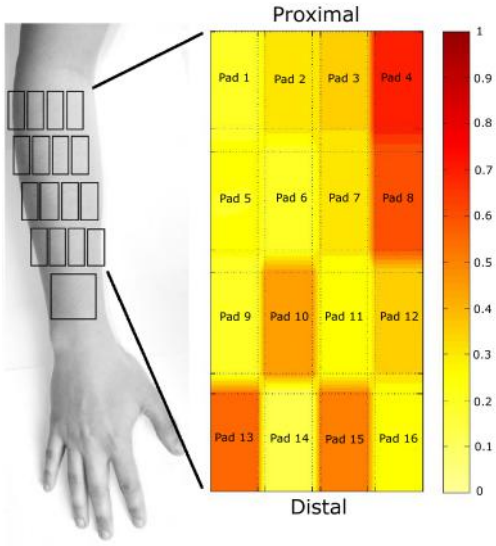

Figure 5.9: Average normalized pain ratings of 11 subjects for posterior forearm. Each square represents one field of the multi-field electrode when placed as shown on the left.

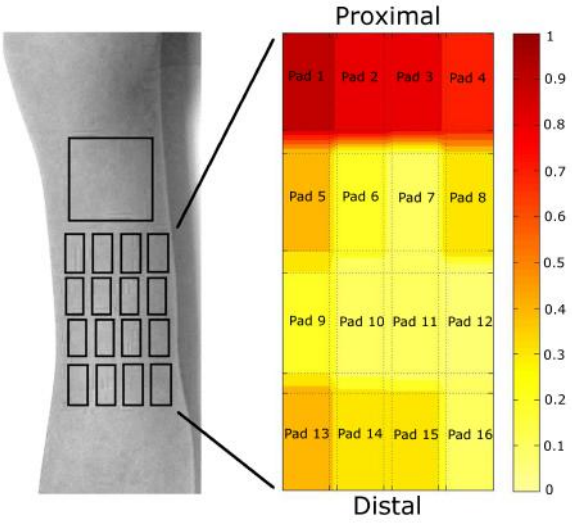

Figure 5.10: Average normalized pain ratings of 11 subjects for anterior upper-arm. Each square represents one field of the multi-field electrode when placed as shown on the left.

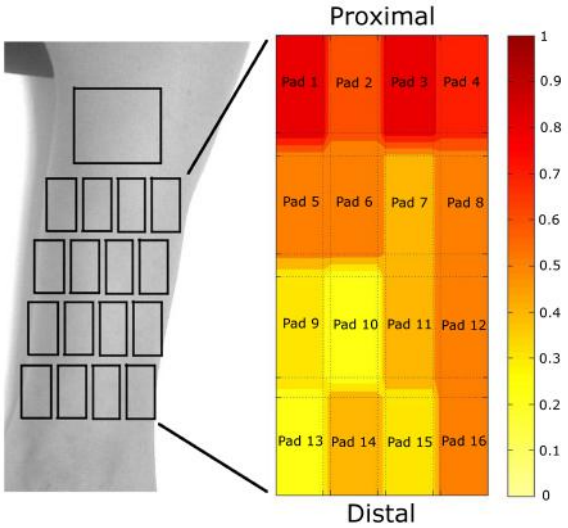

Figure 5.11: Average normalized pain ratings of 11 subjects for posterior upper-arm. Each square represents one field of the multi-field electrode when placed as shown on the left.

5.3.3 Field differences

Differences on pain ratings of different fields could be appreciated in the average pain-maps. However, individual pain-maps showed a great inter-subject variance regarding pain ratings of different fields. Hence, to check if the differences between fields of the average pain-maps were significant or they were just obtained by chance as a result of the big variance between subjects, a statistical analysis was carried out. In this study, first a non parametric Friedman test for repeated measurements [73] was carried out for each of the four areas, to check if there were significant differences between, at least, two fields. If the result showed positive results with a significance level of $\alpha = 0.01$, then a Wilcoxon-Nemenyi-McDonald-Thompson post-hoc analysis [73] was made to examine which fields were significantly different. Table 5.1 shows the results to Friedman test, where significant differences between fields were found in upper-arm areas.

Table 5.1: Friedman test results

Arm area	**p-value**
Anterior forearm	0.4218
Posterior forearm	0.01236
Anterior upper-arm	1.29×10^{-9}*
Posterior upper-arm	0.0090*

* Significant differences between fields were found at $\alpha = 0.01$

Wilcoxon-Nemenyi-McDonald-Thompson post-hoc analysis were carried out for anterior and posterior upper-arm areas. Figure 5.12 and 5.13 show the post-hoc results in forms of bars of anterior and posterior upper-arm respectively. Each bar represents the average pain rating for one field, and these are ordered from most painful to least painful fields. Colors and letters represent different groups, where there are significant differences between groups that do not share the same letter. In Figures 5.14 and 5.15 the post-hoc results are marked in the pain-maps of the anterior and posterior upper-arm respectively, highlighting the significantly different groups. Red color is used for the identification of most painful fields and green color for the least painful fields.

5.4 Discussion

First aspect that could be remarked was the high inter-patient variability of pain ratings obtained in the experiments. This fact could be the result of, on one hand, the inherent subjectivity of pain [72], and on the other hand, the high

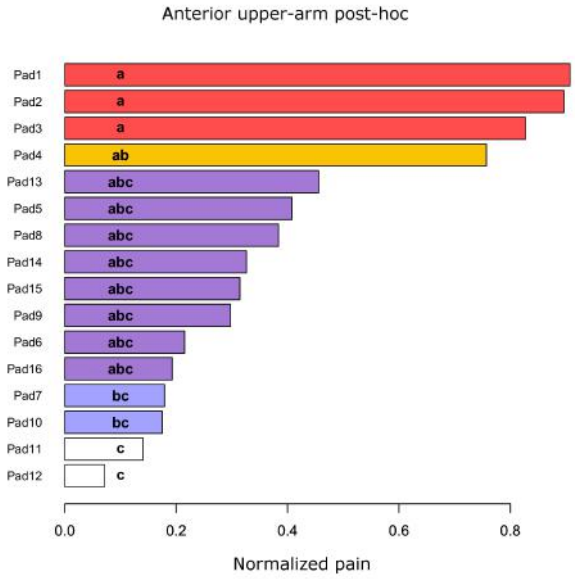

Figure 5.12: Post-hoc results of pain ratings of fields on anterior upper-arm.

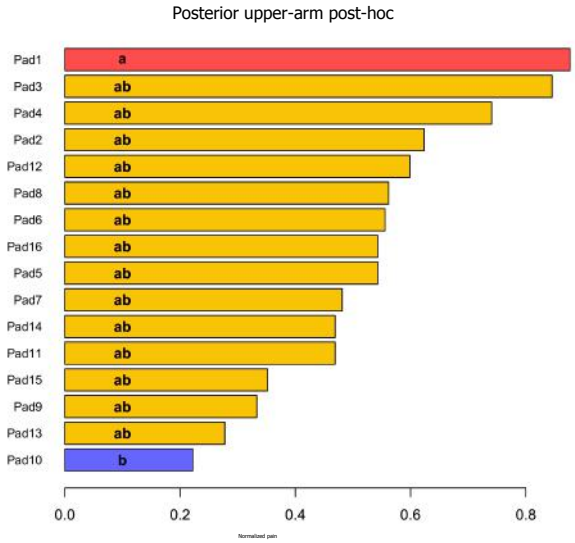

Figure 5.13: Post-hoc results of pain ratings of fields on posterior upper-arm

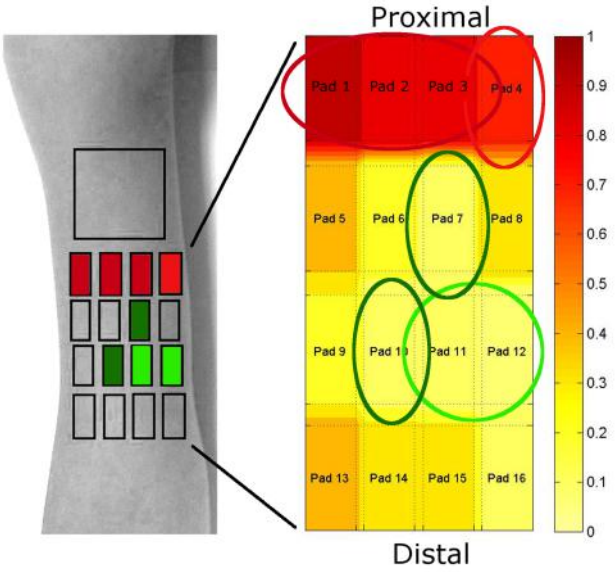

Figure 5.14: Significantly different fields of anterior upper-arm. Being red most painful and green least painful fields.

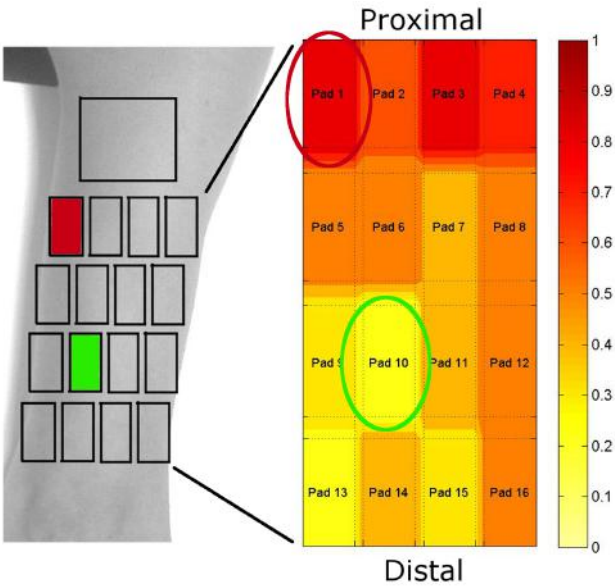

Figure 5.15: Significantly different fields of posterior upper-arm. Being red most painful and green least painful fields.

variability among stroke patient pathologies, where sensitivity is affected at different levels in different patients [39]. Another aspect that could be perceived at first sight was that average pain ratings of the forearm areas showed bigger homogeneity between fields than upper-arm areas, where pain rating differences between fields could be easily perceived. Finally, the statistical analysis carried out at $\alpha = 0.01$, revealed that there were no significant differences on pain ratings between fields for forearm areas, but that there were differences on pain ratings between fields on upper-arm areas. This dissimilarity between forearm and upper-arm areas could come from the physiological differences between muscles that belong to lower and upper areas of the arm. Whereas forearm muscles are smaller, bigger muscles like biceps and triceps require higher amplitudes to generate a contraction, which can lead to discomfort. Regarding the post-hoc analysis on biceps and triceps, it was confirmed that the most painful fields were those located most proximally, close to the return electrode, and the least painful fields were located distally, further from the return electrode. This phenomenon could be caused by the current distribution happening with this electrode configuration. As explained in previous chapters, the distance between the active electrode and the return electrode is important. If electrodes are placed too close, most of the current flows through the superficial layers of the skin, where lower impedance layers like fat are located, bypassing the deeper nerves [7, 8]. Hence, one of the reasons for high pain ratings at these fields could be that higher amplitudes were needed to achieve MT when active fields were too close to the return electrode. Higher amplitudes result in higher current densities, which itself increases discomfort [17, 26]. In summary, we could conclude that there were no significantly painful spots along the forearm areas for the application of FES, but there were significant pain differences between some fields on the upper-arm that could be caused by electrode configuration. To reduce produced pain in these areas, it is therefore recommended to select the active fields located more distally on the arm so the current is forced to go deeper in the skin and can elicit muscle contractions with lower amplitudes. Pain maps shown in this chapter do easily illustrate recommended areas for the use of FES on upper limb with the proposed electrode configuration. These experiments should be carried out in a bigger population to draw more relevant conclusions, and in that case they could be used as a guide or basis for future clinical or research applications and design of more comfortable neuroprostheses.

Part of the work described in this chapter was presented in the 19th Annual Conference of the International Functional Electrical Stimulation Society [74].

II Part Two

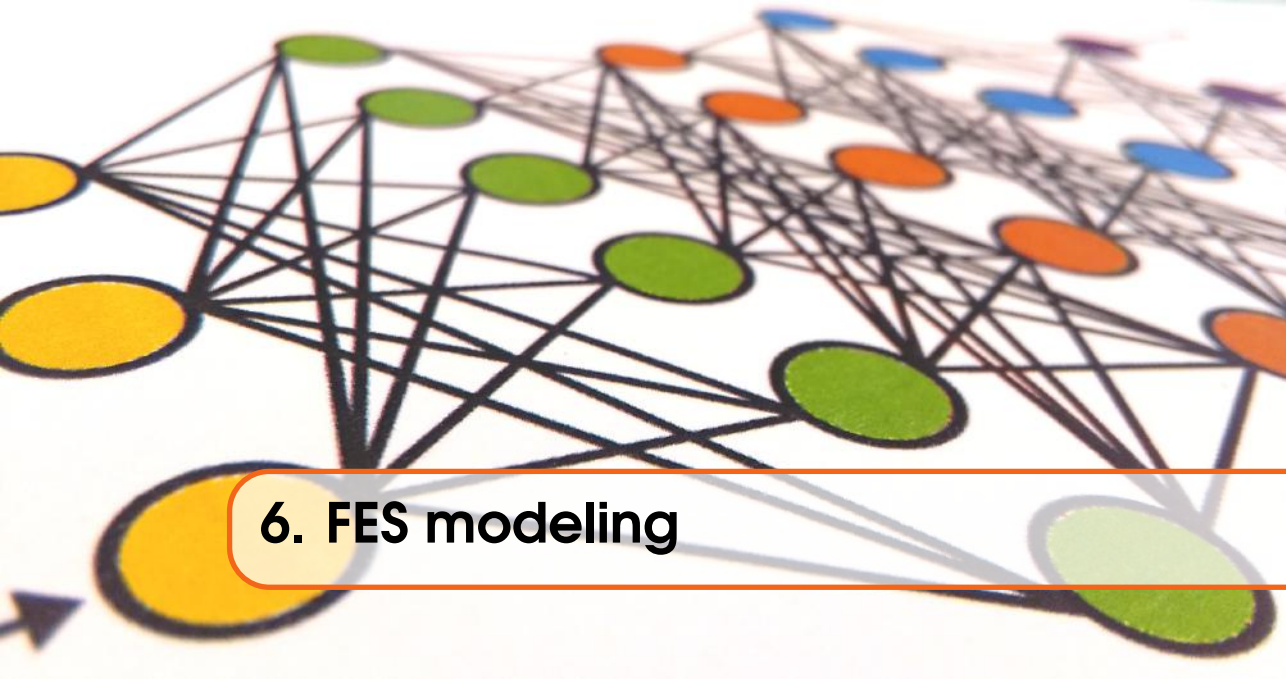

6. FES modeling

Transcutaneous FES systems are complex. They can be divided into smaller subsystems that can be modeled separately and in combinations. Most transcutaneous FES models that relate stimulation parameters with joint dynamics or kinematics are based on the combination of some of the models described below and adaptations of these for particular FES applications.

6.1 Skin and current distribution models

Transcutaneous FES applications aim at exciting target motor nerve fibers with electrodes placed over the skin. Hence, generated currents distribute along the different layers and tissues of the body before reaching the nerve fibers. Proposed skin impedance models and current distribution models provide knowledge on how the electrical fields are spread throughout body tissues.

The skin is inhomogeneus and it is composed by different layers as shown in chapter 2, which results in its non-linear character. Additionally, dynamic changes on skin hydration make it time-variant. However, the skin impedance is broadly resembled with the simple circuit shown in Figure 6.1 that consists on a parallel resistor R_p and capacitor C_p followed by a series resistor R_s [75]. R_s represents the resistance of deep tissues (fat and muscle) and R_p and C_p correspond to the skin impedance [75]. It has been shown that R_s is independent of the stimulation voltage, while there is an inverse relation between R_p and the stimulation voltage [75, 76]. Indeed, most non-linearities of the skin impedance disappear when the most superficial layer of the skin (*stratum corneum*) is

removed, in which case the R_p resistor could be neglected [75, 76]. In order to capture the dynamic properties of the skin impedance, the use of a nonlinear time-dependent resistor R_p has been proposed [77]. However, a later study has shown that the non-linearities of the skin resistivity can be neglected for current regulated FES applications that focus on muscle activation rather than electrode voltage[78].

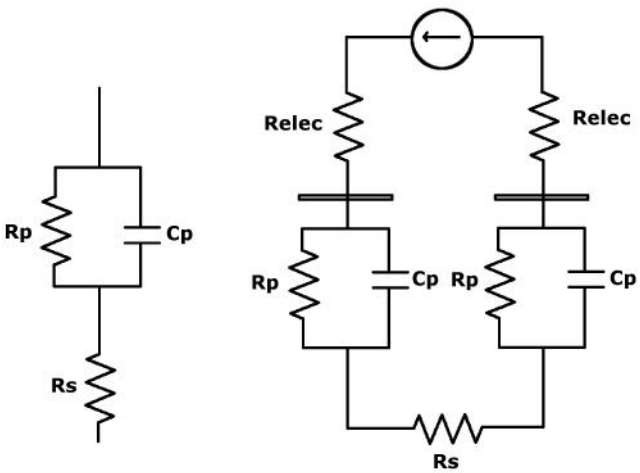

Figure 6.1: The simple skin impedance equivalent circuit is shown on the left and the equivalent circuit model for a current regulated two electrode application is shown on the right, where R_{elec} represents electrode resistance.

Regarding the electrical potential fields, some analytical models have been proposed for calculating intramuscular current distribution on three dimensions caused by application of transcutaneous electrical stimulation, which take into account properties of different tissues (skin, fat, muscle and bone) [79, 80]. Analytical models present low computational cost, but detailed geometries or inhomogeneities are not included [81]. However, a finite difference model and a finite element model have been proposed for calculating the electric field generated in denervated thigh muscles in three dimensions [82, 83]. And another model based on finite elements was proposed for describing the three-dimensional potential field generated by transcutaneous electrical stimulation on the forearm [81]. Although the latter models can describe current distribution in volume conductors with inhomogeneities, main disadvantage relies in their computational cost [84].

6.2 Nerve models

As described in detail in Chapter 2, AP propagate along nerve axons when the membrane potential is depolarized below a threshold value. Nerve models aim at describing the excitation of the nerves and the propagation of AP along their axons. The behavior of a patch of the membrane of a nerve axon can be simulated by an electric circuit as the one shown on the left in Figure 6.2 [85]. In this circuit, the voltage source V_r represents the resting potential, whereas C and R_m are the capacity and resistance of the membrane respectively. Similarly, the propagation of an AP along the axon can be simulated with the extended circuit shown on the right in Figure 6.2, where R_a corresponds to the inneraxonal resistance [85].

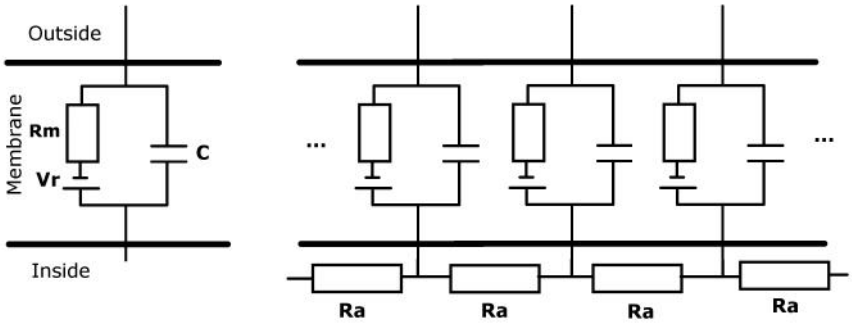

Figure 6.2: Electrical circuit for nerve axon. On the left, a single membrane patch is represented, and on the right, the corresponding electrical network for the axon is shown.

The membrane resistance is non-linear as it is dependent on the voltage-gated ion channels of the membrane. Although the broadly used cable model consists of a constant resistance value, it has been shown that linear models cannot reproduce many properties of axons that are observed in experimental work, so its use should be limited to subthreshold or close to steady state applications [85, 86].

Regarding non-linear models, the most known and broadly used model is the Hodgkin-Huxley model, which is based on experiments with giant unmyelinated squid axons and describe quantitatively the voltage-current relations of a piece of membrane [87]. In contrast to the linear models, membrane resistance is substituted by different conductances which represent the active voltage-gated mechanisms of the cell membrane modeled by means of differential equations [87]. Similarly, the Frankenhaeuser-Huxley model, which was based on experiments with frog nerves, proposed a solution for myelinated nerve axons and used permeabilities instead of conductances for describing sodium, potassium

and leakage currents of the nodes of Ranvier [88]. A mammalian nerve model was also proposed in [85, 89], which was an adaptation of the Hodgkin-Huxley model without taking into account potassium currents. Finally, the MRG model was recently proposed, which incorporated a double cable structure, in order to describe not only membrane currents at the nodes of Ranvier but at internodal sections as well [90].

6.3 Muscle models

Muscle models aim at describing the behavior of muscle contractions at the application of electrical stimulus. The most widely used muscle model is the Hill model [91, 92], which represents the active and passive properties of the musculo-tendinous units by means of three mechanical elements. The structure of the Hill model is shown in Figure 6.3, where the contractile element *CE* models active muscle force; the series elastic element *SE* models tendon and soft tissue stretch; and the parallel elastic element *PE* models passive muscle force [91, 92].

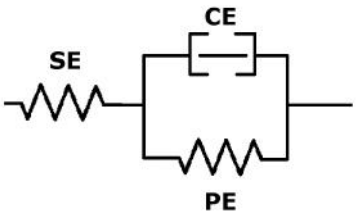

Figure 6.3: Hill muscle model.

Modifications of Hill models and other proposed muscle models have been compared, where a combination of Huxley (based on biophysical cross-bridge mechanisms) and Hill models [93, 94] and a second order system with added static non-linearities [95] have shown best results [96, 97, 98]. However, basic Hill type models are not accurate for predicting muscle forces when the muscle length is variable (non-isometric contractions) [99]. Similarly, the Huxley-Hill model [93, 94] have not been tested yet on non-isometric contractions.

Another popular model for describing the nonlinear muscle activation dynamics is the electrical Hammerstein model, which consists on a static non-linearity followed by a linear subsystem [100, 101] as shown in Figure 6.4. In muscle model applications, the static non-linearity represents the Isometric Recruitment Curve (IRC), which describes the relation between the stimulus level and the output torque at a fixed muscle length. Then, the linear subsystem represents the muscle contraction dynamics. A Wiener-Hammerstein muscle

model has also been proposed and proved to be as accurate as the Hill-Huxley model while being less complex and having less unknown parameters [102].

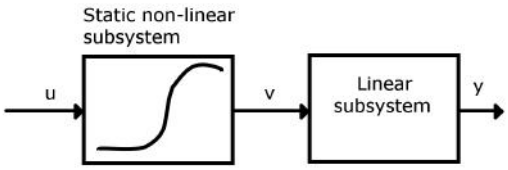

Figure 6.4: Hammerstein model.

6.4 Upper-limb biomechanical models

Although biomechanical models of lower-limb applications are well established (specially for gait), upper-limb biomechanical models are still in early stage due to the complex nature of the upper limb [103]. Main challenges of upper-limb modeling include the variability of non-cyclic task-dependent movements and inter-subject movements, large ranges of motion, high number of DOF, and difficulty of measuring kinematic or dynamic data [103]. However, different approaches have tried to overcome these problems. Some of the simpler proposed biomechanical models for the complete upper-limb consist of three rigid body segments representing upper-arm, forearm and hand, and describe shoulder, elbow and wrist joint kinematics [104, 105]. One of the proposed models, based on visual tracking systems, leads with skin-movement artifacts and describes wrist and elbow angles [104]. Similarly, another kinematic model was developed to obtain joint angles of the trunk, shoulder and elbow using a visual tracking system and validated in stroke patients reaching tasks, proposed for the assessment of stroke rehabilitation [106]. Another approach based on a spatial tracking system includes 7 DOF that describe functional physiological parameters: shoulder abduction-adduction, shoulder flexion-extension, shoulder internal-external rotation, elbow flexion-extension, elbow pronation-supination, wrist flexion-extension and wrist abduction-adduction [105]. Musculoskeletal models are more complex models that aim to describe joint kinematics based on the interaction between muscles and bones. One of the proposed musculoskeletal models for upper-limb includes 13 DOF based on 26 muscle groups for describing relative positions and orientations of 7 bones of the upper-arm (including clavicula and scapula) and forearm [107]. A recent study proposed and compared three different upper-limb models of different complexity for shoulder, elbow and wrist motion, based on the Delft shoulder model[108], and

concluding that best model depends on the simulation task, required accuracy and computational cost [109]. Finally, another model aimed at musculoskeletal surgery applications, including finger and thumb joints in a complete upper-limb model of 15 DOF and 50 muscle compartments, which described shoulder, elbow, forearm, wrist, thumb and index finger kinematics [110].

Although a complete hand has not been included in any upper-limb biomechanical model, hand models have been proposed separately. Kinematic models have been proposed based on visual tracker systems for computer vision applications [111, 112]. However, musculoskeletal models are more challenging due to the anatomical complexity of the hand and wrist, which are composed by a total of 27 bones and 45 muscles, where fingers are controlled by a combination of intrinsic and extrinsic muscles, resulting in a system with at least 23 DOF at the joints [113]. Several groups have proposed different three-dimensional models of human fingers, focusing on specific elements for certain purposes. Some of these include a model for estimating muscle-tendon tension during climbing grips [114], a biomechanical model for the finger pulley system [115], a three-dimensional inverse dynamic model of the index finger for free finger movements [116], finger and thumb models for determining fingertip forces for pinch applications [117, 118, 119], or a finger model based on non-linear optimising techniques adaptable to the study of different escenarios [120]. Most proposed models present a similar configuration, where they use fixed axes of rotation and an indeterminate system of equations with more unknown parameters (muscle forces) than available equations. Recently, a realistic complete biomechanical hand model has been proposed by merging the current knowledge of biomechanics, ergonomics and robotics, for modeling movements (excluding wrist) of the hand and grasps [121, 122]. A complete biomechanical hand model including finger and wrist joints is now being developed at Delft University, which includes the 45 intrinsic and extrinsic muscles of the hand [113].

6.5 Upper-limb FES models

Previously presented analytical models have been designed and validated for specific applications. Some of them have been adapted or taken as a basis for upper-limb FES applications, having stimulation parameters as inputs and joint forces or angles as outputs. One of the upper-arm FES models was developed for shoulder and elbow joints based on the model proposed by the Delft University [108], adapted for the application of percutaneous FES on SCI patients [123]. Blana et al. developed another model for both forward and inverse dynamic simulations of shoulder and elbow joints, which was validated with electromyographical (EMG) data and adapted to high cervical level SCI

subjects [124]. Another model was proposed by Freeman et al. for a FES-based stroke rehabilitation application, where a robotic workstation constrained the forearm to movements on the horizontal plane and FES was applied to triceps muscle [125]. The activation dynamics in this model based on a Hammerstein structure, whose identification used on a recursive approach [126]. Regarding models for hand FES applications, Keller et al. proposed a Hammerstein model for predicting isometric finger forces [127]. Similarly, Westerveld et al. proposed a model for predicting and controlling constrained thumb forces in two dimensions for healthy and stroke subjects [128]. A recent publication includes a simplified model of the hand for FES control purposes consisting on a single composite finger and wrist [129], and a complete ILC based approach for hand posture control based on multi-field surface electrodes [130].

By the time this thesis started, to the author's knowledge, only one model-based FES-induced grasp control application had been proposed with multi-field electrodes [130]. However, it was based on a simplified model of the hand and no model accuracy results were presented as they focused on control. Indeed, stimulation application sites were predefined before the control stage and thus were not taken into account in the model. However, as stated earlier, the electrode configuration and FES application site are key for achieving more selective stimulation. The latter is critical as the relative position of the nerves and the skin change during arm and hand movements [131, 132]. Therefore, we believe that taking both stimulation parameters and application sites into account is essential for obtaining accurate models of FES-induced selective hand movements. The musculoskeletal complexity of the hand and wrist combined with the success of intelligent computing techniques in other FES applications mentioned in the next chapter, brought the present thesis to propose a novel model of surface multi-field FES-induced hand movements. In this thesis, we present the first steps of a modeling approach for a complete FES system based on intelligent computing techniques that pretends to cover the different subsystem models described, from the skin to the biomechanical model. The aim of the proposed models is to support the design and development of new surface FES neuroprostheses and control techniques for hand grasp.

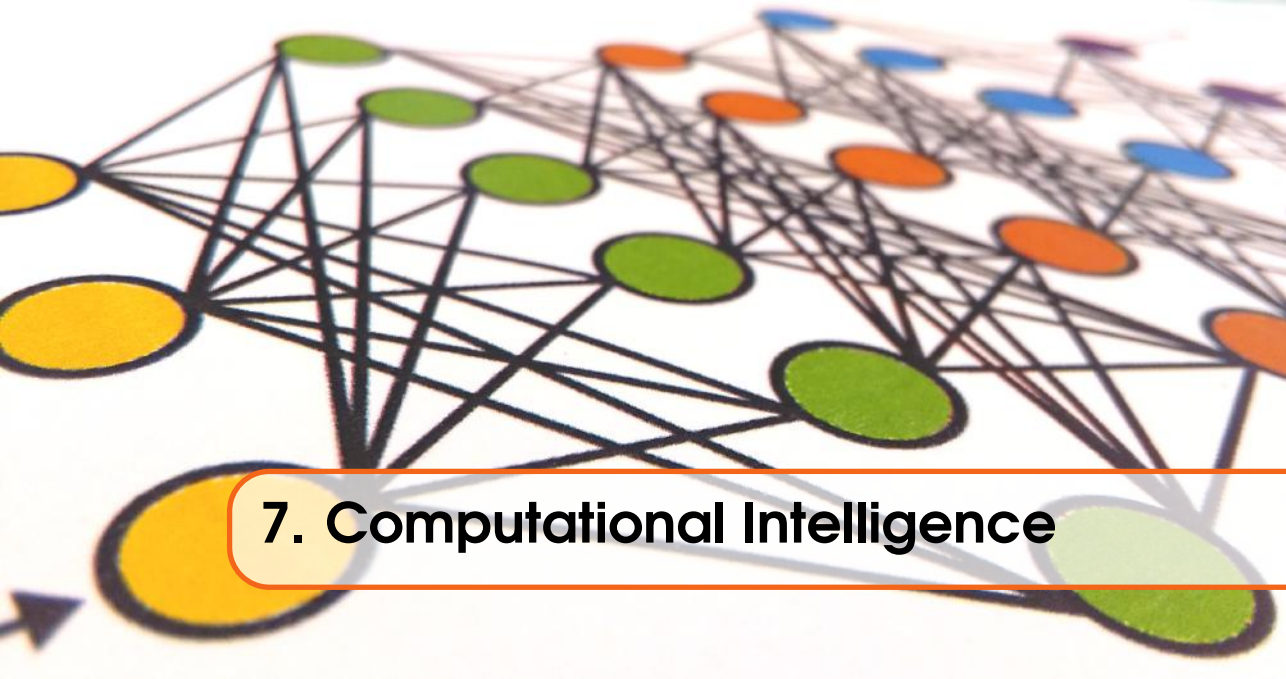

7. Computational Intelligence

Although there is no common definition for the Computational Intelligence (CI) term, it can be described as a combination of Soft Computing and numerical processing techniques for developing systems that simulate intelligent behavior by giving outputs based on experimental evidence and prior knowledge [133]. Hence, CI techniques properly suit complex, nonlinear, time varying or stochastic processes. Although CI is a wide interdisciplinary area covering many fields, the main disciplines covered by CI are fuzzy systems, artificial neural networks (ANN) and evolutionary computation [133]. Despite being these the most established disciplines, many others are also considered as part of CI, such as learning theory, probabilistic methods, swarm intelligence, artificial immune systems or rough sets among others [134, 135]. Different approaches, methods and tools developed in these disciplines and their combinations share a common goal, which is the development of intelligent systems. In the present chapter the basic concepts of those paradigms that relate to this thesis will be briefly described.

7.1 Fuzzy Systems

Fuzzy systems allow handling the concept of partial truth, which enables modeling uncertainties found on linguistic terms. The input space is described by the fuzzy sets and fuzzy terms and these are then mapped to the output space by means of fuzzy logic and fuzzy inference systems based on fuzzy rules.

7.1.1 Fuzzy sets

Fuzzy set elements are described by membership degrees, which determine the certainty that a given element belongs to that set. Formally, a fuzzy set A is characterized by a membership function $\mu_A(x)$ which associates a real number from the interval $[0,1]$ with each point in X. Where X is the domain and $x \in X$ is a specific element of that domain. Thus, the $\mu_A(x)$ value represents the membership degree of x in the set A. In the classical set case, the membership function $\mu_A(x)$ can only take two values, which are 0 or 1, so fuzzy sets are an extension of classical sets. A discrete fuzzy set A is then defined as a set of ordered pairs in a X domain [135]:

$$\begin{aligned} A &= \{(\mu_A(x_i)/x_i) | x_i \in X, i = 1, \cdots, n\} \\ A &= \mu_A(x_1)/x_1 + \mu_A(x_2)/x_2 + \cdots + \mu_A(x_n)/x_n \\ &= \sum_{i=1}^{n} \mu_A(x_i)/x_i \end{aligned} \tag{7.1}$$

In this case the summation should not be confused with the arithmetical operation. It only indicates that the fuzzy set is a collection of ordered pairs.

The membership function $\mu_A(x)$ is therefore used to associate a membership degree of each of the elements of the domain to a certain fuzzy set. Shape of fuzzy terms can be of any type, which is usually defined for specific problems. The only requirement is that the membership function should be bounded between 0 and 1 and that for each $x \in X$ there must be a unique $\mu_A(x)$ value. Most common shapes include triangular, trapezoidal, gaussian or bell-shaped functions. As an illustration, Figure 7.1 shows an example of three fuzzy sets, which are *cold*, *comfortable* and *hot* sets, represented by a descending monotonic, a triangular and an ascending monotonic membership function respectively. Each temperature value is paired with a membership degree for each set. For example, a temperature of 0 °C belongs to the *cold* set with membership value 1 and to *comfortable* and *hot* sets with value 0. However, 25 °C belongs with a certain degree to both *comfortable* and *hot* sets.

When the values of a variable are words or sentences, then it is called linguistic variable, which in fuzzy systems usually correspond to the labels of fuzzy sets. In the Figure 7.1 case, the temperature is a linguistic variable represented by *cold*, *comfortable* and *hot* terms. This capacity of dealing with uncertainty is the essence of the fuzzy systems [135].

7.1.2 Fuzzy logic and inference

Fuzzy logic together with an inference system results in a tool that approximates reasoning. The main core of fuzzy logic are the linguistic fuzzy rules, which

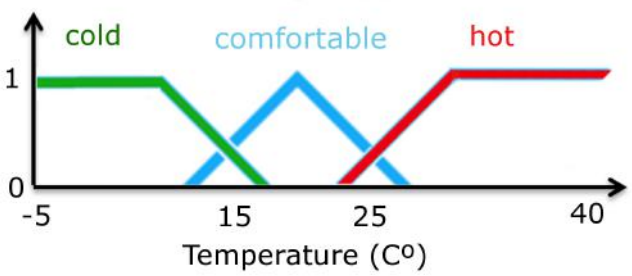

Figure 7.1: Example of fuzzy sets.

characterize the behavior of fuzzy systems and are usually based on human or expert knowledge [135]. Fuzzy rules are usually of the form

$$\text{if} \quad \textit{antecedent}, \quad \text{then} \quad \textit{consequent} \tag{7.2}$$

where both antecedent and consequent are propositions containing linguistic variables. In general, a fuzzy rule can be expressed as

$$\text{if} \quad A \text{ is } a \text{ and } B \text{ is } b, \quad \text{then} \quad C \text{ is } c \tag{7.3}$$

where A, B and C are fuzzy sets. Both antecedent and consequent parts of a rule can be composed by a combination of fuzzy sets by means of fuzzy logic operators, although the consequent part usually consists on a single fuzzy set [135].

Fuzzy sets and fuzzy rules form the basis of fuzzy rule-based reasoning systems, where fuzzification, inference and defuzzification concepts complete the whole system. Fuzzification is the process of converting crisp values into fuzzy input values, which is achieved with membership functions that associate values with their membership grades to fuzzy sets present in the input space. The inverse process of converting fuzzy values into crisp values is called defuzzification. There are many methods on literature for calculating approximate numerical outputs from fuzzy sets, and the selection of the method is dependent on the application. Most common methods include the center of gravity method, the averaging method, the mean-max method or the max-min method, among others. Finally, inference is the process that maps a given input space to the corresponding output space in a non-linear manner. The most used fuzzy inference mechanisms are the Mamdani and Sugeno models [133, 135].

A typical rule of a set of R rules in Mamdani type of fuzzy inference is defined as

$$r_k: \quad \text{if} \quad x \text{ is } A_i^k \text{ and } y \text{ is } B_j^k, \quad \text{then} \quad z \text{ is } C_l^k \tag{7.4}$$

where $k = 1,2,\cdots R$, $i = 1,2,\cdots,N$, $j = 1,2,\cdots,M$, and $l = 1,2,\cdots,L$. N and M are the number of membership functions for inputs, and L the number of membership functions for outputs. Last step of converting the output fuzzy sets into a crisp value is carried out by a defuzzification method.

Sugeno type of inference systems have a crisp function as a consequent part of the fuzzy rules, which have the following form

$$r_k: \quad \text{if} \quad x \text{ is } A_i^k \text{ and } y \text{ is } B_j^k, \quad \text{then} \quad z^k = f(x,y) \tag{7.5}$$

where x and y are the inputs, z is the output, $k = 1,2,\cdots,R$, $i = 1,2,\cdots,N$, $j = 1,2,\cdots,M$, and N and M are the number of input membership functions. $z = f(x,y)$ is the crisp consequent part of the rule, and although it is usually polynomial in the input variables x and y, it can be any function. When this is a first-order polynomial, the resulting inference system is called first-order Sugeno, and if it is a constant value, it is called a zero-order Sugeno. The final output of a Sugeno fuzzy model is obtained with the weighted average of the crisp z^k outputs, avoiding the time-consuming defuzzification process required by Mamdani models [133].

7.2 Artificial Neural Networks

Artificial Neural Networks (ANN) were inspired by the brain and pretend to mimic the behavior of the nervous system. Although research on ANN has lead to a broad and diverse variety of different type of ANN, only the basic concepts of those relevant to the present thesis will be described.

7.2.1 Neuron unit

ANN are composed by many information processing units called *neuron units*, which try to mimic the behavior of biological neurons. Each neuron unit has a vector of inputs $(x_1,x_2,\cdots,x_n)$, with its corresponding weights $(w_1,w_2,\cdots,w_n)$, and a threshold called *bias*. With this information, an activation function determines the output signal of the neuron [135]. The input signal to the activation function is usually determined by a weighted average of the form

$$\sum_{i=0}^{n} x_i w_i \tag{7.6}$$

In some cases the weight of the bias is represented by θ and its input x_0 is assumed to have value 1, in which case, the input signal to the activation function takes the form

$$\sum_{i=1}^{n} x_i w_i + \theta \tag{7.7}$$

The general structure of a single neuron unit is shown in Figure 7.2. The activation function can be of any type, although most used functions include linear, step, ramp, sigmoid, hyperbolic or gaussian functions [135], from which examples are shown in Figure 7.3.

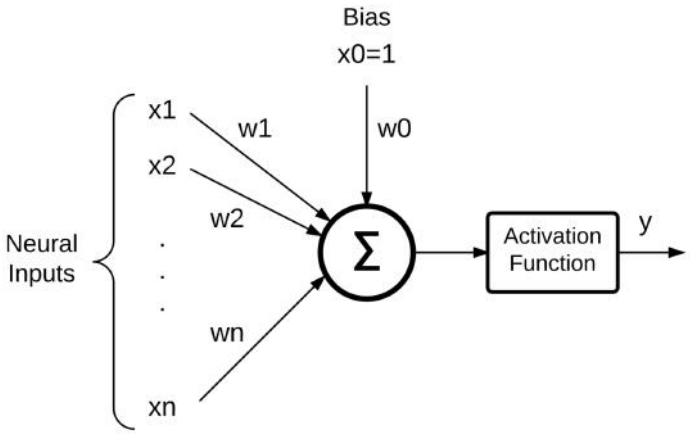

Figure 7.2: Artificial neuron.

7.2.2 Multi-layer feedforward networks and backpropagation

Multi-layered feedforward networks are the standard most used type of ANN and consist on a group of many interconnected artificial neurons organized in multiple layers. These neurons form forward connections only, so information is transmitted from lower layers to higher layers in one direction. Multi-layer feedforward networks are considered static networks as they are characterized by memoryless nonlinear equations. Their morphology consists of an input layer (first layer), an output layer (last layer) and one or more hidden layers between them. In Figure 7.4, an example of a multi-layer feedforward network with two hidden layers is shown.

Regarding general notation, each layer k has N_k number of neurons. Each of them is noted as $N_i^{(k)}$, which refers to neuron number i from layer number k. Similarly, the output of the i-th neuron of layer number k is noted as $y_i^{(k)}$. The detailed scheme and notation of a $N_i^{(k)}$ neuron is shown in Figure 7.5, where usually the activation function is of the sigmoid or hyperbolic tangent form [133].

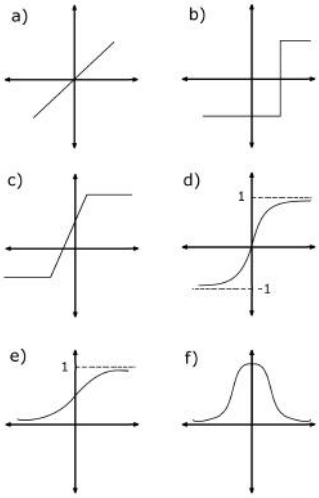

Figure 7.3: Activation function examples: a) linear function, b) step function, c) ramp function, d) hyperbolic tangent function, e) sigmoid function, f) gaussian function.

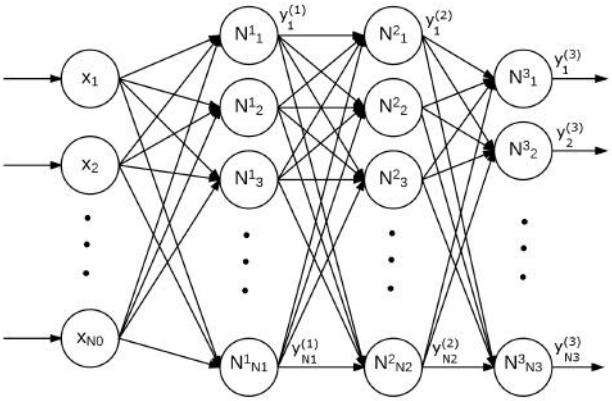

Figure 7.4: Multi-layer feedforward network morphology. An example with one input layer, two hidden-layers and an output layer.

Hence, the output signal of neuron $N_i^{(k)}$ at the instant t, where $t = 1, 2, \cdots$ is defined as

$$\begin{aligned} s_i^{(k)}(t) &= \sum_{j=0}^{N_{k-1}} w_{ij}^{(k)}(t) x_j^{(k)}(t) \\ y_i^{(k)}(t) &= f(s_i^{(k)}(t)) \end{aligned} \tag{7.8}$$

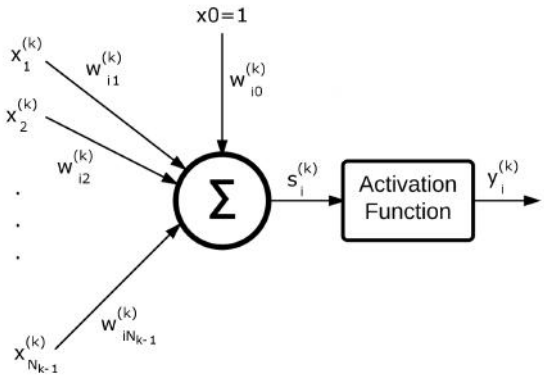

Figure 7.5: Detailed scheme of a multi-layer feedforward neuron: i-th neuron of layer k.

where f is the activation function. The forward pass of a multi-layer feedforward network begins at the input layer, then the outputs of each neuron are updated layer by layer, until reaching the final layer. This is called the output layer, where the outputs of the neurons are the final outputs of the network [133].

Learning in neural networks is the procedure of modifying and tuning the weights and the biases in order to obtain the desired behavior of the ANN. Most ANN are tuned under supervised learning, which is based on a set of input/output data (also called training data) of desired network behavior. As the inputs are applied to the network, the network outputs are compared to the desired outputs. The learning or training algorithm is then used to adjust the weights and biases of the network in order to reduce the difference between obtained and desired outputs. This error reduction is carried out continuously modifying the network parameters until an acceptable error is reached. Although many learning algorithms exist, the most commonly used backpropagation (BP) algorithm will be briefly described, as it is used in the following chapters.

The BP method is based on the gradient descent method, which continuously modifies the weights of the network to reduce the difference between the desired output and the actual output of the network. The error in the output layer is then backpropagated into previous layers, one layer at a time, until the first layer is reached [136]. The error between desired outputs d_j and network outputs y_j, which is also referred to as cost function, can be of different forms, for example

the sum square of the output errors defined as

$$E(t) = \frac{1}{2}\sum_{j=1}^{m}[d_j(t) - y_j(t)]^2 \quad = \frac{1}{2}\sum_{j=1}^{m} e_j(t)^2 \tag{7.9}$$

where m represents the number of outputs and $e_j(t)$ the error at instant t of output j.

According to gradient descent, the correction of the weight vectors are made in the direction of decreasing error function, and thus, are proportional to the negative of the gradient of the error function. The general weight update formula is

$$w_{ij}^{(k)}(t+1) = w_{ij}^{(k)}(t) - \eta \frac{\partial E(t)}{\partial w_{ij}^{(k)}(t)} \tag{7.10}$$

where η represents the learning rate and defines the convergence speed of the updating process. If δ is defined as

$$\delta_i^{(k)}(t) = -\frac{\partial E(t)}{\partial s_i^{(k)}(t)} \tag{7.11}$$

then, the weight update function can be noted as

$$w_{ij}^{(k)}(t+1) = w_{ij}^{(k)}(t) + \eta\, \delta_i^{(k)}(t) x_j^{(k)}(t) \tag{7.12}$$

and the $\delta_i^{(k)}$ in each layer k is updated by the formula

$$\begin{aligned} \delta_i^{(k)}(t) &= f'(s_i^{(k)}(t)) \sum_{l=1}^{N_{(k+1)}} \delta_l^{(k+1)}(t) w_{li}^{(k+1)}(t) \\ &= f'(s_i^{(k)}(t)) \varepsilon_i^{(k)}(t) \end{aligned} \tag{7.13}$$

where f' is the differential of the activation function and $\varepsilon_i^{(k)}$ represents the backpropagation error and is defined as

$$\varepsilon_i^{(k)}(t) = \sum_{l=1}^{N_{(k+1)}} \delta_l^{(k+1)}(t) w_{li}^{(k+1)}(t) \tag{7.14}$$

This is the basic BP algorithm, which is widely used for its simplicity and online adapting nature. One of its disadvantages is that it can be trapped in local minimum and so, it is highly dependent on the initial weight values. However, many modifications to the basic BP algorithm have been proposed to reduce this problem [133, 136]. A very common modification is the inclusion of a

momentum term α, which involves modifying the weight update equation 7.12 like this

$$w_{ij}^{(k)}(t+1) = w_{ij}^{(k)}(t) + \eta \delta_i^{(k)}(t) x_j^{(k)}(t) + \alpha[w_{ij}^{(k)}(t) - w_{ij}^{(k)}(t-1)] \quad (7.15)$$

The momentum term α determines the influence of the past weight changes on the current direction of movements in the weight space, which usually results in a reduction of oscillations.

7.2.3 Recurrent neural networks

Recurrent neural networks (RNN) are called like this because they include recurrences or feedback loops in their structure, which allow them to emulate dynamic processes. Thus, they are also known as dynamic neural networks.

Similar to the neuron unit presented in the previous section, the dynamic neuron unit has the form shown in Figure 7.6, where a self-recurrence weighted connection makes it able to process information from the past and store current information for future usage. f_i represents the activation function and g_i the neural output function.

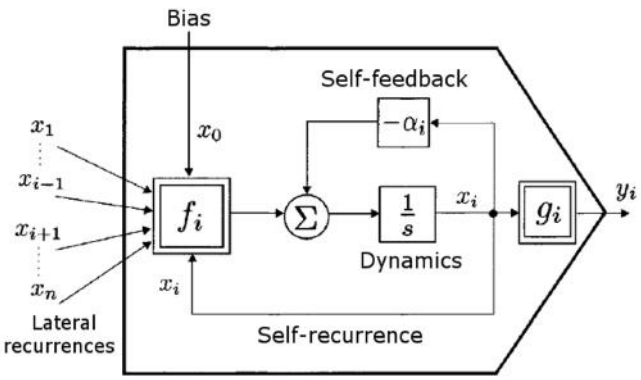

Figure 7.6: Scheme of a general dynamic neuron unit *i* [136].

RNN networks can be formed by dynamic or static neuron units, but unlike multiple-layer feedforward networks, their structure contains feedback connections. There are many types and modifications of RNN, but as an illustration, only the morphology of the three most known networks will be shown, which are the Elman, Jordan and Hopfield structures. Elman and Jordan RNN consist on modifications of the already described multiple-layer feedforward network. Elman structure makes a copy of the hidden layer called *context layer*, whose purpose is to feed the hidden layer with previous network states. Similarly,

the Jordan structure makes a copy of the output layer called *state layer*, which feeds the hidden layer with previous network output states [133, 135]. Figure 7.7 shows basic examples of both Elman and Jordan RNN. On the other hand, Hopfield structure is a one-layer network with a regular structure, which consists on a fully connected network, except for self-connections as shown in a simplified scheme in Figure 7.8 [136].

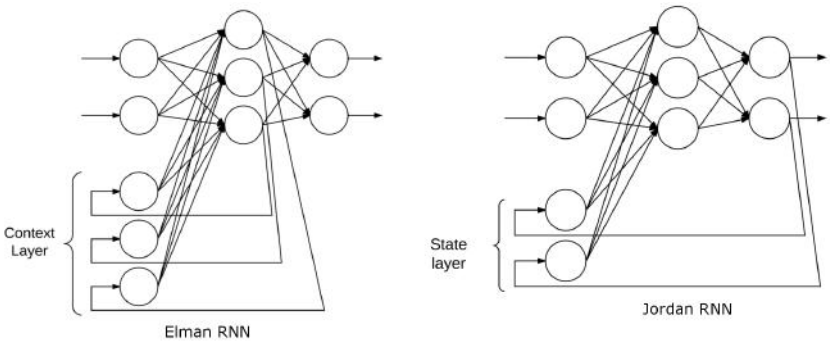

Figure 7.7: Elman and Jordan recurrent networks.

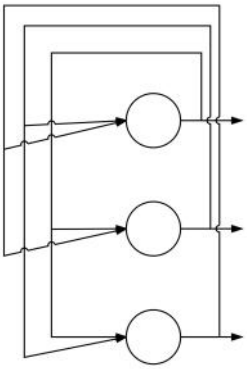

Figure 7.8: Hopfield neural network.

Main advantage of RNN in general is that they are nonlinear dynamic networks, which make them appropriate for identification and control of nonlinear dynamic systems [136].

7.3 Neuro-fuzzy systems

Fuzzy logic systems are based on linguistic expressions, but construction of membership functions and fuzzy rules depend on expert knowledge and can be a tedious or difficult task in complex systems. On the contrary, ANN automatically learn their parameters from experience, but their morphology and parameters are abstract and not related to linguistic terms. Both are mathematical model-free systems with different advantages and drawbacks. However, merging both approaches into neuro-fuzzy systems result in systems that are able to learn from experiential data by means of learning algorithms, while representing linguistic knowledge by means of fuzzy sets. Thus, neuro-fuzzy systems take advantages of both systems and solve some of the drawbacks present when any of the systems is used independently. Neuro-fuzzy systems can be of different forms depending on the aim and the way they are combined. In this section cooperative neuro-fuzzy systems and hybrid neuro-fuzzy systems will be briefly described.

7.3.1 Cooperative neuro-fuzzy systems

The aim of the cooperative combination is that the neural network determines or assists in the definition of certain parameters of the fuzzy system or vice versa, where both systems work independently. In some combinations, the fuzzy system provides prerequisite information to an ANN in order to speed up the learning. On the contrary, in other cases the ANN is used to determine the membership functions of the fuzzy system by learning from obtained data [133]. An example scheme of both approaches is shown in Figure 7.9.

7.3.2 Hybrid neuro-fuzzy systems

Unlike in cooperative systems, in hybrid approaches both the fuzzy system and the ANN are merged. On one hand, the rule base is replaced by an ANN and so, inference is simplified. And on the other hand, the parameters of the fuzzy system (membership functions) are found by learning methods obtained from ANN. In order to achieve this, usually in hybrid approaches the fuzzy system is represented in a network-type structure. Like this, learning algorithms such as BP can be applied [133]. Again, although many hybrid neuro-fuzzy approaches are available on the literature, the most well known adaptive networks will be briefly described, which are the Adaptive Neuro-Fuzzy Inference System (ANFIS) and its homologous multiple output system CoActive Neuro-Fuzzy Inference System (CANFIS).

The ANFIS is an adaptive network that is functionally equivalent to a fuzzy inference system [137]. A basic ANFIS scheme representing a first-order

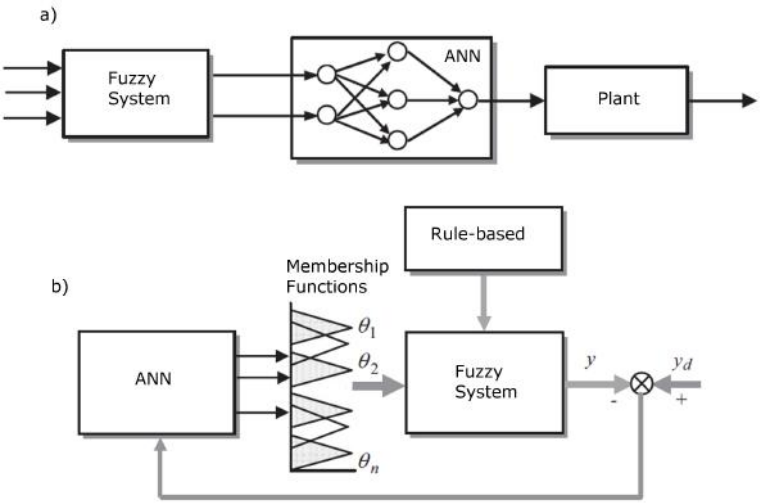

Figure 7.9: Cooperative neuro-fuzzy examples: a) a fuzzy system determines the inputs of an ANN, and b) an ANN adapts the membership functions by learning from data. Adapted from [133]

Sugeno fuzzy model of two inputs, two rules and one output is shown in Figure 7.10 and described below.

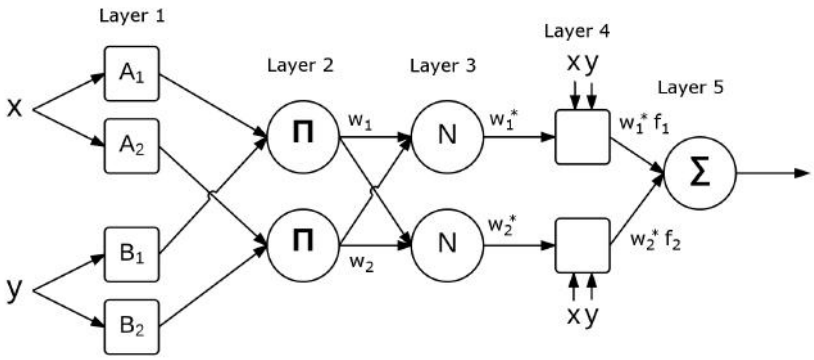

Figure 7.10: ANFIS scheme equivalent to a first-order Sugeno fuzzy model of two inputs, two rules and one output.

ANFIS usually consist of five layers, where the first layer is the membership layer. The nodes corresponding to this layer are adaptive, where the outputs represent the grade of membership of the inputs to the corresponding fuzzy sets.

In the example shown in Figure 7.10, the outputs are:

$$\begin{aligned} O_{1,i} &= \mu_{A_i}(x), \quad \text{for} \quad i = 1,2 \\ O_{1,i} &= \mu_{B_{i-2}}(y), \quad \text{for} \quad i = 3,4 \end{aligned} \tag{7.16}$$

The parameters of the membership functions, which adapt with the learning algorithm, are called premise parameters. The nodes of the second layer are fixed and represent the rules. Their outputs are the product of all the incoming signals, in this case:

$$O_{2,i} = w_i = \mu_{A_i}(x)\mu_{B_i}(y), \quad \text{for} \quad i = 1,2 \tag{7.17}$$

The nodes of the third layer are also fixed and they calculate the ratio of the firing strength over the sum of all firing strengths, also called normalized firing strengths:

$$O_{3,i} = w_i^* = \frac{w_i}{\sum_i w_i} \tag{7.18}$$

The nodes from the fourth layer are adaptive nodes, which in this case are represented by a first-order Sugeno function

$$O_{4,i} = w_i^* f_i = w_i^*(p_i x + q_i y + r_i) \tag{7.19}$$

where p_i, q_i and r_i are called consequent parameters and are modified by the learning algorithm.

Finally, the nodes of the last layer are fixed and compute the network output as the summation of all the incoming signals:

$$O_{5,1} = \sum_i w_i^* f_i = \frac{\sum_i w_i f_i}{\sum_i w_i} \tag{7.20}$$

The adaptive network structure of the ANFIS permits learning the premise and consequent parameters with different training algorithms, such as the previously described BP [137].

CANFIS is a generalized ANFIS that can be applied to multiple-input multiple-output (MIMO) systems. A basic CANFIS scheme representing a first-order Sugeno fuzzy model of two inputs, two rules and two outputs is shown in Figure 7.11. As it can be seen, it follows the same structure as the ANFIS except the normalization layer, which in the CANFIS case is carried out in the last layer [137].

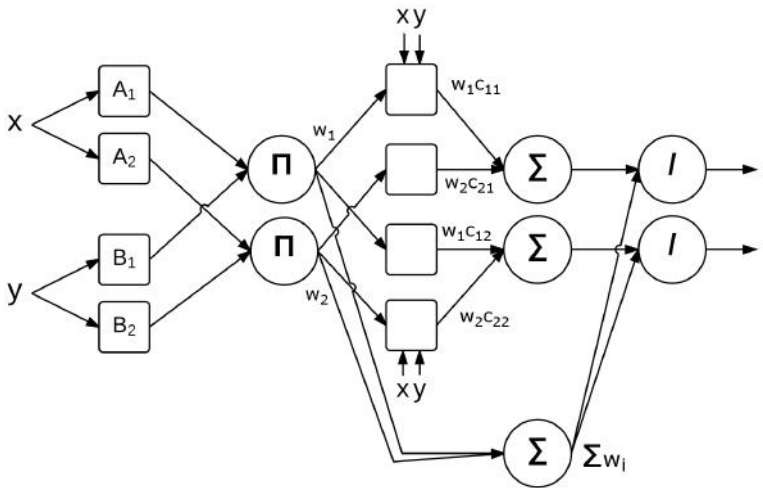

Figure 7.11: CANFIS scheme equivalent to a first-order Sugeno fuzzy model of two inputs, two rules and two outputs.

7.4 Evolutionary algorithms

Evolutionary computing is the emulation of the process of natural selection in a search procedure adapted to optimization problems, where more fit individuals have the opportunity to mate most of the time, and thus, expect that the offspring will have similar or better fitness. Although there are many different variants of evolutionary algorithms, the common underlying idea is the same for all. Given a population of individuals, the natural selection process causes a particular group of individuals to survive depending on the fitness [138]. Main concepts common to most evolutionary algorithms will be briefly described followed by the description of differential evolution (DE) algorithm, which is the algorithm used in the present work.

7.4.1 Main concepts

In nature, traits or features of organisms are represented in long chains of *genes* that contain coded information called *chromosomes*. Similarly, in evolutionary algorithms, chromosomes are usually called individuals and are represented by a vector of elements, where each of these elements represents one parameter of the optimization problem. The coding of these chromosomes can be done in different ways depending on the algorithm and application [138]. The population in evolutionary algorithms represents the search space and it is composed by individuals. The maximum number of individuals in a population is called the population size [138]. At the beginning, this population is usually

defined by a randomly chosen or generated set of individuals, and generation by generation, the population changes or adapts towards a solution. The size of the population is an important parameter for any evolutionary algorithm, as small populations can limit the diversity and miss good individuals, and on the contrary, large populations are computationally more expensive and converge slower towards the solution [138]. The population is updated in each generation by a new set of individuals, which represent potential solutions to the optimization problem, and this new generation is usually formed through the application of three operators: selection, crossover and mutation [138].

The selection operator selects individuals from the population to be copied for possible inclusion in the next generation. The chance of an individual of being selected usually depends on its fitness value, which is determined by an evaluation function that is specific to each application. In each generation, the selected individuals are placed into a mating pool, for creating the offspring for the next generation. There are many selection operators, such as random selection, where individuals are selected randomly; rank-based or proportional selection, where individuals with higher fitness have more chances to be selected; or elitist selection, where individuals with highest fitness are selected; among others [138]. Crossover operator, also known as recombination, mates selected individuals to produce new individuals based on the genes or parameters of the parents. The aim is to create new individuals with higher fitness values that form the new generation. Crossover probability determines the probability that a selected individual will undergo a crossover operation or not, so unless this probability is 1, there will always be a set of individuals that are copied without changes to the new generation. Depending on the crossover operation method the offspring can have a single parent, two parents or multiple parents. Different and diverse crossover operators are available, which determine the way the combination of parent individuals is carried out to give birth to the new individuals [133, 138]. Finally, the mutation operator randomly changes a gene or parameter value of an individual with a mutation probability, which is usually very small. This operation ensures diversity on the population, and thus, can overcome problems derived by a bad initial population [138].

Evolutionary algorithms are based on these concepts, and most popular algorithms include evolution strategies, evolutionary programming, genetic algorithms, genetic programming or DE [133, 138]. In the next subsection, DE, which is used in the present work, will be briefly described.

7.4.2 Differential evolution

Like other evolutionary algorithms, DE is a population-based optimizer which has a population of randomly selected individuals as a starting point. Each

individual consists of a vector of parameters, and in the initial population these individuals are chosen randomly from within boundaries fixed for the specific application. From then on, DE generates new individuals by combining and perturbing existing ones driving the population towards a optimum solution, as described next.

Individuals in DE consist of a vector of parameters x of length D, and the most versatile implementation of DE is based on two populations with N_p individuals each, where Px represents the current population and Pu represents the trial population [139]. Individuals and populations are defined like this:

$$\begin{aligned} P_x &= \{X_1, X_2, \cdots, X_{N_p}\} \\ X_i &= \{x_{1i}, x_{2i}, \cdots, x_{Di}\} \end{aligned} \tag{7.21}$$

$$\begin{aligned} P_u &= \{U_1, U_2, \cdots, U_{N_p}\} \\ U_i &= \{u_{1i}, u_{2i}, \cdots, u_{Di}\} \end{aligned} \tag{7.22}$$

After initializing the population within the predefined boundaries, DE mutates and recombines the population to produce a new population of Np trial vectors. Mutation in DE consists of adding a scaled, randomly sampled (for every mutant) vector difference to a third vector [139]. Each of the mutant vectors V_i is therefore formed as follows:

$$V_i = X_{r0} + F \cdot (X_{r1} - X_{r2}) \tag{7.23}$$

where $r0$, $r1$ and $r2$ represent randomly chosen individual indexes, and F is a positive real number that controls the rate at which the population evolves. The base vector X_{r0} can also be selected following other criteria, depending on the DE version [139]. A graphical example with two dimensional vectors is shown in Figure 7.12.

Apart from mutation, a crossover strategy is also applied in DE, which builds trial vectors from parameter values copied from current population vectors and mutant vectors [139]. The crossover probability C_r controls the fraction of parameter values that are copied from the mutant V_i to the trial vector U_i as follows:

$$\begin{aligned} U_i &= \{u_{1i}, u_{2i}, \cdots, u_{Di}\} \\ u_{ji} &= \begin{cases} v_{ji} & \text{with} \quad prob = C_r \quad \text{or} \quad j = j_{rand} \\ x_{ji} & \text{otherwise} \end{cases} \end{aligned} \tag{7.24}$$

In addition, the trial parameter with randomly chosen index j_{rand} will be taken from the mutant to ensure that the trial vector U_i is not identical to the

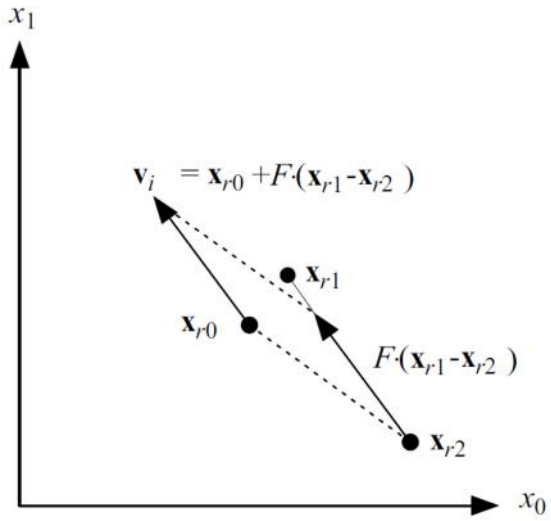

Figure 7.12: Differential mutation is performed by adding a weighted difference $F \cdot (X_{r1} - X_{r2})$ to a base vector X_{r0} [139].

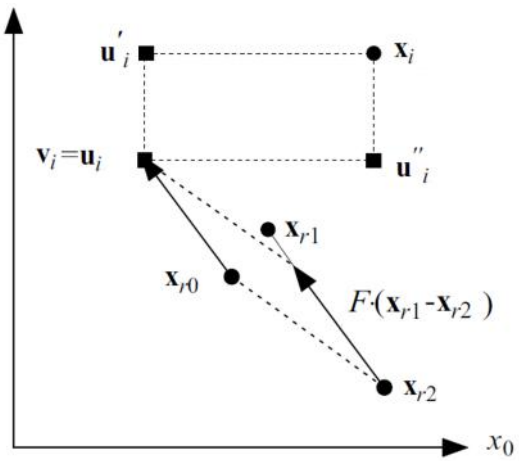

Figure 7.13: Crossover DE: possible U_i trial vectors after crossing V_i and X_i [139].

current population vector X_i. An illustration of possible trial vectors resulting from the crossover is shown in Figure 7.13.

Once the trial population P_u is formed, the current population P_x updates its values according to a selection process. Thus, this selection process determines the population of the next generation [139]. If the trial vector U_i has a lower

cost value (or higher fitness value), than its target vector X_i, then it replaces the target vector in the next generation, otherwise the target vector remains:

$$X_{i,new} = \begin{cases} U_i & \text{if} \quad f(U_i) \leq f(X_i) \\ X_i & \text{otherwise} \end{cases} \tag{7.25}$$

where, f is the cost function.

Once the new population is built, the process of mutation, crossover and selection is repeated until a predefined termination criteria (maximum number of iterations, error threshold,...) is satisfied. Although many versions and modifications of DE have been proposed for different applications [139], these are the basic principles that describe the concept of DE algorithm.

7.5 FES applications

CI techniques have been applied to FES applications. Most of these approaches involve the use of ANN due to their capacity of learning and adapting from experiential data, where different ANN approaches have been proposed for lower-limb applications [140, 141, 142, 143] and upper-limb applications, which include applications for control of elbow [144, 145], shoulder and elbow [146, 147] or classification of surface multi-field electrodes for hand movements [148]. Solutions based on fuzzy logic controllers have also been proposed for FES applications such as rowing [149], FES-induced leg swinging motion [150], or standing [151]. Neuro-fuzzy approaches have also been proposed for FES applications. Lower limb applications include a comparison of different neuro-fuzzy approaches for simulating FES-induced leg swing [152]; a comparison of FES-induced knee extension analytical and ANFIS models, where a combination of both showed best results [153]; an application for controlling the leg swing with a neuro-fuzzy system combined with reinforcement learning [154]; and recently, a FES standing control application where a combination of an ANFIS and a Proportional-Integral-Derivative (PID) controller is proposed [155]. Regarding upper-limb applications, a cooperative system of ANN and fuzzy logic for indoor rowing exercise has been investigated [156, 157]. A neuro-fuzzy approach has also been used in FES-induced reaching applications, where the control is carried out cooperatively between a neuro-fuzzy system and the CNS [158].

As stated in the previous chapter, the complexity of the analytical model of the hand and wrist for FES-induced movements, combined with the success of CI techniques in other FES applications, brought the present thesis to propose a novel approach based on CI techniques for FES-induced hand movements. Based on the linguistic interpretability of fuzzy systems and the

learning capacity of ANN, we selected a neuro-fuzzy approach for combining both characteristics. Thus, in this thesis, we present the first steps of an modeling approach based on a combination of CI techniques for its application on surface FES neuroprostheses for grasping.

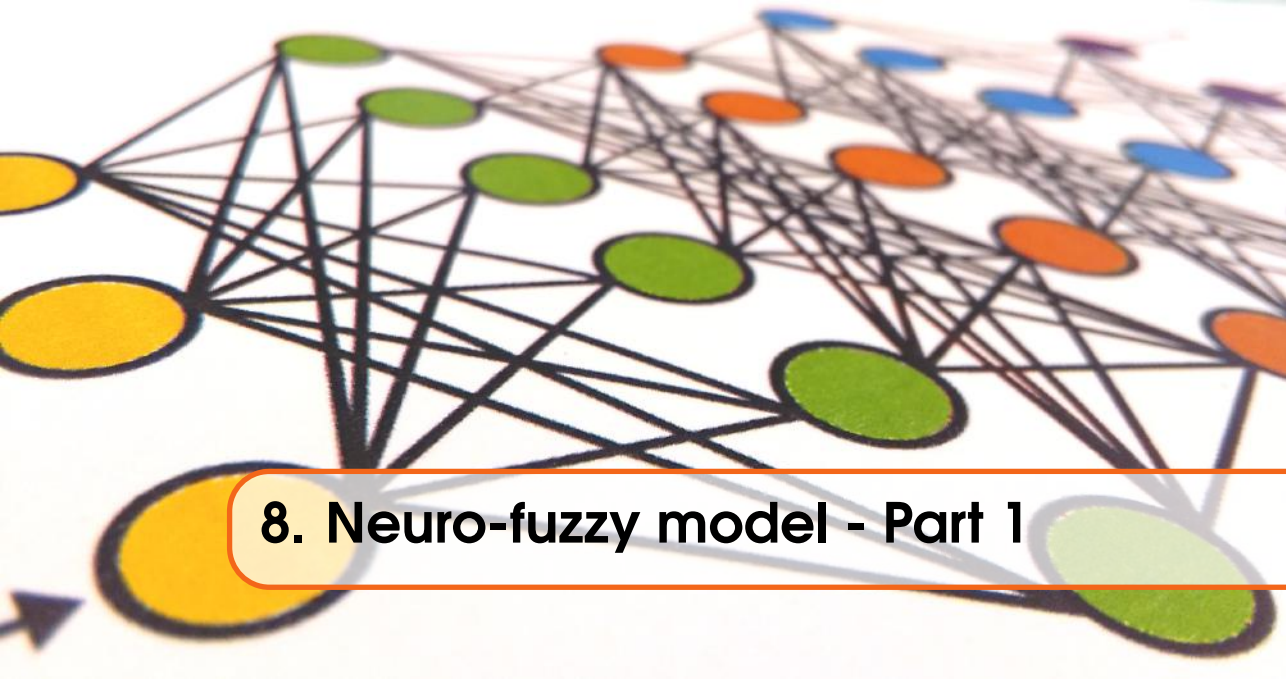

8. Neuro-fuzzy model - Part 1

CI techniques have successfully been applied to other FES applications as described in the previous chapter but not to FES-induced hand movements. Regarding analytical methods, to date only one simplified model for FES-induced hand movements with surface multi-field electrodes has been published [130]. It was designed for control purposes, where electrode configuration was predefined and remained constant. However, electrode configuration and FES application site are key for achieving selective movements. Indeed, the relative position of the nerves and the skin change during arm and hand movements [131, 132]. Thus, a model that takes into account stimulation parameters together with spatial application sites is needed for the development of more selective neuroprostheses. Due to the complexity and dimensionality of the upper-limb and specially the hand, we believe that CI techniques could bring new modeling and control possibilities to the field of upper-limb surface neuroprostheses in the near future, and thus, speed up the process of designing successful surface neuroprostheses.

The aim of the work presented in this chapter was to check the feasibility of using a neuro-fuzzy approach for modeling FES-induced hand movements with multi-field electrodes. Two different neuro-fuzzy systems were tested and trained with data collected from two stroke patients. Data collection was carried out in collaboration with the ADACEN (Acquired Brain Injury Association of Navarra) center.

8.1 Materials

The materials used in this set of experiments consist of a FES system and a sensor system for measuring wrist and finger flexion/extension, which were fully controlled by a custom-made GUI built on Matlab Software.

8.1.1 FES system

The FES system that we used in these experiments was the same as the one presented in chapter 5. The system consisted on an IntFESV2 stimulator shown in Figure 5.1 and two regular matrix electrodes shown in Figure 5.2, which were used for the stimulation of the anterior and posterior forearm. The details of the system are given in chapter 5. Additionally, conventional single electrodes (50x50 mm) and Compex stimulators were used for the adaptation sessions as therapists were more familiar to them.

8.1.2 Sensor system

The sensor system for measuring hand and finger flexion/extension consisted of a combination of two separated systems based on inertial sensors and optic fiber based sensors. For the measurement of finger flexion/extension the 5Data instrumented glove from Fifth Dimension Technologies was used, which is shown in Figure 8.1. It contained 5 optic fiber sensors, one for each finger, which provided the percentage of curvature of both metacarpophalangeal and proximal interphalangeal joints with respect to a previously defined maximum value. In this experiment, the maximum and minimum values were defined by the passive range of motion (PROM) measured at the beginning of the sessions. The PROM is the maximum range of motion at a given joint when this is moved by the therapist.

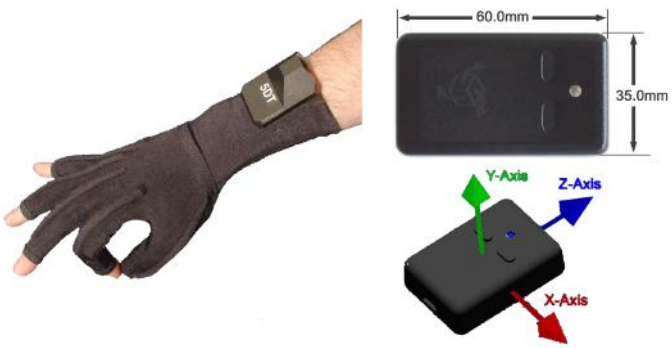

Figure 8.1: 5Data glove (on the left) and 3-Space sensor size and axes (on the right).

Wrist flexion/extension was measured with two 3-Space wireless inertial sensors from YEI Technology shown in Figure 8.1. One of them was mounted on the posterior side of the palm and the other one was mounted on the posterior side of the forearm, close to the wrist. Euler pitch angles were collected from these sensors and their difference was taken as an approximation of the wrist joint angle, which was also scaled to PROM values. Data from all sensors were collected at 20Hz and they were all calibrated at the beginning of the session as described in next section.

8.2 Methods

The objective of this first experiment was to check the feasibility of using neuro-fuzzy systems for modeling FES-induced hand movements in stroke patients. For this purpose, FES-induced hand movement data was collected from two volunteer chronic stroke patients at the ADACEN center. The protocol was approved by ADACEN and both participants signed an informed consent. Both subjects were left side affected and times from stroke were 3 and 4 years for Subject 1 and Subject 2 respectively.

8.2.1 Adaptation sessions

The aim of these sessions was to make the subjects familiar to the feeling produced by transcutaneous FES and at the same time train the forearm muscles before carrying out the main session. These sessions were carried out on the week before the main session and consisted of 30 minutes of electrical stimulation carried out daily on both sides of the forearm. As mentioned before, a preprogrammed Compex stimulator and conventional single electrodes were used for these sessions because therapists already had experience handling them.

Electrode pairs were placed longitudinally on the forearm, with the return electrodes placed on the wrist and active electrodes placed covering extensor/flexor muscles of the forearm. The stimulation was carried out in three phases, where a sequence of 5 seconds of stimulation on posterior forearm, 5 seconds on anterior forearm and 5 seconds of rest was followed all the time:

- Phase 1: frequency 25 Hz, pulse-width 150 µs and low amplitude (above sensory threshold but below motor threshold). (5 minutes)

- Phase 2: frequency 25 Hz, pulse-width 250 µs and high amplitude (above motor threshold, as high as tolerated). (20 minutes)

- Phase 3: frequency 5 Hz, pulse-width 250 µs and low amplitude (above sensory threshold but below motor threshold). (5 minutes)

8.2.2 Main session

After the adaptation week, the main session was carried out, which had a duration of around 60 minutes in total. Parameters during the whole session were set at 25 Hz frequency and 200 µs pulse-width.

The first stage consisted of donning the electrodes and sensor system on subjects' arm, where the electrode placement was the same as the one shown in Figure 5.3 in chapter 5, with medial and lateral epycondiles taken as a reference. An elastic sleeve was put on top of the electrodes to ensure hydrogel-skin contact throughout the experiment. Finally, the instrumented glove was donned. Figure 8.2 shows the arm of a subject after the donning stage.

Figure 8.2: Donned FES and sensor systems.

After the donning stage, the calibration stage followed. At this point, the subject was seated in a chair and rested his arm on top of a table with an elbow angle of 90 degrees. The forearm rested on top of a pillow and was kept in neutral position throughout the whole experiment. Firstly, PROM ranges were registered by collecting maximum extension/flexion of wrist angles and maximum and minimum flexion percentages of fingers. Afterwards, the subjects were asked to extend/flex the wrist and open and close the hand at their maximum to register the active ranges of motion (AROM). Finally, maximum tolerated amplitudes were registered for posterior and anterior areas by activating a single field in each area and increasing the amplitude up to the subject's tolerance level. The selected fields for determining maximum amplitude limits were chosen as the fields that got rated as most painful on average on experiments presented in chapter 5. These corresponded to the most proximal-lateral field (field 4) for the posterior forearm and most medial and halfway-distal field (field 12) for the anterior forearm.

Finally, the data collection stage took place. In this phase the subject was asked to not make any voluntary movements and to relax the forearm and hand while the forearm was kept in neutral position. The stimulation consisted of 4 repetitions of randomly activating all the fields of the two electrode matrices.

Each field started at 20 mA and increased in steps of 1 mA and 1 second of duration until the amplitude limit for that subject was reached. The starting point was set to 20 mA to speed up the process because no motor response was observed below 25 mA in either subject. The sequence followed an order, which was activation of fields located over the extensors first and activation of fields located over the flexors next with approximately 10 seconds of rest between each field, and 1 minute of rest between the repetitions. These frequent and long resting periods were applied to avoid fatigue interfere in this preliminary study. If the subject felt discomfort at any time during the experiment, the stimulation was stopped for the corresponding forearm area and stimulation continued in the next stage. A flowchart describing the data collection sequence in shown in Figure 8.3.

8.2.3 Neuro-fuzzy models

Two neuro-fuzzy models were tested with the data collected in this experiment. The first model consisted of the CANFIS hybrid neuro-fuzzy structure, described in the previous chapter, which is an adaptation of the broadly used ANFIS structure for MIMO systems. This model was selected because it was the most used neuro-fuzzy system in other FES applications. The second model consisted of a Recurrent Fuzzy Neural Network (RFNN). This model was chosen because like the CANFIS, it is a hybrid approach that has the learning capacity of ANN and the linguistic interpretability of fuzzy systems. Moreover, it is a dynamic network, as its structure contains recurrent connections, and so, has shown successful results when dealing with non-linear dynamic applications [159, 160, 161]. The structure of the CANFIS structure was shown in Figure 7.11 in the previous chapter, and the structure of the RFNN used in this tests, which is the one proposed in [160], is shown in Figure 8.4.

As it can be seen in the scheme, it includes an internal recurrence in the second layer, which brings the ability of temporarily storing information of previous states. Similar to the CANFIS layer structure defined in the previous chapter, the first layer applies the membership functions to the inputs and the second layer emulates the rules. However, the normalization and consequent layers of the CANFIS do not apply to the RFNN. In the RFNN case, the last layer performs a linear combination of the values obtained by the rules multiplied by the link weights, which are tuned by the learning algorithm [160]. Thus, both systems are hybrid neuro-fuzzy systems, able to adapt the parameters of the membership functions to minimize the error between the network outputs and desired outputs. However, the CANFIS adapts the consequent parameters as well, whereas the RFNN adapts the link weights.

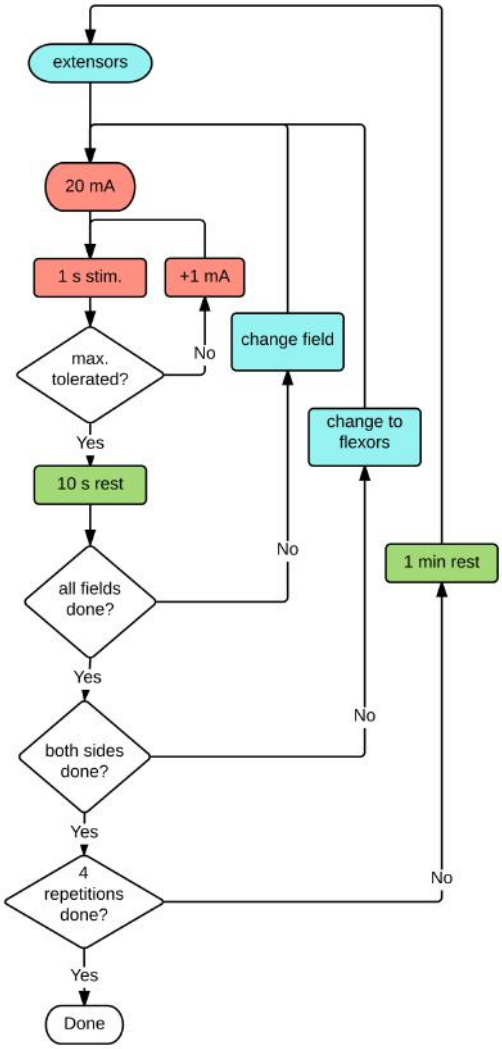

Figure 8.3: Data collection session flowchart.

We wanted to train a forward model that was able to predict finger and wrist flexion/extension from stimulation amplitudes and activation sites on the forearm, therefore, models were provided with 3 inputs and 6 outputs. One of the inputs represented the amplitude, and the other two inputs represented the coordinates of the activated field on the arm in proximal-distal and medial-lateral dimensions. Regarding the outputs, they represented the flexion/extension of

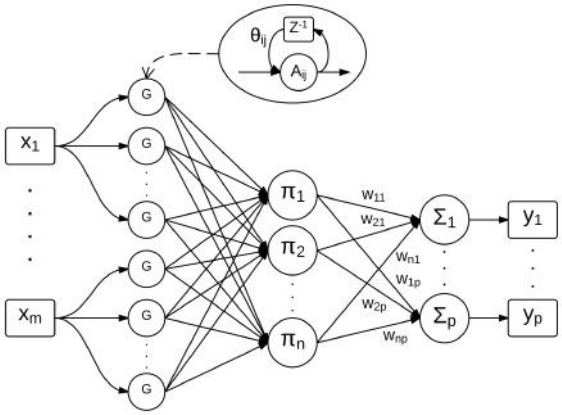

Figure 8.4: RFNN scheme.

wrist and fingers. Indeed, apart from the proposed structure with 3 inputs and 6 outputs, an additional approach with a fourth input consisting on the wrist feedback was tested with both systems. The aim was to see if the models improved when a feedback from the output was included in the structure. In this case, only the wrist feedback was used because additional feedback would mean an increase on the network size and because wrist was considered to carry the most important information regarding hand kinematics. Figure 8.5 shows the scheme used for the training with both approaches.

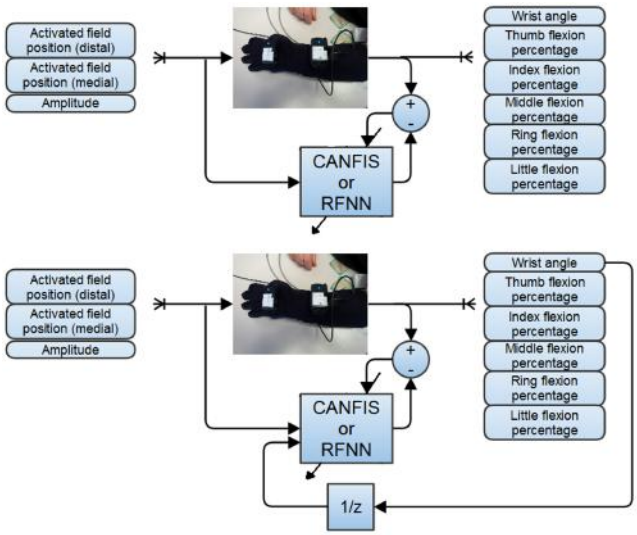

Figure 8.5: Model training schemes, top: no feedback, bottom: wrist feedback.

8.2.4 Data

As stated previously, the 3 inputs provided information of stimulation intensity and application site, whereas the 6 outputs provided flexion/extension values of the wrist and 5 fingers. The only data preprocessing carried out before training consisted in scaling. Data was scaled in order to handle similar magnitudes and support a better training of the models. The input that represented the amplitude was scaled by being 1 the maximum amplitude tolerated by the subject and 0 being the absence of current. The input corresponding to the proximal-distal dimension was represented by being zero the reference point located at the elbow and being 1 the most distal row. In the case of the lateral-medial dimension, data was scaled to the range (-1,1), where negative values represented fields over the posterior forearm and positive values fields over the anterior forearm. Zero value or reference value referred to the ulna area. An illustration of scaled distal and medial coordinates is shown in Figure 8.6.

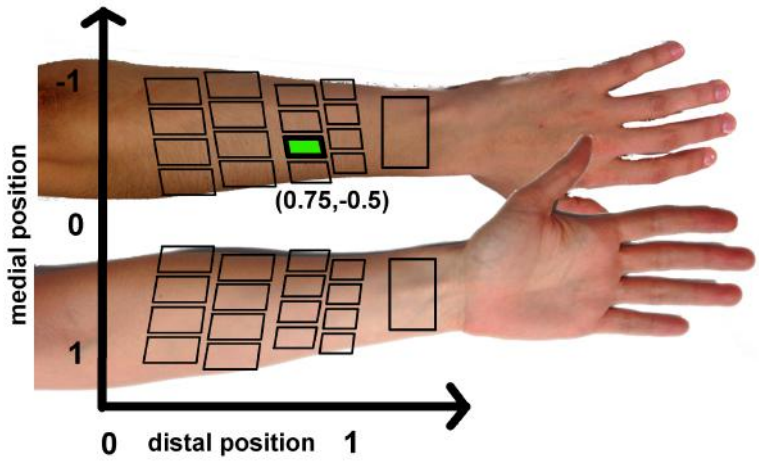

Figure 8.6: Coordinates on distal and medial dimensions, where the field with coordinates (0.75,0.5) is highlighted as an example.

Regarding the outputs, the finger flexion percentages provided by the glove were scaled by being 0 the minimum flexion and 1 the maximum flexion, according to PROM values. The wrist angles were scaled to the range (-1,1) over the PROM, where negative and positive values represented extension and flexion positions respectively.

Once data was scaled, 80% of the samples were used for training, whereas the remaining 20% were used for validation.

8.2.5 Model training

As the aim of the present experiments was to check the feasibility of using neuro-fuzzy models, a basic qualitative ad-hoc analysis was carried out to select appropriate model parameters for these preliminary neuro-fuzzy models. In all the cases the models were trained with gradient descent BP.

Once data was collected and scaled, 50% of the training data (40% of the total data) was trained with different model parameters for each subject. The model parameters included the learning rate η, the number of input terms and the membership function initialization. Two learning rate values $\eta = 0.1$ and $\eta = 0.01$ were tested resulting in better qualitative results with $\eta = 0.1$ for both subjects. Membership functions were selected as Gaussian functions and two initialization methods were tested, which were an online initialization method [162] and the uniform distribution of the membership functions along the input space. The latter gave better qualitative results for both subjects. Finally, regarding the membership layer, from 5 to 10 numbers of input terms were tested for each subject. Best qualitative results were obtained with 10 input terms for Subject 1 and 7 input terms for Subject 2.

8.3 Results

The results shown in this section correspond to the model parameters selected in the previous qualitative analysis, which were a learning rate $\eta = 0.1$, 10 input terms for Subject 1, 7 input terms for Subject 2, and gaussian membership functions initiated uniformly distributed throughout the input space.

8.3.1 No feedback approach

Training the CANFIS and RFNN systems without any feedback information resulted in the behavior shown in Figures 8.7 and 8.8 for Subject 1, which represent training and validation periods respectively. Similarly, Figures 8.9 and 8.10 represent training and validation periods for Subject 2. As an illustration, wrist and one finger (index) outputs are shown, but the behavior was similar for all outputs. It can be seen that training data was approximated by both approaches on both subjects. However, peaks were present throughout the predicted data, which were more prominent with the CANFIS approach. Regarding the validation case, better predictions were obtained for Subject 1 than for Subject 2 by both approaches.

Tables 8.1 and 8.2 show the MSE of the scaled values of CANFIS and RFNN results respectively. We could see that higher peak values of CANFIS in the learning period resulted in higher MSE values, whereas MSE differences

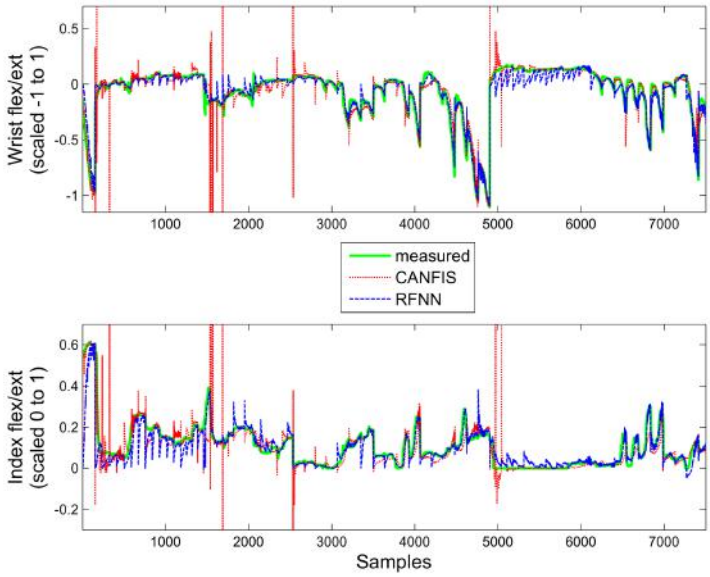

Figure 8.7: No feedback training results - Subject 1.

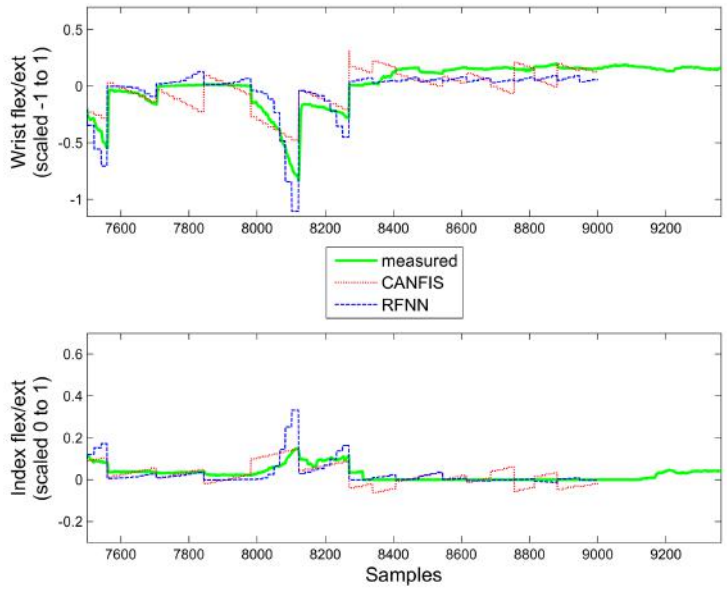

Figure 8.8: No feedback validation results - Subject 1.

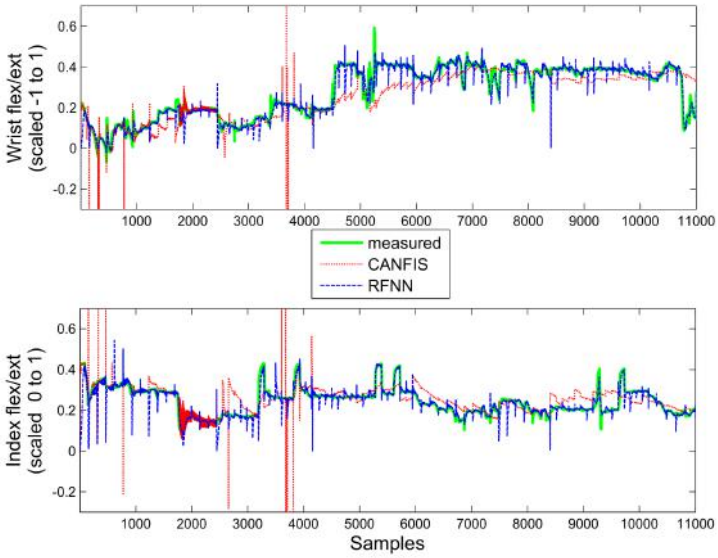

Figure 8.9: No feedback training results - Subject 2.

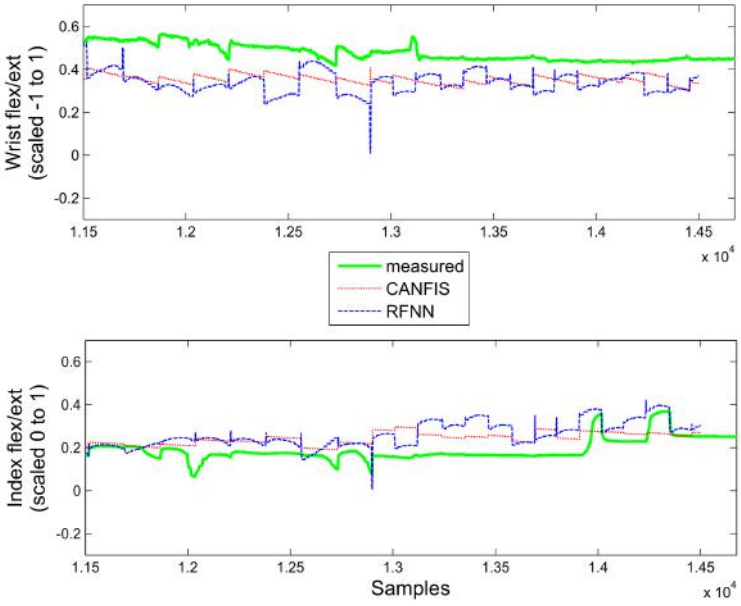

Figure 8.10: No feedback validation results - Subject 2.

were small and dependent on subject and output type in the case of validation period.

Table 8.1: CANFIS MSE - no feedback approach

Subj.	Wrist	Thumb	Index	Middle	Ring	Little
			Training			
1	1.0166	0.0154	1.0665	0.0160	0.0625	0.5526
2	0.0796	0.3702	2.2323	4.923	0.7771	4.2618
			Validation			
1	0.0143	0.0004	0.0012	0.0001	0.0035	0.0058
2	0.0169	0.0005	0.0056	0.0004	0.0009	0.0015

Table 8.2: RFNN MSE - no feedback approach

Subj.	Wrist	Thumb	Index	Middle	Ring	Little
			Training			
1	0.0041	0.0004	0.0031	0.0011	0.0014	0.0017
2	0.001	0.0009	0.0013	0.0038	0.0004	0.0018
			Validation			
1	0.0123	0.0005	0.0014	0.0003	0.0005	0.0034
2	0.0238	0.0003	0.0082	0.0024	0.0003	0.0059

8.3.2 Wrist feedback approach

Training the CANFIS and RFNN systems with the wrist feedback resulted in the behavior shown in Figures 8.11 and 8.12 for Subject 1, which represent training and validation periods respectively. Similarly, Figures 8.13 and 8.14 represent training and validation periods for Subject 2. Once more, the training data was approximated by both approaches on both subjects, and peak values produced by CANFIS had lower values than in the previous case. Regarding the validation period, worse predictions than in the previous case were observed. None of the both approaches captured the system characteristics properly, specially the CANFIS case, which for Subject 2 predicted values above the maximum scaled value 1.

Tables 8.3 and 8.4 show the MSE of the scaled values of CANFIS and RFNN results respectively. Once again, peak values of CANFIS in the learning

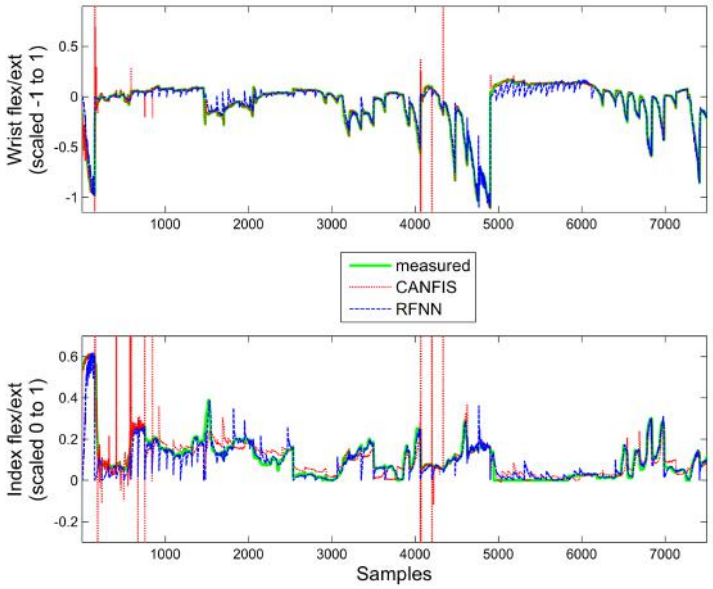

Figure 8.11: Wrist feedback training results - Subject 1.

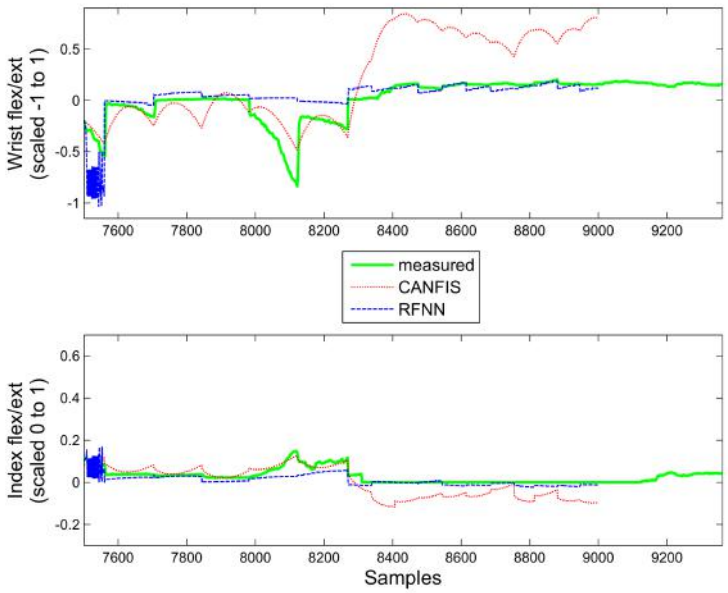

Figure 8.12: Wrist feedback validation results - Subject 1.

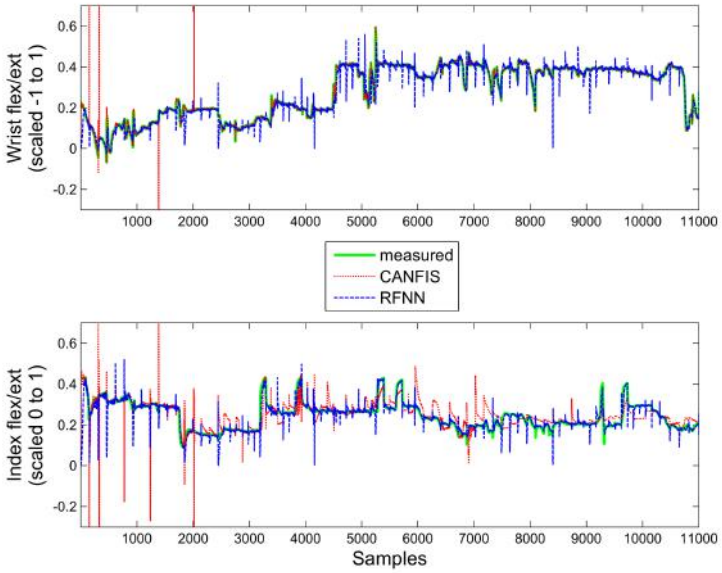

Figure 8.13: Wrist feedback training results - Subject 2.

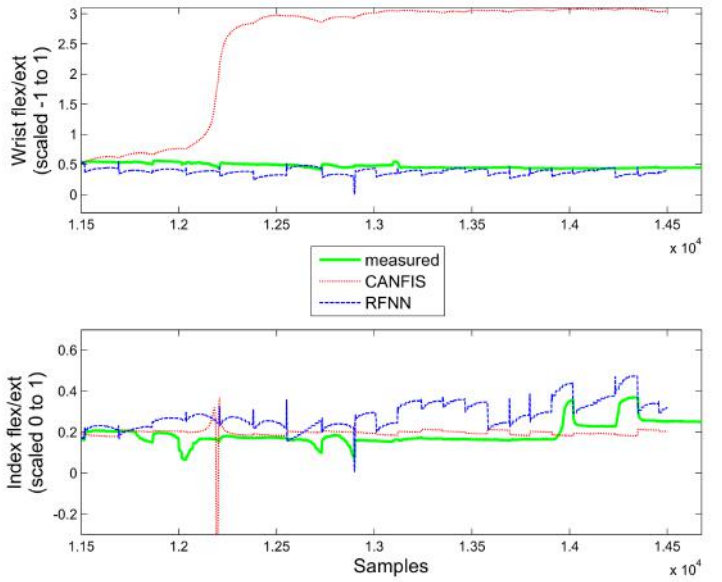

Figure 8.14: Wrist feedback validation results - Subject 2.

period resulted in higher MSE than RFNN. In the validation period, RFNN showed smaller MSE values for all outputs and both subjects, however, as already mentioned, it was not able to capture the system characteristics as well as in the previous case.

Table 8.3: CANFIS MSE - wrist feedback approach

Subj.	Wrist	Thumb	Index	Middle	Ring	Little
			Training			
1	0.0108	0.0634	0.5291	0.2514	0.1791	0.1721
2	0.0007	0.0024	0.2550	1.3505	0.2805	1.5714
			Validation			
1	0.1411	0.0036	0.0028	0.0003	0.0024	0.0061
2	4.96	0.1113	0.0041	0.0050	0.0228	0.0535

Table 8.4: RFNN MSE - wrist feedback approach

Subj.	Wrist	Thumb	Index	Middle	Ring	Little
			Training			
1	0.0029	0.0003	0.003	0.001	0.0011	0.0016
2	0.001	0.0008	0.0011	0.0032	0.0004	0.0016
			Validation			
1	0.0356	0.0005	0.0008	0.0002	0.0004	0.0045
2	0.0136	0.0004	0.0126	0.0067	0.0005	0.0082

8.3.3 Membership functions

As mentioned in the previous section, membership functions were initialized uniformly distributed along the input space, and they were modified during training. Means and standard deviations of gaussian functions were adjusted in order to adapt to the specific subject. This type of information could bring clues and knowledge about the system that was being analysed. As an illustration, the resulting 10 membership functions for each input after training with RFNN and CANFIS are shown in Figures 8.15 and 8.16 respectively. Both correspond to Subject 1 and no feedback approach, however, results were similar with the other subject and other approach.

Membership functions tend to expand in order to wrap those values which lead to similar results. They tend to become narrower to differentiate between

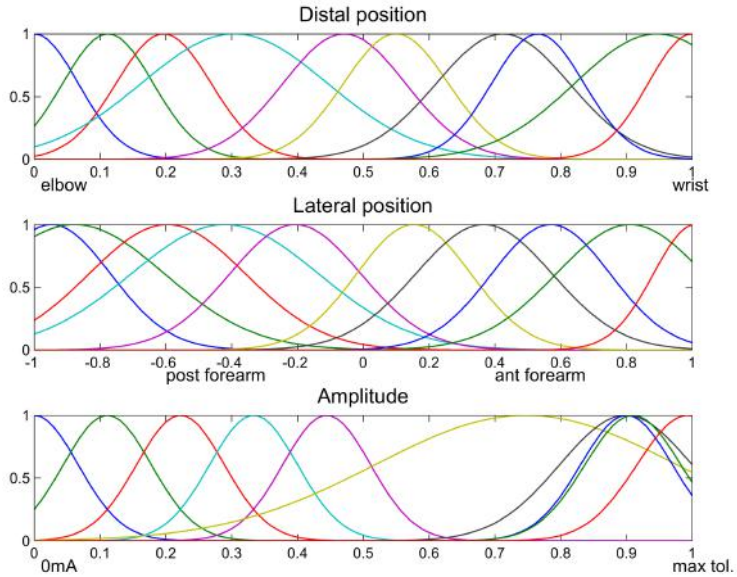

Figure 8.15: Membership functions after RFNN training for Subject 1 and no feedback approach.

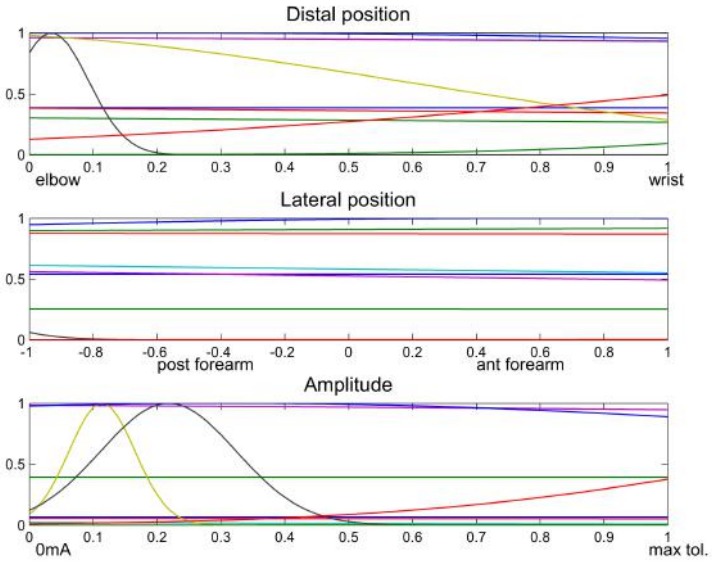

Figure 8.16: Membership functions after CANFIS training for Subject 1 and no feedback approach.

values that lead to distinct rule results. Thus, analyzing the membership functions of Figure 8.15, we could point out or extract few conclusions. For example, one of the membership functions that represented distal position extended almost from elbow to middle forearm, which could mean that similar movements were achieved when any field located in this area was active. The lateral position showed similar behavior on the posterior forearm side. Conversely, membership functions that represented distal position from middle forearm to wrist and lateral position on the anterior forearm became slightly narrower. This fact could tell us that Subject 1 had higher selectivity of FES-induced movements on the anterior forearm rather than on the posterior side, and on the distal part of the forearm rather than on the proximal part. In the case of stimulation amplitudes, different membership functions merged and became narrower around 0.9, which could indicate the motor threshold of the subject. Conversely, one of the membership function became very wide, representing the lack of movement that was common to lower amplitude values. It should be noted that membership functions that represented amplitudes from 0 to 20mA (0-0.5) did not change because those values were not present in the data used for training, therefore, membership functions remained unchanged as in initialization.

However, if Figure 8.16 is analyzed, we can see a completely different behavior. After training with CANFIS, some of the membership functions expanded to such an extent that gaussian shape could not be observed anymore. This effect was present in both subjects and both feedback approaches. So, although CANFIS was able to predict training and validation data up to some degree, the membership function modifications after training, lack linguistic (or fuzzy) meaning. Thus, no information could be extracted from these membership functions. This effect could be a result of bad parameter fitting or initialization of membership functions. In any case, CANFIS presented the same behavior for both subjects and both approaches.

8.4 Discussion

The aim of the work presented in this chapter was to check the feasibility of using a hybrid neuro-fuzzy system for modeling FES-induced hand movements, more specifically, the model aimed at predicting finger and wrist flexion/extension positions from stimulation parameters and a spatial application site. Two neuro-fuzzy systems, CANFIS and RFNN, and two feedback approaches were tested on these preliminary results, and showed promising results. Both systems were able to approximate training data to some extent, although worse results were found in the validation case, specially for Subject 2. Inclusion of an additional input consisting of wrist feedback led to an improvement on training data, but it resulted in increased validation errors, specially for

Subject 2. This effect was the opposite to what was expected, as we faced a dynamic problem and thus, expected an overall improvement when previous output information was added as an input. However, it could be an effect caused by the increase of the structure, which involved a difficulty in the learning stage because more parameters needed to be tuned; or an overtraining effect, where adding an output feedback led to better tuning the parameters for training data and less generalization occurred. Indeed, for both approaches, the presence of noise or small voluntary movements when no stimulation was applied, could have disturbed the training of the model and affected performance.

When comparing both neuro-fuzzy systems, there was a difference in the training data, where CANFIS showed high peaks in all cases, which led to higher MSE than RFNN. For the validation data, there were no so clear differences on the approach without feedback, but with wrist feedback, the RFNN showed better results, specially with Subject 2, where values predicted by CANFIS exceeded the maximum scaled limits. Moreover, the membership functions that resulted from training with the RFNN could be used for extracting some general information of the system, whereas those membership functions obtained with CANFIS lacked linguistic meaning.

Summing up, these preliminary results showed that hybrid neuro-fuzzy systems were able to learn main characteristics from data recorded in two stroke subjects, and could construct membership functions from which combined physiological and stimulation features could be interpreted or extracted. Regarding neuro-fuzzy system comparison, the RFNN showed more stable and slightly better overall results than CANFIS system in terms of MSE and membership functions, specially for the wrist feedback approach. The reason for this could be that the RFNN is a dynamic network that includes self-recurrences and therefore, it is more suitable for these type of dynamic nonlinear problems. These were the first steps towards neuro-fuzzy modeling of FES-induced hand movements, hence, still much work needs to be done in terms of deeper testing and analyzing different methods and aspects of neuro-fuzzy systems for the presented application.

The most significant results of the work described in this chapter were presented in the XXXVI Jornadas de Automática [163] and in the 9th IFAC Symposium on Biological and Medical Systems [164].

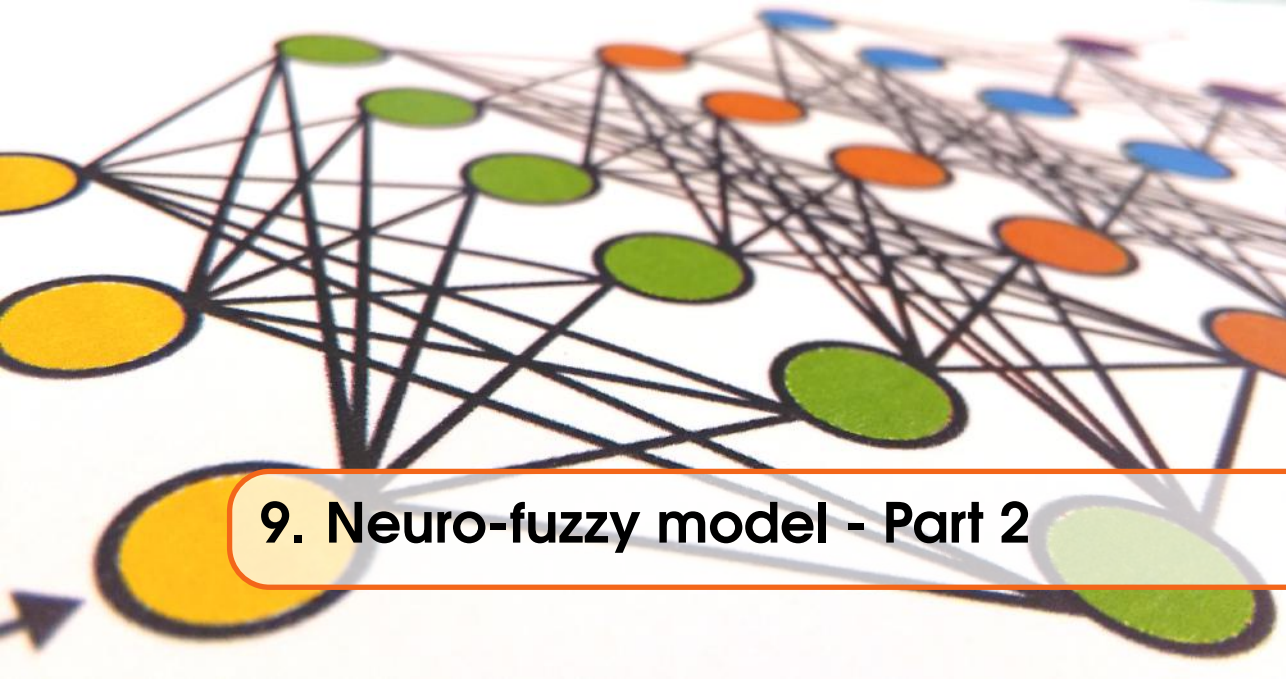

9. Neuro-fuzzy model - Part 2

In the previous chapter a feasibility study was presented, which showed the capacity of neuro-fuzzy systems to approximate FES-induced hand movements of stroke subjects. However, the aim of these models was to support the design process of subject-specific forearm surface neuroprostheses, as well as to provide a basis for development of new control techniques. Therefore, the reliability and accuracy of the models should be high and they should adapt to different types of subjects and physiologic characteristics. In order to achieve this, still many aspects of neuro-fuzzy models of FES-induced movements should be tested. In this chapter, the RFNN system that showed the best results in the previous chapter was further analyzed and tested with two different learning methods. The data collected from three stroke subjects and three healthy subjects was used in order to have a heterogeneous subject sample. Data collection was again carried out in collaboration with the ADACEN center.

9.1 Materials

As in the previous set of experiments, the materials include a FES system and a sensor system for measuring wrist and finger flexion/extension, which were fully controlled by a custom-made GUI built on Matlab Software.

9.1.1 FES system

The FES device that we used in these experiments was the *Fes:a* device shown in Figure 9.1. This stimulator was a wireless single channel electronic with

included 32 channel demultiplexer stimulator that provided current-regulated biphasic stimulation pulses. The output ranges were from 0 mA to 100 mA for amplitude, from 0 Hz to 100 Hz for frequency, and from 0 µs to 500 µs for pulse-width. It could be controlled through the incorporated touchpad or remotely via Bluetooth.

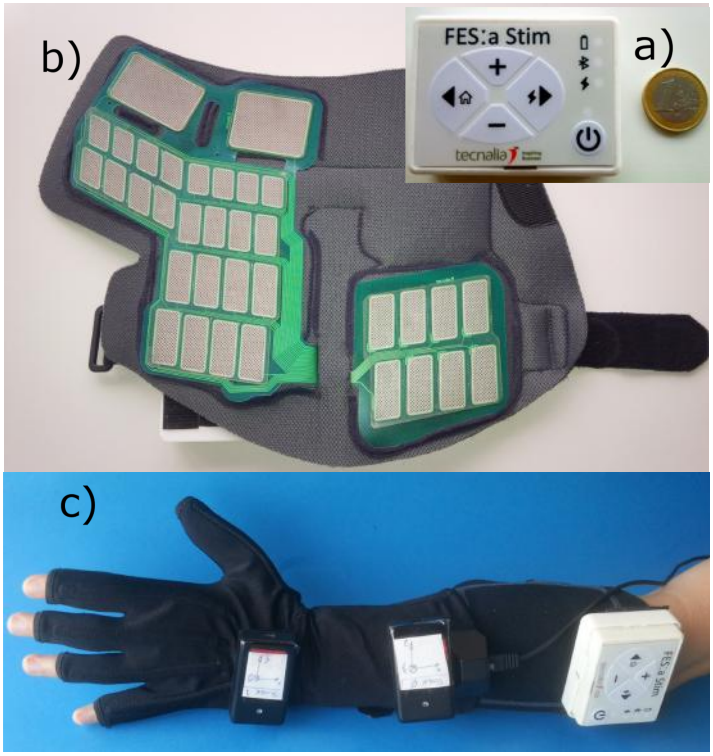

Figure 9.1: *Fes:a* system: a) stimulator, b) garment and electrodes, and c) full system donned, including sensors.

The *Fes:a* stimulator was able to control up to two 16-field IntFES electrodes (32 fields in total), and as with the stimulators described previously, amplitude and pulse-width of each field could be independently controlled. For these experiments a pseudo-matrix electrode formed by 32 fields and two return electrodes, based on the regular matrix described in chapter 5, was designed to be embedded into a garment, as shown in Figure 9.1b. The garment with integrated electrodes ensured proper electrode-skin contact and simplified significantly the donning process. The whole FES system together with the sensor system is shown in Figure 9.1c.

9.1.2 Sensor system

The sensor system for measuring hand and finger flexion/extension was the same as the one described in the previous chapter. An instrumented glove was used for measuring flexion/extension of fingers, and two inertials sensors were used for measuring wrist flexion/extension as shown in Figure 9.1c. The details of the system are given in the previous chapter. Data were recorded at a sampling frequency of 10Hz.

9.2 Methods

The objective of this set of experiments was to further analyze the performance of a RFNN system for modeling FES-induced hand movements in subjects with different characteristics. For this purpose, FES-induced hand movement data was collected from three healthy subjects and three chronic acquired brain injury subjects. The model was trained with different parameters, different structures and different learning methods and their effect was analyzed. The protocol for the data acquisition session was approved by ADACEN and all participants signed an informed consent.

9.2.1 Subjects

Data from three healthy subjects and three chronic acquired brain injury subjects were collected in order to test the model with an heterogeneous group. The three chronic acquired brain injury patients were suffering from a left hemiparesis. Age and time from injury of all is summarized in Table 9.1.

Table 9.1: Subjects

Subject	Gender	Age	Brain injury cause	Time from injury
1	Female	27	- (healthy)	- (healthy)
2	Male	29	- (healthy)	- (healthy)
3	Male	38	- (healthy)	- (healthy)
4	Male	53	Trauma	4 years
5	Female	65	Stroke	4 years
6	Female	61	Stroke	10 years

All the participants were familiar with FES, as each of them had received at least 60 hours of electrical stimulation during the month prior to the data collection session.

9.2.2 Main session

The data acquisition was carried out in one session of approximately 45 minutes overall duration. The parameters during the whole session were set to 25 Hz frequency and 200 µs pulse-width. The first stage consisted in donning the electrodes and sensor system on the subject's arm, where the garment was attached taking the ulna as a reference. Then the instrumented glove was donned. Figure 9.1c shows the arm of a subject after the donning phase. After the donning, the calibration stage took place, which was the same procedure as the one described in detail in the previous chapter. The subject was seated in a chair and rested his arm on top of a table with an elbow angle of 90 degrees. The forearm was rested on a pillow and was kept in neutral position throughout the whole experiment. Finally, PROM and AROM values were recorded, followed by maximum tolerated amplitudes for posterior and anterior parts of the forearm.

In the data collection stage the subject was asked to not make any voluntary movements and to relax the forearm and hand while the forearm was kept in neutral position. The stimulation consisted of repeated random activation of the 32 electrode-fields with different amplitude patterns shown in Figure 9.2 to cover the full range of amplitudes (0 mA to maximum amplitude tolerated by each subject), including both ramps and steps.

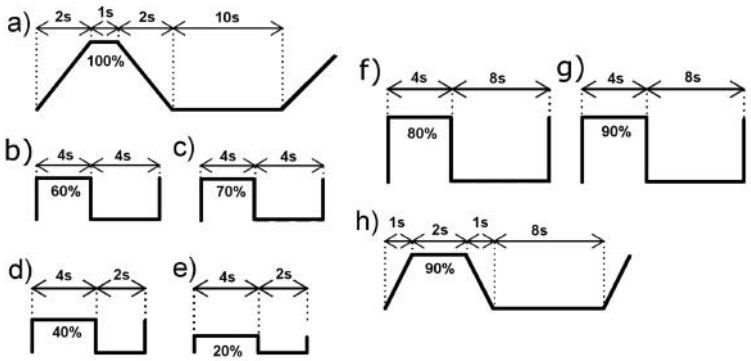

Figure 9.2: Amplitude patterns applied in the data acquisition session.

The amplitude patterns are represented in percentages with respect to the maximum amplitude tolerated by the subjects. Resting periods, also shown in Figure 9.2, were introduced between stimulation periods in order to avoid fatigue affecting the experiment. Data corresponding to stimulation patterns from Figure 9.2a to 9.2g were used for training, whereas data obtained by

applying the pattern shown in Figure 9.2h were used for testing. If the subjects indicated discomfort with a specific field, stimulation was immediately stopped and the session continued with the activation of the next field.

9.2.3 Data

The input/output approach was the same as the one presented in the previous chapter, consisting of three inputs and six outputs. The inputs represented the amplitude and the spatial coordinates on distal and medial dimensions, as shown in Figure 8.6, and the six outputs were the flexion/extension of the wrist and five fingers. However, in the experiments carried out on the previous chapter we realized that noise or small movements made during the resting periods could be affecting the learning process. Therefore, this time, data recorded by sensors were preprocessed before the training was carried out. First, all values were scaled to PROM values, and then, a smoothing of the signal with a moving average window of 9 samples was carried out. Finally, as our main concern was the behavior of the system when stimulation was applied, the offset or values at the resting periods were removed. Like this we focused on the stimulation periods and avoided noise or small movements happening at resting periods to disturb the training of the model. As a result, the six outputs were held in the -1 to 1 range, where negative and positive values represented extension and flexion positions respectively. An example of the result of this process is shown in Figure 9.3.

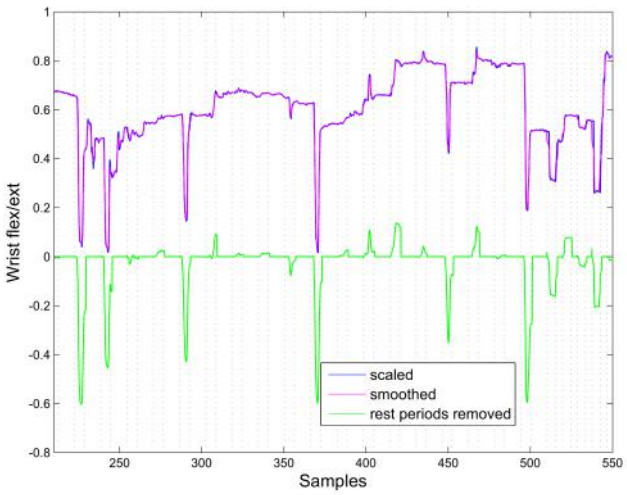

Figure 9.3: Data preprocessing example, showing scaled, smoothed and final data with resting periods removed.

9.2.4 Model training

Based on the results from previous chapter, the RFNN system was chosen for training. The previously presented RFNN was tested with different structure approaches for each subject. These involved different numbers of fuzzy terms, different feedback approaches and combinations of them. The aim of making this analysis was to find the best structure of the RFNN for modeling FES-induced hand movements of subjects with different characteristics.

Regarding number of fuzzy terms, in the RFNN, like in the previously described fuzzy systems, each of the inputs was defined by a number of fuzzy terms, which, in this case, were represented by gaussian membership functions. 3 to 7 numbers of fuzzy terms were tested in this case. The lower limit was set to 3 because clearly different behavior is present in at least three stimulation areas on the forearm. These are the posterior forearm, the radial part and the anterior forearm, which present different neuromuscular anatomy as described in chapter 2. The upper limit was set to 7 because we thought that 7 fuzzy terms were enough to describe each of the three inputs: amplitude, distal position and medial position. Higher number of fuzzy terms significantly increase the network structure, number of parameters and computational cost. Regarding the feedback approaches, as in the previous chapter, we assumed that providing the system with additional inputs with previous output information would improve or support the RFNN results because we were dealing with a dynamic application. However, adding a feedback for each of the outputs implies a big increase on the network structure, number of parameters and computational cost. Therefore, we decided to test the RFNN with a limited amount of feedback combinations that included wrist, index and ring finger feedbacks. This selection was done taking into account the independence of the digits and wrist [165]. Seven feedback approaches were tested in total, which implied: one with no feedback, three with a single feedback (wrist, index, ring), two with two feedbacks (wrist and index, wrist and ring) and one with three feedbacks (wrist, index and ring). Figure 9.4 shows the general schemes of training and validation stages with the feedback approach. Thus, the 35 different combinations of numbers of fuzzy terms and feedback approaches were tested with each subject.

Finally, apart from the effect of structure parameters, the learning method was also analyzed. BP based on gradient descent is a commonly used learning algorithm because of its simplicity and low computational cost. However, it can miss the optimal solution by being stuck in a local minimum [133]. Therefore, and due to the success of the combination of RFNN and DE in other applications [166, 167], we decided to carry out the training for all the cases and all the subjects with both BP and DE learning strategies.

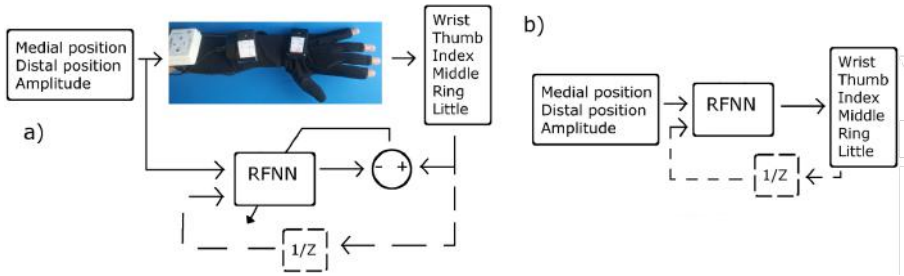

Figure 9.4: Schemes for a) training and b) validation.

9.3 Results

The model performance was evaluated with two complementary values. First of them was the average MSE value of the six outputs, and the other one was the success rate value. The success rate value was defined as the percentage of successful predictions over all the stimulation periods, and it was obtained by comparing the maximum/minimum values of the peaks/valleys resulting from each stimulation period to their corresponding predicted values. A successful prediction was assumed when the absolute error between the recorded and the predicted peak/valley values was less than 5% of the output range.

9.3.1 Backpropagation

BP was carried out with learning rate $\eta = 0.01$ and 100 epochs for all the cases, determined in preliminary qualitative tests where most subjects were found to converge towards the desired behavior. Membership functions were gaussian functions and they were initialized uniformly distributed along the input space for all cases as well.

For space issues, the results of the 35 cases for each of the six subjects cannot be shown. However, an example of an intermediate case is shown in Figures 9.5 and 9.6, which correspond to Subject 4 (brain injured subject) when the RFNN was trained with 3 fuzzy terms and wrist and ring finger feedback, resulting in a training success rate of 99.65% and validation success rate of 80.56%. Figure 9.5 shows a portion of the training data, where the recorded data and predicted outcomes are shown, with green circles representing successful predictions of each stimulation period and red crosses representing unsuccessful ones. Similarly, Figure 9.6 shows the validation results. If we analyze the figures qualitatively, it can be noted that for the selected subject and case, training data were successfully approximated by the RFNN for most stimulation periods. However, the model failed to correctly predict the response of the middle, ring and little fingers for some stimulation periods for validation data.

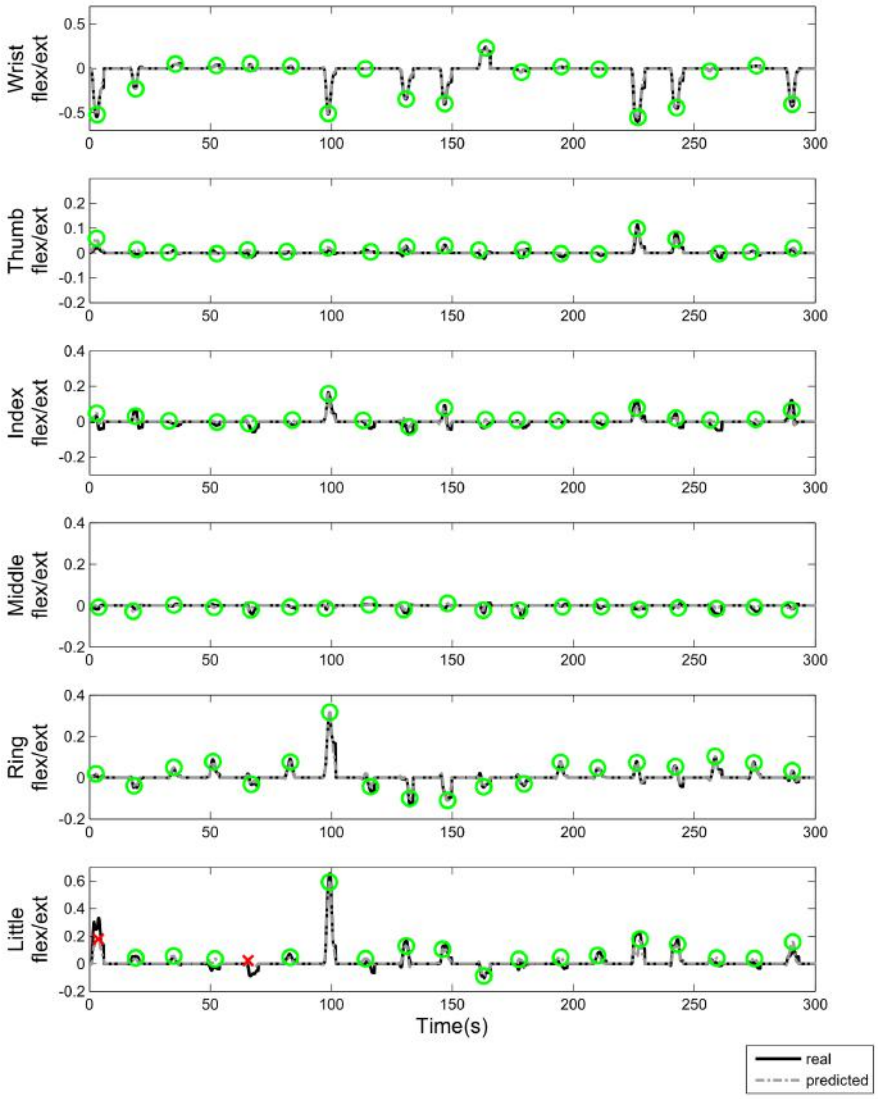

Figure 9.5: BP training results – Recorded vs. Predicted outcomes for 3 fuzzy terms and wrist+ring feedback case for Subject 4. Successful predictions are represented with a green dot and not successful ones with a red cross.

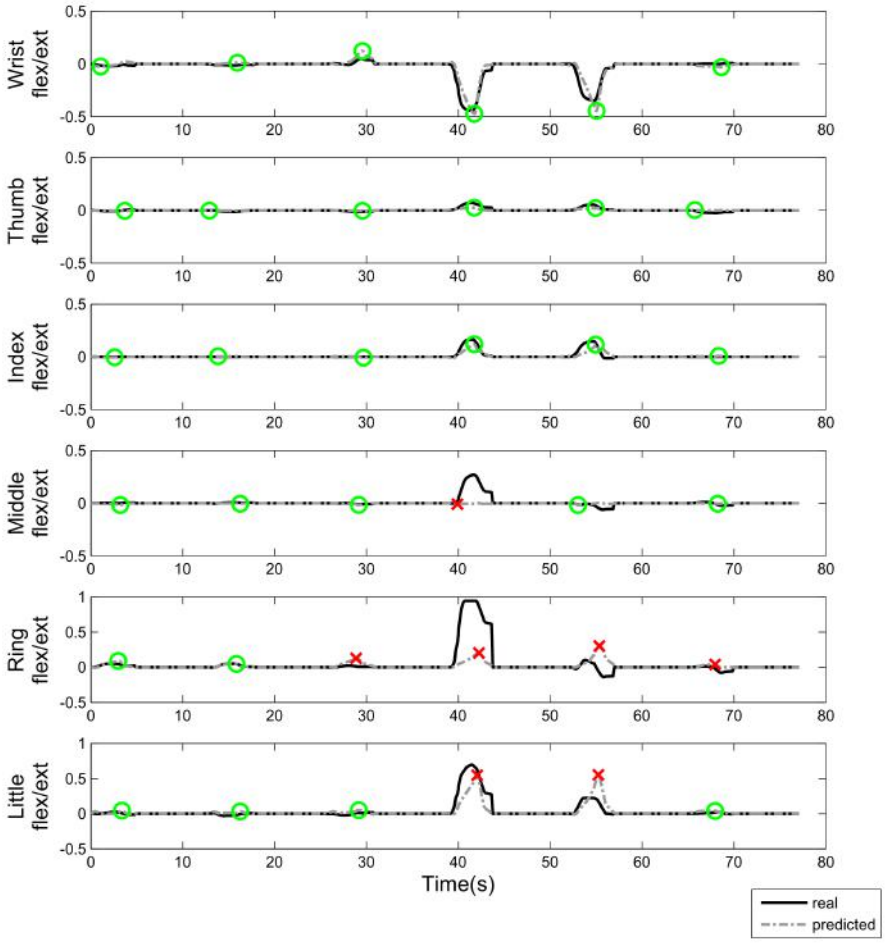

Figure 9.6: BP validation results – Recorded vs. Predicted outcomes for 3 fuzzy terms and wrist+ring feedback case for Subject 4. Successful predictions are represented with a green dot and not successful ones with a red cross.

Table 9.2 summarizes the results obtained in the 35 cases by showing mean, best and worst average MSE, and success rates for each of the subjects. This table only shows the results for the validation data. Regarding the training data, mean success rates for the 35 cases of the six subjects were in the range 87.81%-99.68%, best cases in the range 92.84%-100% and worst cases in the range 78.26%-99.21%.

Table 9.2: BP validation results

	Subjects	**Mean**	**Best case**	**Worst case**
Average MSE	1	0.00464	0.00301	0.00879
	2	0.00153	0.00049	0.00353
	3	0.00081	0.00028	0.00255
	4	0.00846	0.00592	0.01099
	5	0.00018	0.00003	0.00147
	6	0.00787	0.00228	0.02384
Succes Rate	1	61.75%	77.78%	44.44%
	2	90.63%	97.22%	83.33%
	3	92.70%	97.22%	83.33%
	4	80.48%	88.89%	75%
	5	98.65%	100%	91.67%
	6	60.32%	88.89%	30.56%

At a first glance, it can be observed that there was a high variation in the average MSE values and success rates across different subjects. Four subjects showed successful results with mean success rates comprised between 80.48% and 98.65%, best success rates between 88.89% and 100% and worst success rates between 75% and 91.67%. However, poor results were obtained for Subject 1 and Subject 6, which were a healthy and a brain injured subject respectively and resulted in mean success rates of 61.75% and 60.32% respectively. Best success rate for Subject 1 was 77.78%, corresponding to four fuzzy terms and no feedback case, and worst success rate was 44.44% corresponding to three fuzzy terms and wrist and index feedback. Similarly, Subject 6 achieved the best success rate of 88.89% in the seven fuzzy terms and ring feedback case, and the worst success rate of 30.56% for the five fuzzy terms and wrist feedback case.

For analyzing the effect of the number of fuzzy terms, a non-parametric Friedman test was carried out for each of the subjects. The purpose was to find if there were statistically significant differences among the validation average MSE values obtained by training the RFNN with different numbers of

fuzzy terms. Significance level was set to $\alpha = 0.05$ and for post-hoc analysis the Bonferroni correction method was applied. Figure 9.7 shows the average MSE values of each subject grouped by number of fuzzy terms in a boxplot configuration. Significant differences between groups were only found in two of the subjects, in which the performance was completely opposite. One of them presented lower average MSE values with less fuzzy terms, whereas the other one showed the opposed effect.

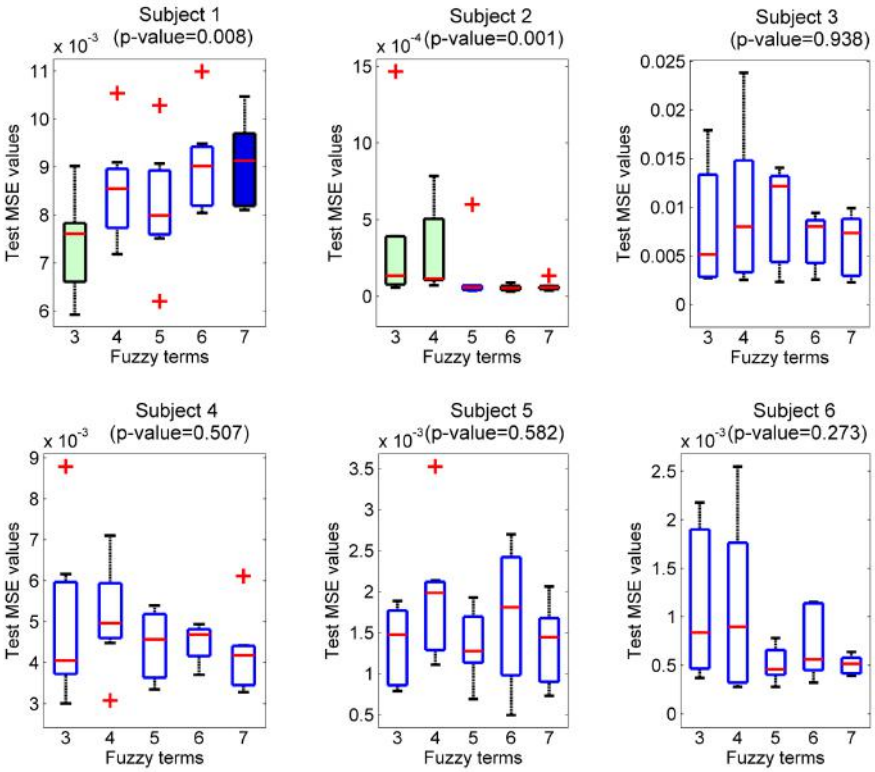

Figure 9.7: BP validation average MSE grouped by fuzzy terms. Significantly different groups are represented with different colors.

A similar procedure was carried out to find if there were statistically significant differences among the different feedback approaches. Figure 9.8 shows the validation average MSE values of each subject grouped by feedback approaches. Significant differences between groups were found in five out of six subjects by the Friedman test. However, in some cases the Bonferroni correction method was too conservative to find which groups were statistically different. This was probably due to the small data sample and the high number of groups to be compared. Nevertheless, it can be easily seen that there are differences in the

average MSE values across different groups. However, these did not follow a common trend across different subjects. Indeed, feedback approaches which resulted in low average MSE values in some subjects resulted in high average MSE values in others.

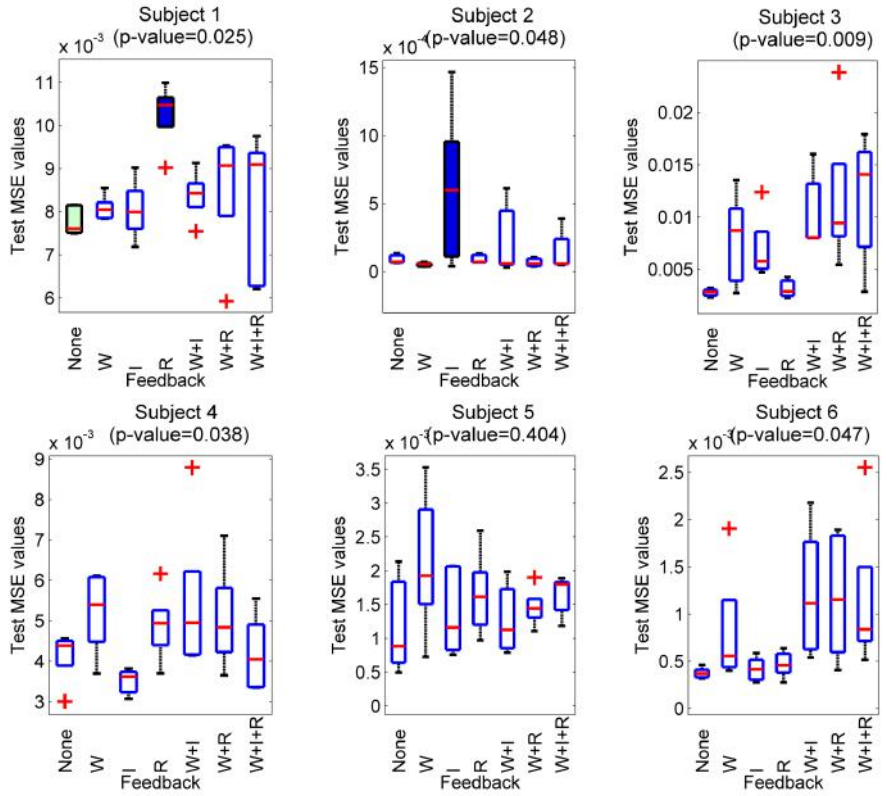

Figure 9.8: BP validation average MSE grouped by feedback approaches, with W=wrist, I=index and R=ring. Significantly different groups are represented with different colors.

Finally, the difference in performance between healthy and brain injured subject groups was analyzed by carrying out a Kruskal-Wallis analysis on validation average MSE values. The result showed a significant difference between both groups, showing lower validation average MSE errors on the healthy group than on the brain injured subject group as it is shown in Figure 9.9.

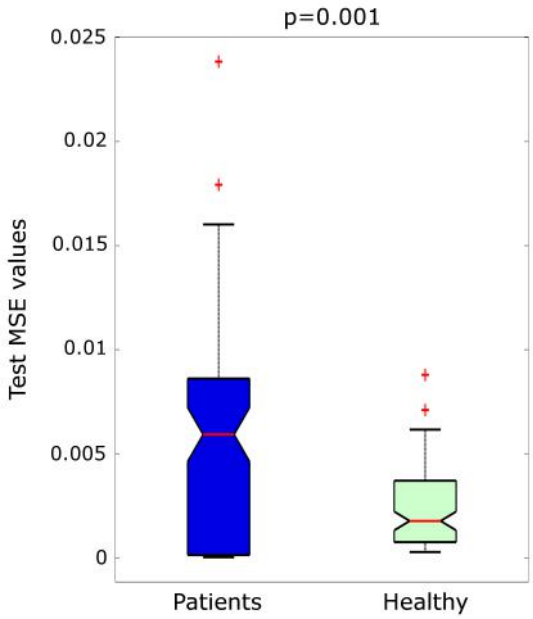

Figure 9.9: BP validation average MSE grouped by subject type.

9.3.2 Differential Evolution

Same analysis as the one with BP was carried out with DE training strategy. However, due to computational costs and memory requirement issues, only the cases comprising 3 to 5 fuzzy terms were analyzed, which reduced the number of cases from 35 to 21. An increase of fuzzy terms resulted in a larger structure and higher number of parameters to be tuned. As the DE is based on populations of parameter vectors, it turned out to be a problem for high numbers of fuzzy terms. However, additional inputs corresponding to different feedback approaches did not increase the number of parameters so much, so all the feedback approaches were tested. The DE training parameters for all the cases were set as $F = 0.7$ and $C_r = 0.9$, population size was set to 80, the number of epochs was 100, and the DE strategy chosen was the DE/target-to-best/1/bin, which usually converges faster than the most classical version of DE [139]. Two cost functions were used in this DE: the average MSE value and the failure rate. The failure rate was the opposite of the success rate, and the selection was carried out as

$$X_{i,new} = \begin{cases} U_i & \text{if} \quad mse(U_i) \leq mse(X_i) \quad \text{and} \quad failrate(U_i) \leq failrate(X_i) \\ X_i & \text{otherwise} \end{cases}$$

(9.1)

where, *mse* and $failrate$ were the MSE and failure rate cost functions respectively.

Unlike BP, DE is iniatilized by a population of randomly chosen vectors of parameters. Therefore, the membership functions used were gaussian functions, but their parameters were randomly initialized with values comprising from -1 to 1. To avoid bad performance results due to a bad initialization, 10 training trials for each of the cases were carried out. So, for each of the subjects 10 training trials for each of the 21 cases were tested, resulting in 210 training trials for each of the subjects.

As an example, the same case as in the previous section is shown in Figures 9.10 and 9.11, which correspond to Subject 4 when the RFNN was trained with DE and 3 fuzzy terms and wrist and ring finger feedback, resulting in a training success rate of 95.31% and validation success rate of 77.78%. Figure 9.10 shows a portion of the training data, where the recorded data and predicted outcomes are shown, with green circles representing successful predictions and red crosses representing unsuccessful ones. Similarly, Figure 9.11 shows the validation results. If we analyze the figures, it can be noted that for the selected subject and case, predictions failed more often than with BP, specially for the validation case, where the only successful predictions corresponded to stimulation periods where no movement occurred.

Table 9.3 summarizes the results obtained in the 210 training trials for each subject by showing mean, best and worst average MSE values and success rates. This table only shows the results for the validation data. Regarding the training data, mean success rates for the total of training trials of the six subjects were in the range 83.59%-98.22%, best cases in the range 85.55%99.21% and worst cases in the range 82.03%-97.75%.

Like in the previous case, it can be observed that there was a high variation in the average MSE values and success rates across different subjects. Five subjects showed acceptable results with mean success rates comprised between 74.79% and 97.35%, best success rates between 83.33% and 100% and worst success rates between 61.11% and 97.22%. However, Subject 1 got slightly lower results, with mean success rate 65.19%, best success rate 72.22% and worst success rate 61.11%. Although in general, performance was a bit lower than with BP, there were no extremely bad cases as we found with BP, with 30.56 and 44.44% success rates.

As in the previous section, a non-parametric Friedman test was carried out for each of the subjects to analyze the effect of the number of fuzzy terms. Significance level was set to $\alpha = 0.05$ and for post-hoc analysis the Bonferroni correction method was applied. Figure 9.12 shows the average MSE values

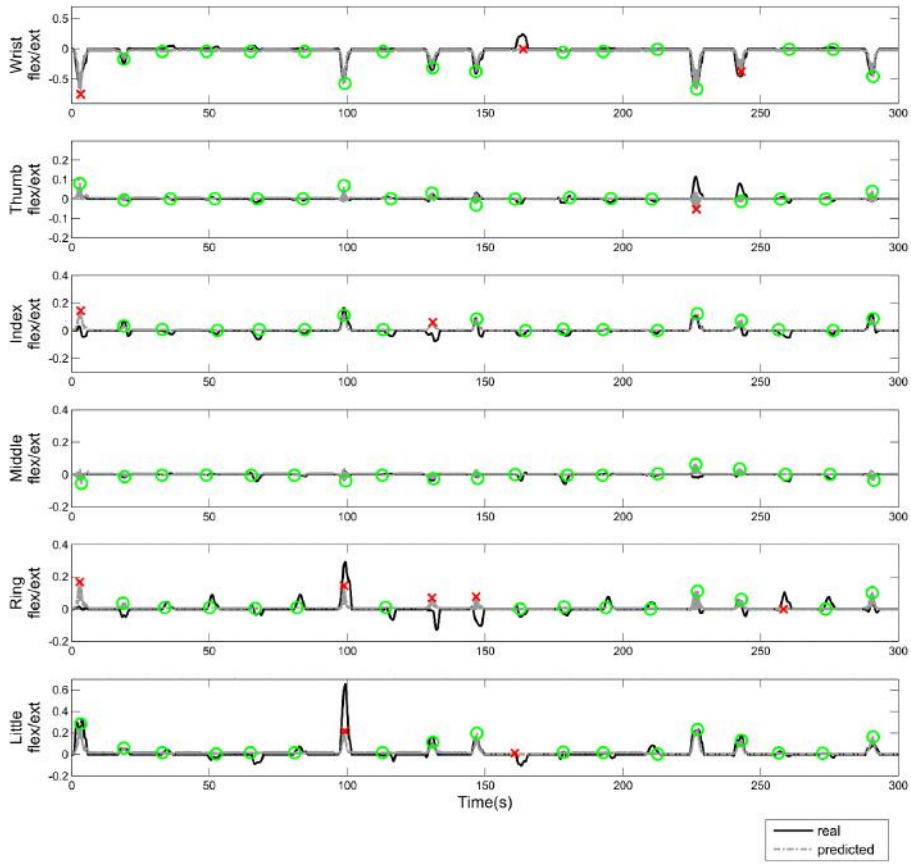

Figure 9.10: DE training results – Recorded vs. Predicted outcomes for 3 fuzzy terms and wrist+ring feedback case for Subject 4. Successful predictions are represented with a green dot and not successful ones with a red cross.

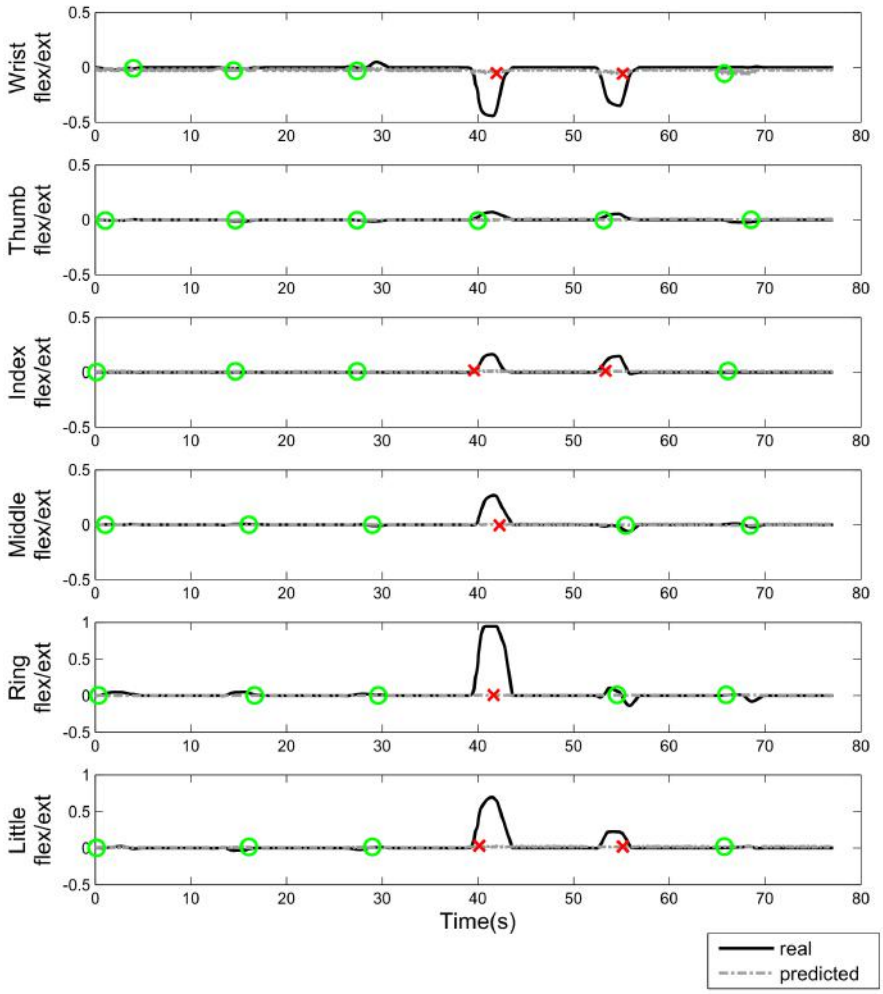

Figure 9.11: DE validation results – Recorded vs. Predicted outcomes for 3 fuzzy terms and wrist+ring feedback case for Subject 4. Successful predictions are represented with a green dot and not successful ones with a red cross.

Table 9.3: DE validation results

	Subjects	Mean	Best case	Worst case
Average MSE	1	0.00375	0.00292	0.03192
	2	0.00356	0.00264	0.00394
	3	0.00177	0.00034	0.18772
	4	0.01163	0.00713	0.22101
	5	0.00021	0.00004	0.00028
	6	0.00552	0.00378	0.04254
Succes Rate	1	65.19%	72.22%	55.56%
	2	86.04%	94.44%	83.33%
	3	92.35%	97.22%	63.89%
	4	76.36%	88.89%	66.67%
	5	97.35%	100%	97.22%
	6	74.79%	88.33%	61.11%

of each subject grouped by number of fuzzy terms in a boxplot configuration. Significant differences between groups were only found for Subject 2. The post-hoc analysis with Bonferroni correction failed to point out which groups were significantly different.

A similar procedure was carried out to find if there were statistically significant differences among the different feedback approaches. Figure 9.13 shows the validation average MSE values of each subject grouped by feedback approaches. Again, significant differences between groups were found in five out of six subjects by the Friedman test. However, the Bonferroni correction method resulted too conservative to find which groups were statistically different. This was probably due to the small data sample and the high number of groups to be compared. Nevertheless, as in the BP case, there was not a clear trend across different subjects.

Finally, the difference in performance between healthy and brain injured subject groups was analyzed by carrying out a Kruskal-Wallis analysis on validation average MSE values. The result shown in Figure 9.14 was similar to the BP case, showing a significant difference between both groups and lower validation average MSE errors on the healthy group than on the brain injured subject group.

9.3.3 Backpropagation vs. Differential Evolution

Finally, in order to compare the performance of both learning strategies, a Kruskal-Wallis test was carried out on validation average MSE and validation

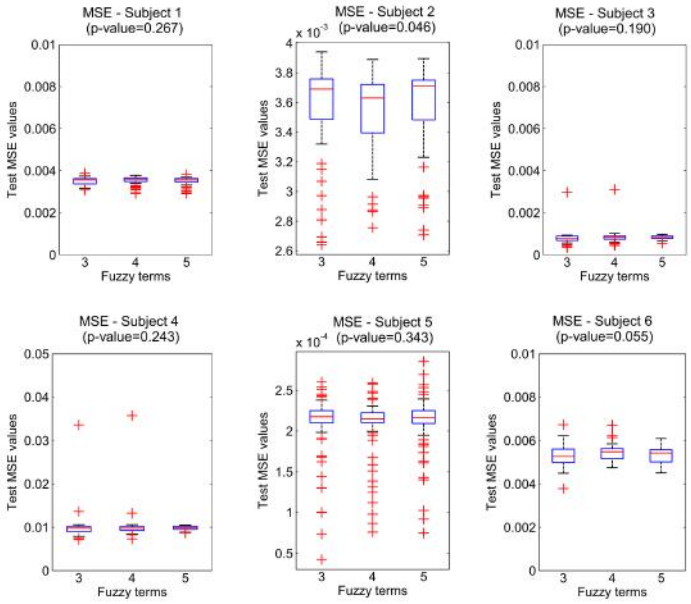

Figure 9.12: DE validation average MSE grouped by fuzzy terms.

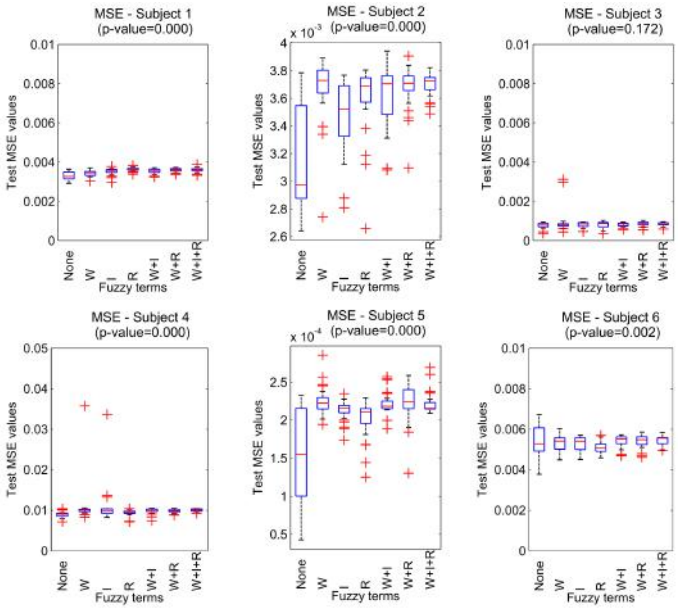

Figure 9.13: DE validation average MSE grouped by feedback approaches, with W=wrist, I=index and R=ring.

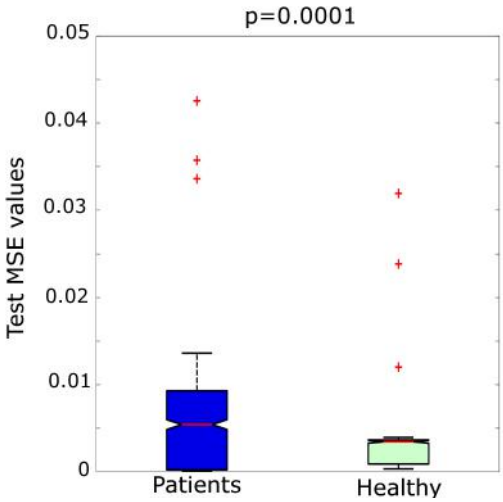

Figure 9.14: DE validation average MSE grouped by subject type.

success rate values for each subject. Results grouped by learning strategy are shown in Figures 9.15 and 9.16, where MSE and success rate values are shown respectively. Significant differences were found on most subjects between learning methods. For Subject 1 DE showed better results, but for Subjects 2, 4 and 5, BP showed better results. For Subject 3 there were no significant differences between methods and for Subject 6 a significant improvement only in success rates was found with DE.

9.4 Discussion

In this chapter, an analysis of the RFNN approach for modeling FES-induced hand movements has been presented. It has been based on data collected from three healthy and three brain injured subjects. The RFNN has been trained with different combinations of fuzzy terms and feedback approaches, as well as different learning strategies. Results obtained with both strategies showed a great inter-subject variability on the effect of fuzzy terms and feedback approaches. From this we conclude that there is not a specific structure that works best for all, as best structure parameter combinations are greatly dependent on subject-specific data characteristics. Thus, depending on the desired accuracy, a subject-specific structure parameter tuning stage is recommended to select best structure parameters for each subject. Healthy subjects got significantly lower validation average MSE values than brain injured subjects. This could be a result of the increased response to FES that is present in healthy subjects compared to brain injured subjects, which would result in a richer training data

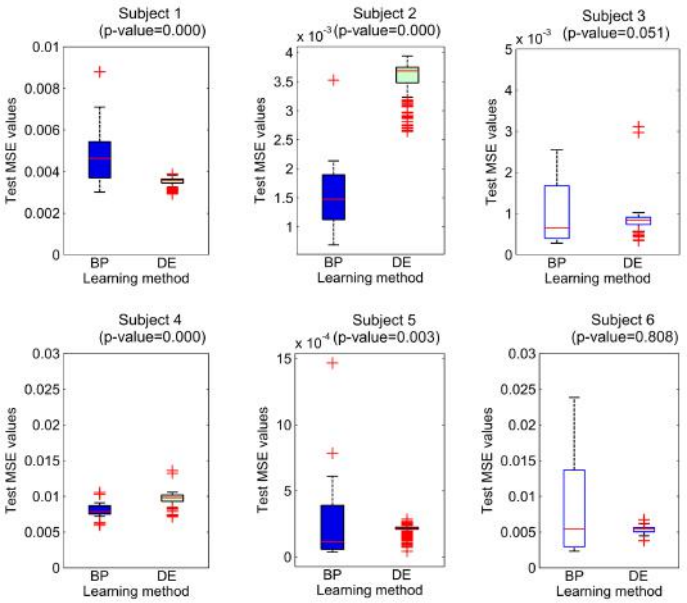

Figure 9.15: Validation average MSE grouped by learning strategy. Significantly different groups are represented with different colors.

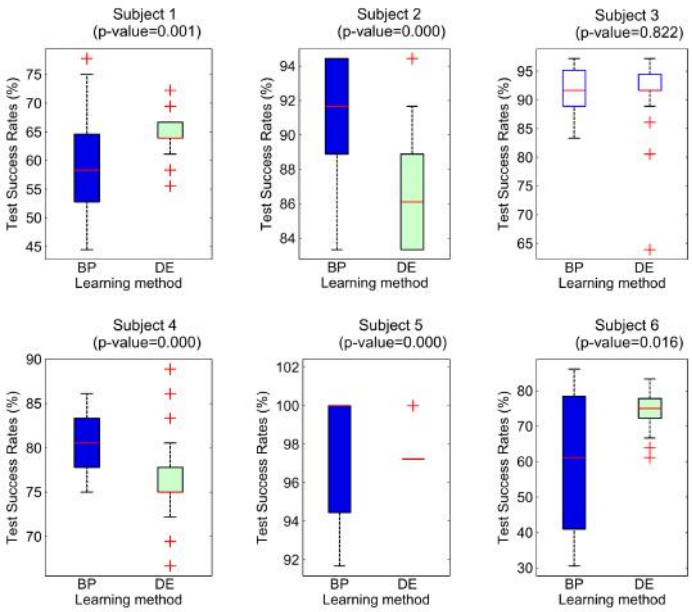

Figure 9.16: Validation success rates grouped by learning strategy. Significantly different groups are represented with different colors.

set, and thus, better results. Finally, the comparison between BP and DE showed that in most subjects BP achieved significantly better validation results than DE. However, worst cases obtained on Subject 1 and Subject 6 with BP were worse than those obtained with DE for the same subjects. The reason could be that BP converged to a local minimum in certain cases. To avoid this effect, a hybrid approach could be tested in future experiments, where DE is applied for some iterations followed by BP. Like this, advantages of both strategies may be merged.

To sum up, taking into account the complexity of the application, we can conclude that BP showed better results than DE and it is computationally less expensive, therefore it is the preferred method. Although in some specific cases poor results were obtained, all the subjects showed results with success rates on the range 77.88% to 100% in at least one of the cases with BP and 72.22% to 100% with DE. We believe that results are positive as the RFNN shows the capacity of approximating the response to FES for all subjects, which comprised two groups with completely different characteristics (healthy and brain injured subjects). Further work could include the testing of different neuro-fuzzy structures, the design of a fast parameter tuning method, a bigger subject sample or other training strategies.

The most significant results obtained with the BP approach described in this chapter were submitted to the special issue Advances in FES Modeling & Control of the peer-reviewed Medical Engineering & Physics journal [168].

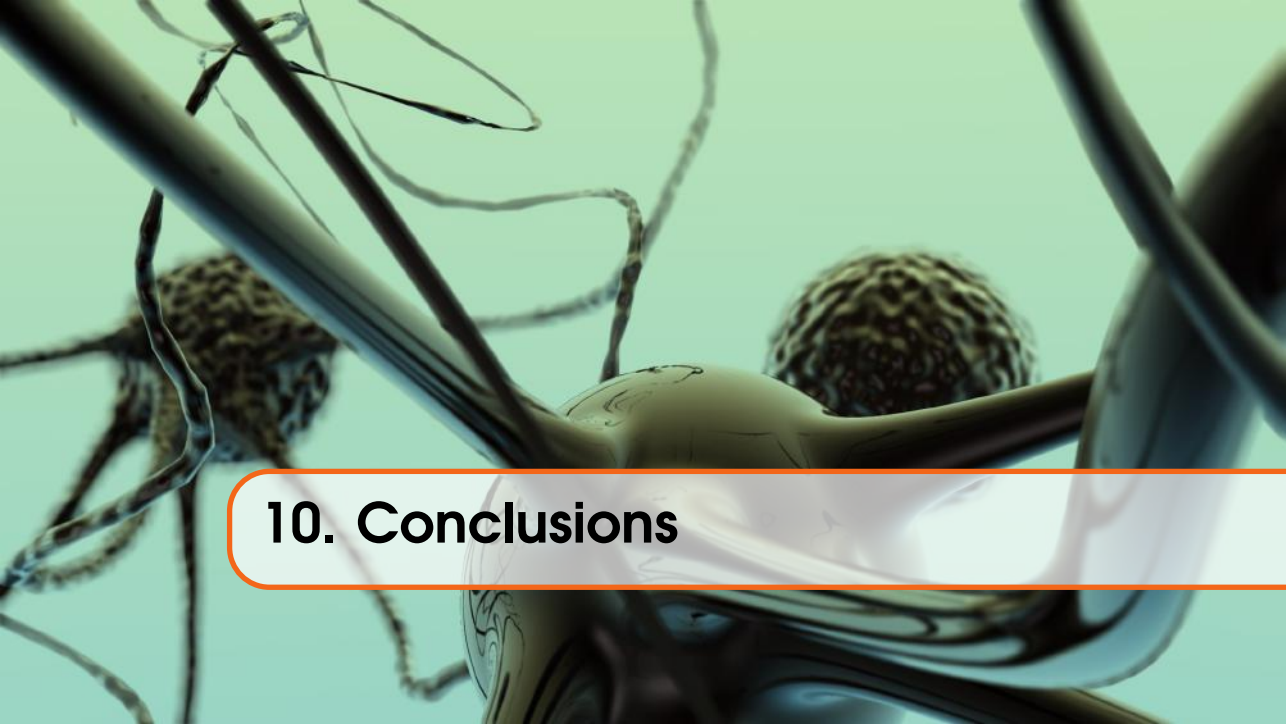

10. Conclusions

The aim of the present thesis was to apply intelligent computing techniques for modeling hand movements induced by surface FES neuroprostheses. Main challenges of the present application relate to the biomechanical complexity of the hand and wrist and the difficulty of selectively exciting the desired motor nerves by surface FES. Indeed, this selectivity issue results in an undesired excitation of afferent nerves corresponding to cutaneous receptors, which can cause pain or discomfort in some cases. For this reason, an analysis in order to find less painful stimulation methods and less painful arm areas was carried out first, followed by an analysis of using neuro-fuzzy modeling for FES-induced hand movements.

Two different experiments, described in Chapters 4 and 5, were carried out in order to analyze pain or discomfort caused by surface FES. The aim of the first experiment was to compare different stimulation methods to find the one that produces less discomfort, whereas the second experiment aimed at identifying potentially painful arm areas to the application of surface FES. The first experiment, presented in Chapter 4, was motivated by the lack of studies regarding discomfort caused by stimulation techniques that new multi-field electrodes make possible. Asynchronous and synchronous stimulation methods and different electrode-field configurations were tested and compared in order to find a method that could ensure good performance producing as lowest discomfort as possible. This was carried out by recording wrist forces and pain ratings from 15 healthy subjects while different stimulation methods and electrode-field configurations were applied. Results showed that synchronous

stimulation produced significantly higher deep discomfort than asynchronous stimulation when distant fields were activated, which limited the performance of the system, failing to reach the target in many subjects. This effect could be caused by higher current densities present on the return electrode with synchronous stimulation than with asynchronous stimulation, which could result in the activation of a bigger amount of afferent fibers corresponding to deep cutaneous receptors. On the other hand, asynchronous stimulation showed stable discomfort rates and successful attempts for all the cases. Taking into account the results, and the previously reported benefits on fatigue and selectivity of asynchronous stimulation [29, 30], we assumed that it was the best method tested so far with multi-field electrodes in terms of discomfort, so this method was used for the rest of the experiments.

After comparing different stimulation methods, the spatial distribution of discomfort caused by surface FES on the arm was studied and presented in Chapter 5. The aim of this second experiment on discomfort was to create pain-maps, which were graphical representations of pain ratings of different sites of the arm. These could point out painful spots on the arm that should be avoided or less painful spots that should be preferred for applying FES, which could be used as a reference for the design of more comfortable neuroprostheses. Subjects suffering from neural disorders such as stroke usually suffer from sensory impairments and their discomfort or pain thresholds are different to healthy subjects [39], therefore this experiment was carried out with 12 chronic stroke subjects. The experiment consisted of the application of surface FES at different sites of the arm and the recording of corresponding pain ratings for each of these areas. The inherent subjectivity of pain [72], and the high variability among stroke patient pathologies [39] resulted in a high inter-subject variability of pain-maps. Results showed no significant differences on pain ratings between fields for forearm areas, but significant differences on pain ratings between fields on upper-arm areas. This dissimilarity between forearm and upper-arm areas could come from the physiological differences between muscles that belong to lower and upper areas of the arm, where bigger muscles like biceps and triceps required higher amplitudes to generate a contraction, which could lead to higher discomfort. The most painful areas of posterior and anterior upper-arm were those located most proximally to the return electrode, and the least painful fields were those located distally from the return electrode. One of the reasons for recording significantly higher pain ratings at these fields could be that higher amplitudes were needed to achieve motor threshold when active fields were too close to the return electrode, causing discomfort. This phenomenon is caused because most of the current flows through the superficial layers of the skin, where lower impedance layers like fat are located

[7, 8], which can result in a bypass of the deeper nerves when the active and return electrodes are close. In summary, we could conclude that there were no significantly painful spots along the forearm areas for the application of FES, but there were significant pain differences between some fields on the upper-arm that could be caused by electrode configuration. It is therefore recommended to select the active fields located more distally on the upper-arm so the current is forced to go deeper in the skin. Pain maps shown in Chapter 5 do easily illustrate recommended areas for the use of FES on upper limb with the proposed electrode configuration. However, these experiments should be carried out in a bigger population to draw more relevant conclusions, and in that case they could be used as a guide or basis for future clinical or research applications and the design of more comfortable neuroprostheses.

After the discomfort analysis was carried out, experiments for checking the feasibility of using neuro-fuzzy systems for modeling FES-induced hand movements were carried out, followed by a study of the effect of different structure parameters on the performance of these models. Models of FES-subject systems are essential for designing and testing new control methods of neuroprostheses without involving patients with neurological disorders in the design loop. However, these models can be very complex to achieve analytically, specially in the case of hand movements, due to its anatomical complexity and high amount of DOF [4, 113, 169]. Therefore, an approach based on neuro-fuzzy systems was proposed and tested. The aim of the work presented in Chapter 8 was to check the feasibility of using a neuro-fuzzy approach for modeling FES-induced hand movements with surface multi-field electrodes. Two different neuro-fuzzy systems were tested and trained with data collected from two chronic stroke patients. After collecting data from both chronic stroke patients, two neuro-fuzzy systems, CANFIS and RFNN, with two different feedback approaches were trained. The aim of these models was to predict finger and wrist flexion/extension positions from stimulation parameters and spatial application site. Both systems were able to approximate training and validation data. Inclusion of an additional input consisting of wrist feedback led to an improvement on training data, but it resulted in worse validation results. This effect was the opposite to what we expected from a nonlinear dynamic system, as an overall improvement was expected when previous output information was added to the model structure. However, it could be an effect caused by the increase of the structure, which involved a difficulty in the learning stage because more parameters needed to be tuned; or an over-training effect, where adding an output feedback led to tuning the parameters for the training data and less generalization occurred. When comparing both neuro-fuzzy systems, the RFNN showed more stable and slightly better overall results

than the CANFIS system due to its dynamic character based on self-recurrences, which makes it more suitable for modeling a dynamic nonlinear system. Indeed, the membership functions that resulted from training with RFNN could be used for extracting some general information of the system or subject due to their linguistic interpretability. Thus, these preliminary results showed that hybrid neuro-fuzzy systems were able to learn main characteristics from data recorded from subjects, and could construct membership functions from which combined physiological and stimulation features could be interpreted or extracted.

After checking the feasibility of using hybrid neuro-fuzzy models for the present application, a deeper analysis of the effect of different structure parameters was carried out, which was presented in Chapter 9. The RFNN was trained with data collected from three healthy and three brain injured subjects. Different RFNN structures were trained with different combinations of fuzzy terms and feedback approaches, as well as two different learning strategies based on gradient descent and evolutionary algorithms. Results obtained with different numbers of fuzzy terms and feedback approaches showed a high inter-subject variability. From this we concluded that there was no specific structure that worked best for all, but that best structure parameter combinations were greatly dependent on subject-specific data characteristics. Model predictions of healthy subjects got significantly higher performance than model predictions from brain injured subjects, which could be caused by the increased response to FES of healthy subjects during the training data set. Finally, the comparison between backpropagation (BP) and differential evolution (DE) learning strategies showed that in most subjects BP achieved significantly better validation results than DE, and it was computationally less expensive. However, worst cases obtained with BP were worse than worst cases obtained with DE, which could be caused by eventual convergence to a local minimum with BP in certain cases. In any case, the RFNN showed the capacity of approximating the response to FES for all subjects, which comprised two groups with completely different characteristics (healthy and brain injured subjects) with best validation success rates comprised between 77.88% to 100% with BP and 72.22% to 100% with DE. However, these results were obtained with different structure parameters for each of the subjects. Taking into account the complexity of the application, the presented results were positive as a starting point. However, further work should be carried out to test other neuro-fuzzy systems or structures, other training strategies, a bigger population sample or other automatic parameter tuning methods.

In conclusion, the presented thesis has shown the possibility of using intelligent control techniques for modeling such a complex system as a surface neuroprosthesis for hand grasp. Although analytical models have been suc-

cessfully applied in other FES applications, hand movements imply additional difficulties mainly due to its dimensionality, which involves a high amount of DOF. Hybrid neuro-fuzzy approaches have shown their capacity for successfully modeling FES-induced hand movements when applied to both healthy and brain injured patients, while providing linguistically interpretable information in terms of membership functions. Hence, this work has opened a new research line that brings new possibilities to the field of surface neuroprostheses for hand grasp, where intelligent computing techniques should be further analyzed and tested in the near future in order to develop successful neuroprostheses for upper-limb neurorehabilitation purposes.

10.1 Limitations

The present work suffered from several limitations of different nature. First of all, it should be noted that the present thesis is located in the multidisciplinary neurorehabilitation area, which required not only technical skills, but also required deep understanding on different biological processes and neurological pathologies. Although advice from professionals of the medical field was taken into account, the thesis was focused more from a technical point of view, which could result in overlooking some important medical aspects unintentionally. Another limitation related to the medical implication of the thesis was the reduced number of neurologically impaired subjects involved in the experiments. Carrying out experiments that involve patients requires support from a medical/rehabilitation center or a medical/therapist team. Besides, recruitment of patients, approving clinical protocols and scheduling experiments with volunteers and clinical professionals is a long time-consuming process that disturbs both patients and clinical professionals. Therefore, few subjects were involved in these preliminary tests in order to avoid disturbing a big amount of volunteers and clinicians until a preliminary conclusion was drawn. From the technological point of view, other limitations also arose. One of the main limitations relied on the hand sensor system. In order to obtain more accurate models and analyze grasps, having a complete and reliable sensor system measuring angles of all DOF on hand and finger joints, velocities, accelerations, and forces (grasping different weight objects), would help. However, the sensor system should be wearable and fast to don/doff as well as providing enough freedom for performing different hand-movements and grasps. Moreover, the spasticity present in the hand of some neurologically impaired patients makes it even more difficult to don/doff sensors if hand opening is required. Therefore, a balance between a complete accurate sensor system and wearability should be found, which made us select the sensorized glove system described in Chapter 8. The main limitation of the described system relied on the limited information

given by the finger sensors, where the percentage of curvature of two joints for each finger was given respect to a predefined value. This was a limitation specially for the thumb, because the sensor system was not able to capture the different DOF present in the thumb. Finally, another limitation was that the performance of the neuro-fuzzy models for FES-induced hand movements presented here could not be compared to previously proposed models, because to our knowledge, only one simplified model-based FES-induced grasp control application has been proposed with multi-field electrodes [130]. However, stimulation application sites were predefined before the control stage and no model accuracy results were presented as they focused on control. Therefore, the results obtained with the proposed model could not be contrasted against any previously proposed model.

10.2 Future work

Regarding future research, many tasks arise from the presented thesis. With respect to discomfort, as stated earlier, experiments involving a bigger amount of subjects would help to draw more relevant conclusions regarding spatial distribution of discomfort related to FES on the arm. Indeed, two different stimulation methods were compared, but new stimulation methods such as a combination of both asynchronous and synchronous stimulation could also be analyzed in terms of discomfort. Actually, not only discomfort but a performance analysis based on motor threshold could also be performed between different stimulation methods, as the aim of the neuroprostheses is to elicit muscle contractions and achieve functions. Thus, best stimulation methods should be defined taking into account the balance between performance and discomfort. Regarding hybrid neuro-fuzzy modeling, different possibilities arise. Although a RFNN structure was proposed, other dynamic structures involving other self-recurrences could also be tested. Besides, the input space partition was fixed a-priori in the presented models, but having seen that best structure parameters are dependent on subjects, an online method for defining the number of fuzzy terms could also be applied. Other learning strategies could be tested, for example a hybrid approach starting with a global optimization algorithm such as DE and switching to a local learning algorithm based on gradient descent like BP, which might merge advantages of both algorithms by avoiding the BP falling into local minima while speeding up the DE learning.

Finally, it should be noted that the aim of the presented models is to support the development of successful neuroprostheses for hand grasp neurorehabilitation purposes. The obtained models allow us to speed up the design and development stages of novel control methods without disturbing or affecting clinicians and neurologically impaired patients. Therefore, new CI techniques

could also be applied for controlling FES-induced hand grasps. Few FES control systems have been proposed for hand grasp applications so far. Actually, the proposed approaches for FES-induced hand grasp are either aimed at implanted systems [170, 171, 172, 173]; open-loop, which cannot deal with disturbances or dynamic changes of the system [29, 32, 174]; or use fixed or predefined electrode applications sites during hand grasp [130, 175, 176]. As stated earlier, one of the main challenges of surface FES grasping lies in reduced selectivity, due to the spreading of the current into neighboring tissues of the targeted motor nerves. Indeed, the relative position of the nerves and the skin change during arm and hand movements [131, 132]. Thus, the control of both the stimulation parameters and the spatial application sites of FES during hand movements would help to achieve more selective grasps. Although this fact adds complexity to the FES-induced hand grasp control problem, the application of different CI techniques might deal with its complexity and dimensionality, which could be more challenging for analytical methods. Due to the dynamic characteristics of the surface FES-induced grasping and the repetitive goal-oriented therapies aimed at stroke patients [177], we believe that a Reinforcement Learning (RL) approach could be used to control FES-induced hand grasps. RL is inspired by animal or biological learning systems, where the basic idea consists on learning by means of awards (or punishments) depending on the actions taken. In short, it is a closed loop goal-directed learning, which explores the environment in order to find the actions that maximize the rewards. Moreover, RL systems have shown the capacity of successfully adapting to non-stationary problems [178, 179, 180]. Therefore, we believe that this control method could fit well to most common therapeutic applications that are based on repetitive goal-oriented exercises.

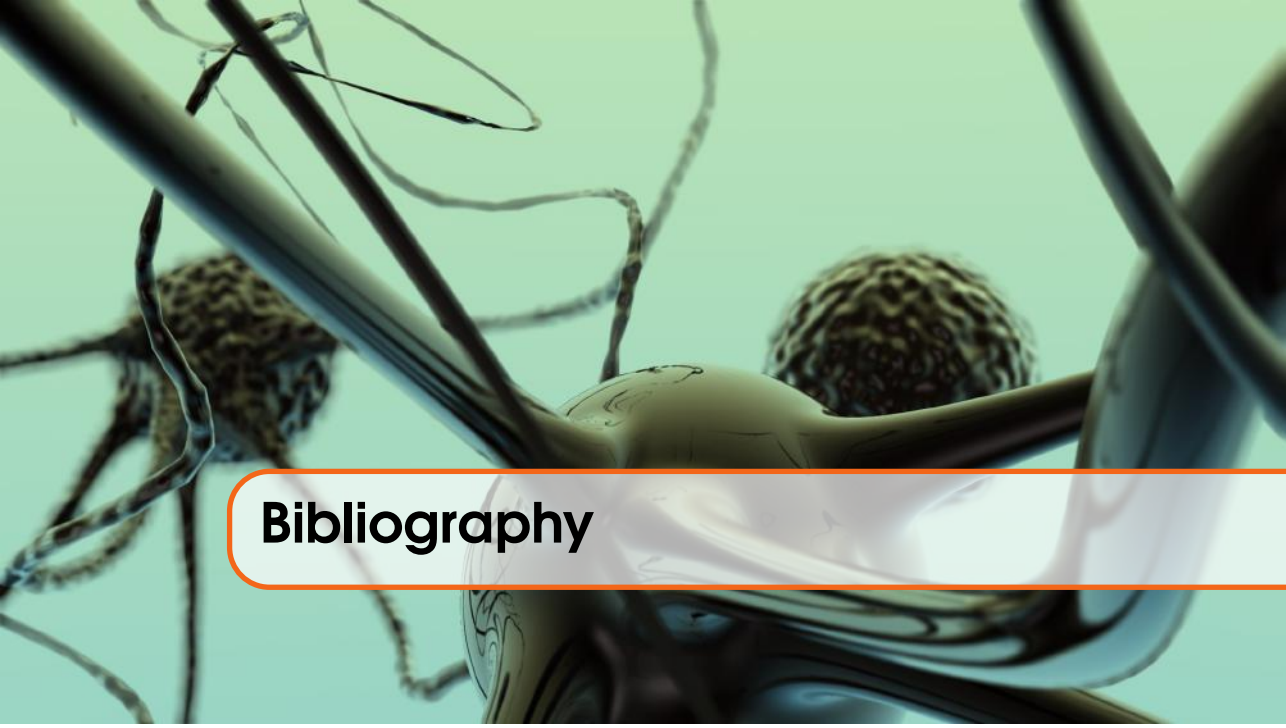

Bibliography

[1] E. R. Kandel, J. H. Schwartz, and T. M. Jessell. *Principles of Neural Science*. 4th ed. McGraw-Hill, 2000.

[2] *Neuroscience Online*. The University of Texas Medical School, Department of Neurobiology and Anatomy. Jan. 2016. URL: `http://neuroscience.uth.tmc.edu/`.

[3] *Pixabay*. Jan. 2016. URL: `https://www.pixabay.com`.

[4] E. N. Marieb and K. Hoehn. *Human Anatomy & Physiology*. 7th ed. Benjamin Cummings, Pearson Education Inc., 2006.

[5] K. S. Saladin. *Anatomy & Physiology: The Unity of Form and Function*. 6th ed. McGraw-Hill, 2011.

[6] F. H. Netter, J. A. Craig, J. Perkins, J. T. Hansen, and B. M. Koeppen. *Atlas of Neuroanatomy and Neurophysiology*. Icon Custom Communications, 2002.

[7] P. H. Peckham and J. S. Knutson. "Functional electrical stimulation for neuromuscular applications". In: *Annual Review of Biomedical Engineering* 7 (2005), pages 327–360.

[8] L. L. Baker, D. R. McNeal, L. A. Benton, B. R. Bowman, and R. L. Waters. *Neuro Muscular Electrical Stimulation: A Practical Guide*. 3th ed. California: Los Amigos Research & Education Institute, 1993.

[9] D. R. Merril, M. Bikson, and J. G. Jefferys. “Electrical stimulation of excitable tissue: design of efficacious and safe protocols”. In: *Journal of neuroscience methods* 141 (2005), pages 171–198.

[10] B. R. Bowman and L. L. Baker. “Effects of waveform parameters on comfort during transcutaneous neuromuscular electrical stimulation”. In: *Annals of biomedical engineering* 13 (1985), pages 59–74.

[11] G. Kantor, G. Alon, and H. S. Ho. “The effects of selected stimulus waveforms on pulse and phase characteristics at sensory and motor thresholds”. In: *Physical Therapy* 74 (1994), pages 951–962.

[12] A. Wongsarnpigoon, J. P. Woock, and W. M. Grill. “Efficiency analysis of waveform shape for electrical excitation of nerve fibers”. In: *IEEE Transactions on Neural Systems and Rehabilitation Engineering* 18 (2010), pages 319–328.

[13] D. M. Durand, W. M. Grill, and R. Kirsch. “Neural Engineering”. In: Springer, 2005. Chapter Electrical stimulation of the neuromuscular system. In Neural engineering, pages 157–191.

[14] D. N. Rushton. “Functional electrical stimulation”. In: *Physiological measurement* 18 (1997), pages 241–275.

[15] T. Kesar and S. Binder-Macleod. “Effect of frequency and pulse duration on human muscle fatigue during repetitive electrical stimulation”. In: *Experimental physiology* 91 (2006), pages 967–976.

[16] M. Lawrence. “Transcutaneous Electrode Technology for Neuroprostheses”. PhD thesis. ETH Zurich, 2009.

[17] A. Kuhn, T. Keller, M. Lawrence, and M. Morari. “The influence of electrode size on selectivity and comfort in transcutaneous electrical stimulation of the forearm”. In: *IEEE Transactions on Neural Systems and Rehabilitation Engineering* 18 (2010), pages 255–262.

[18] J. P. Uhlir, R. J. Triolo, J. Davis, and C. Bieri. “Performance of epimysial stimulating electrodes in the lower extremities of individuals with spinal cord injury”. In: *IEEE Transactions on Neural Systems and Rehabilitation Engineering* 12 (2004), pages 279–287.

[19] W. D. Memberg, P.H. Peckham, and M. W. Keith. “A surgically-implanted intramuscular electrode for an implantable neuromuscular stimulation system”. In: *IEEE Transactions on Rehabilitation Engineering* 2 (1994), pages 80–91.

[20] W. Mayr et al. “Multichannel Stimulation of Phrenic Nerves by Epineural Electrodes: Clinical Experience and Future Developments”. In: *American Society of Artificial Internal Organs Journal* 39 (1993), pages 729–735.

[21] G. G. Naples, J. T. Mortimer, A. Scheiner, and J. D. Sweeney. “A spiral nerve cuff electrode for peripheral nerve stimulation”. In: *IEEE Transactions on Biomedical Engineering* 35 (1988), pages 905–916.

[22] K. S. Wuolle et al. “Satisfaction with and usage of a hand neuroprosthesis”. In: *Archives of physical medicine and rehabilitation* 80 (1999), pages 206–213.

[23] E. B. Marsolais and R. Kobetic. “Implantation techniques and experience with percutaneous intramuscular electrodes in the lower extremities”. In: *Journal of rehabilitation research and development* 23 (1986), pages 1–8.

[24] J. S. Knutson, G. G. Naples, P. H. Peckham, and M. W. Keith. “Electrode fracture rates and occurrences of infection and granuloma associated with percutaneous intramuscular electrodes in upper-limb functional electrical stimulation applications”. In: *Journal of rehabilitation research and development* 39 (2002), pages 671–684.

[25] E. B. Marsolais and R. Kobetic. “Development of a practical electrical stimulation system for restoring gait in the paralyzed patient”. In: *Clinical orthopaedics and related research* 233 (1988), pages 64–74.

[26] T. Keller and A. Kuhn. “Electrodes for transcutaneous (surface) electrical stimulation”. In: *Journal of Automatic Control* 18 (2008), pages 35–45.

[27] N. Sha et al. “The effect of the impedance of a thin hydrogel electrode on sensation during functional electrical stimulation”. In: *Medical engineering & physics* 30 (2008), pages 739–746.

[28] A. J. Westerveld, A. C. Schouten, P.H. Veltink, and H. van der Kooij. “Selectivity and resolution of surface electrical stimulation for grasp and release”. In: *IEEE Transactions on Neural Systems and Rehabilitation Engineering* 20 (2012), pages 94–101.

[29] A. Popovic-Bijelic et al. “Multi-Field Surface Electrode for Selective Electrical Stimulation”. In: *Artificial organs* 29 (2005), pages 448–452.

[30] N. M. Malesevic, L. Z. Popovic, L. Schwirtlich, and D. B. Popovic. “Distributed low-frequency functional electrical stimulation delays muscle fatigue compared to conventional stimulation”. In: *Muscle & nerve* 42 (2010), pages 556–562.

[31] N. Malesevic, L. Popovic, G. Bijelic, and G. Kvascev. “Muscle twitch responses for shaping the multi-pad electrode for functional electrical stimulation”. In: *Journal of Automatic Control* 20 (2010), pages 53–58.

[32] D. B. Popovic and M. B. Popovic. “Automatic determination of the optimal shape of a surface electrode: Selective stimulation”. In: *Journal of neuroscience methods* 178 (2009), pages 174–181.

[33] K. T. Ragnarsson. “Functional electrical stimulation after spinal cord injury: current use, therapeutic effects and future directions”. In: *Spinal Cord* 46 (2008), pages 255–274.

[34] C. L. Barrett, G. E. Mann, P. N. Taylor, and P. Strike. “A randomized trial to investigate the effects of functional electrical stimulation and therapeutic exercise on walking performance for people with multiple sclerosis”. In: *Multiple Sclerosis* 15 (2009), pages 493–504.

[35] D. B. Popovic, T. Sinkjaer, and M. B. Popovic. “Electrical stimulation as a means for achieving recovery of function in stroke patients”. In: *Neurorehabilitation* 25 (2009), pages 45–58.

[36] P. A. Wright and M. H. Granat. “Therapeutic effects of functional electrical stimulation of the upper limb of eight children with cerebral palsy”. In: *Developmental Medicine & Child Neurology* 42 (2000), pages 724–727.

[37] S. D. Cook. *Handbook of multiple sclerosis*. 3th ed. Marcel Dekker, 2001.

[38] F. Miller. *Physical therapy of cerebral palsy*. Springer, 2007.

[39] J. P. Mohr et al. *Stroke: pathophysiology, diagnosis, and management*. Elsevier Health Sciences., 2011.

[40] T. Brandt, L. R. Caplan, J. Dichgans, H. C. Diener, and Christopher Kennard. *Neurological disorders: course and treatment*. Academic Press, San Diego, 2003.

[41] T. M. Skirven, A. L. Osterman, J. Fedorczyk, and P. C. Amadio. *Rehabilitation of the hand and upper extremity*. 6th ed. Mosby, Elsevier, 2011.

[42] M. C. Cirstea and F. L. Mindy. “Compensatory strategies for reaching in stroke”. In: *Brain* 123 (2000), pages 940–953.

[43] G. M. Lyons, T. Sinkjaer, J. H. Burridge, and D. J. Wilcox. “A review of portable FES-based neural orthoses for the correction of drop foot”. In: *IEEE Transactions on Neural Systems and Rehabilitation Engineering* 10 (2002), pages 260–279.

[44] A. I. Kottink et al. “The orthotic effect of functional electrical stimulation on the improvement of walking in stroke patients with a dropped foot: a systematic review”. In: *Artificial Organs* 28 (2004), pages 577–586.

[45] D. Guiraud, T. Stieglitz, K. P. Koch, J. L. Divoux, and P. Rabischong. “An implantable neuroprosthesis for standing and walking in paraplegia: 5-year patient follow-up”. In: *Journal of neural engineering* 3 (2006), pages 268–275.

[46] V. K Mushahwar, P. L. Jacobs, R. A. Normann, R. J. Triolo, and N. Kleitman. “New functional electrical stimulation approaches to standing and walking”. In: *Journal of neural engineering* 4 (2007), pages 181–197.

[47] W. D. Memberg et al. “Implanted neuroprosthesis for restoring arm and hand function in people with high level tetraplegia”. In: *Archives of physical medicine and rehabilitation* 95 (2014), pages 1201–1211.

[48] M. R. Popovic, D. B. Popovic, and T. Keller. “Neuroprostheses for grasping”. In: *Neurological research* 24 (2002), pages 443–452.

[49] S. Hamid and R. Hayek. “Role of electrical stimulation for rehabilitation and regeneration after spinal cord injury: an overview”. In: *European Spine Journal* 17 (2008), pages 1256–1269.

[50] T. A. Thrasher, V. Zivanovic, W. McIlroy, and M. R. Popovic. “Rehabilitation of reaching and grasping function in severe hemiplegic patients using functional electrical stimulation therapy”. In: *Neurorehabilitation and neural repair* 22 (2008), pages 706–714.

[51] E. C. Field-Fote and D. Tepavac. “Improved intralimb coordination in people with incomplete spinal cord injury following training with body weight support and electrical stimulation”. In: *Physical Therapy* 82 (2002), pages 707–715.

[52] T. J. Kimberley et al. “Electrical stimulation driving functional improvements and cortical changes in subjects with stroke”. In: *Experimental Brain Research* 154 (2004), pages 450–460.

[53] D. G. Everaert, A. K. Thompson, S. L. Chong, and R. B. Stein. “Does functional electrical stimulation for foot drop strengthen corticospinal connections?” In: *Neurorehabilitation and neural repair* 24 (2009), pages 168–177.

[54] K. Sasaki, T. Matsunaga, T. Tomite, T. Yoshikawa, and Y. Shimada. "Effect of electrical stimulation therapy on upper extremity functional recovery and cerebral cortical changes in patients with chronic hemiplegia". In: *Biomedical Research* 33 (2012), pages 89–96.

[55] A. H. Bakhtiary and E. Fatemy. "Does electrical stimulation reduce spasticity after stroke? A randomized controlled study". In: *Clinical Rehabilitation* 22 (2008), pages 418–425.

[56] T. P. Seib, R. Price, M. R. Reyes, and J.F. Lehmann. "The quantitative measurement of spasticity: effect of cutaneous electrical stimulation". In: *Archives of physical medicine and rehabilitation* 75 (1994), pages 746–750.

[57] J. Glinsky, L. Harvey, and P. van Es. "Efficacy of electrical stimulation to increase muscle strength in people with neurological conditions: a systematic review". In: *Physiotherapy research international* 12 (2007), pages 175–194.

[58] R. Velik, N. Malesevic, L. Popovic, U. Hoffmann, and T. Keller. "INTFES: A multi-pad electrode system for selective transcutaneous electrical muscle stimulation". In: *Procceedings of the 16th Annual Conference of the International Functional Electrical Stimulation Society (IFESS)*. Sao Paulo, Brazil, 2011.

[59] N. M. Malesevic et al. "A multi-pad electrode based functional electrical stimulation system for restoration of grasp". In: *Journal of NeuroEngineering and Rehabilitation* 9 (2012), pages 66–77.

[60] T. P. Ryan. *Modern Engineering Statistics*. John Wiley & Sons, 2007.

[61] A. Kuhn, T. Keller, S. Micera, and M. Morari. "Array electrode design for transcutaneous electrical stimulation: a simulation study". In: *Medical engineering & physics* 31 (2009), pages 945–951.

[62] E. Imatz, U. Hoffmann, J. Veneman, N. Malesevic., and T. Keller. "Stimulation Discomfort Comparison of Asynchronous and Synchronous Methods with Multi-Field Surface Electrodes". In: *18th Annual Conference of the International Functional Electrical Stimulation Society (IFESS)*. 2013.

[63] M. F. Nolan. "Two-Point Discrimination Assessment in the Upper Limb in Yound Adult Men and Women". In: *Physical Therapy* 62 (1982), pages 965–69.

[64] A. B. Vallbo and R. S. Johansson. "Properties of cutaneous mechanoreceptors in the human hand related to touch sensation". In: *Human Neurobiology* 3 (1984), pages 3–14.

[65] A. C. Grant, R. Fernandez, P. Shilian, E E. Yanni, and M. A. Hill. “Tactile spatial acuity differs between fingers: a study comparing two testing paradigms”. In: *Perception & psychophysics* 68 (2006), pages 1359–1362.

[66] G. O. Gibson and J. C. Craig. “Tactile spatial sensitivity and anisotropy”. In: *Perception & psychophysics* 67 (2005), pages 1061–1079.

[67] M. Solomonow, J. Lyman, and A. Freedy. “Electrotactile Two-Point Discrimination as a Function of Frequency, Body Site, Laterality, and Stimulation Codes”. In: *Annals of Biomedical Engineering* 5 (1977), pages 47–60.

[68] K. Kaczmarek, J. G. Webster, P. Bach-y-Rita, and W.J. Tompkins. “Electrotactile and vibrotactile displays for sensory substitution systems”. In: *IEEE Transactions on Biomedical Engineering* 38 (1991), pages 1–16.

[69] D. J. Gladstone, C. J. Danells, and S. E. Black. “The Fugl-Meyer assessment of motor recovery after stroke: a critical review of its measurement properties”. In: *Neurorehabilitation and neural repair* 16 (2002), pages 232–240.

[70] T. Platz et al. “Reliability and validity of arm function assessment with standardized guidelines for the Fugl-Meyer Test, Action Research Arm Test and Box and Block Test: a multicentre study”. In: *Clinical Rehabilitation* 19 (2005), pages 404–411.

[71] P. E. Bijur, W. Silver, and E. J. Gallagher. “Reliability of the visual analog scale for measurement of acute pain”. In: *Academic emergency medicine* 8 (2001), pages 1153–1157.

[72] H. Breivik et al. “Assessment of pain”. In: *British journal of anaesthesia* 101 (2008), pages 17–24.

[73] M. Hollander, D. A. Wolfe, and E. Chicken. *Nonparametric statistical methods*. John Wiley & Sons, 2013.

[74] E. Imatz, A. Cuesta, J. Iglesias, M. Carratala, and T. Keller. “Transcutaneous FES-induced pain maps on post-stroke upper limb: Preliminary study.” In: *IEEE 19th Annual Conference of the International Functional Electrical Stimulation Society (IFESS)*. 2014.

[75] J. P. Reilly. *Applied bioelectricity: from electrical stimulation to electropathology*. Springer Science & Business Media, 1998.

[76] A. Van Boxtel. “Skin resistance during square-wave electrical pulses of 1 to 10 mA”. In: *Medical and Biological Engineering and Computing* 15 (1977), pages 679–687.

[77] S. J. Dorgan and R. B. Reilly. “A model for human skin impedance during surface functional neuromuscular stimulation”. In: *IEEE Transactions on Rehabilitation Engineering* 7 (1999), pages 341–348.

[78] A. Kuhn, T. Keller, B. Prenaj, and M. Morari. “The relevance of nonlinear skin properties for a transcutaneous electrical stimulation model”. In: *11th Annual Conference of the International Functional Electrical Stimulation Society (IFESS)*. Zao, Japan, 2006.

[79] L. Mesin and R. Merletti. “Distribution of electrical stimulation current in a planar multilayer anisotropic tissue”. In: *IEEE Transactions on Biomedical Engineering* 55 (2008), pages 660–670.

[80] L. M. Livshitz, J. Mizrahi, and P. D. Einziger. “Interaction of array of finite electrodes with layered biological tissue: effect of electrode size and configuration”. In: *IEEE Transactions on Neural Systems and Rehabilitation Engineering* 9 (2001), pages 355–361.

[81] A. Kuhn, T. Keller, M. Lawrence, and M. Morari. “A model for transcutaneous current stimulation: simulations and experiments”. In: *Medical & biological engineering & computing* 47 (2009), pages 279–289.

[82] J. Martinek, M. Reichel, F. Rattay, and W. Mayr. “Analysis of calculated electrical activation of denervated muscle fibers in the human thigh”. In: *Artificial organs* 29 (2005), pages 444–447.

[83] Y. Stickler, J. Martinek, C. Hofer, and F. Rattay. “A finite element model of the electrically stimulated human thigh: changes due to denervation and training”. In: *Artificial organs* 32 (2008), pages 620–624.

[84] A. Kuhn. “Modeling Transcutaneous Electrical Stimulation”. PhD thesis. ETH Zurich, 2008.

[85] F. Rattay. *Electrical nerve stimulation*. Springer-Verlag Wien, 1990.

[86] M. Moffitt, C. C. McIntyre, and W. M. Grill. “Prediction of myelinated nerve fiber stimulation thresholds: limitations of linear models”. In: *IEEE Transactions on Biomedical Engineering* 51 (2004), pages 229–236.

[87] A. L. Hodgkin and A. F. Huxley. “A quantitative description of membrane current and its application to conduction and excitation in nerve”. In: *The Journal of physiology* 117 (1952), pages 500–544.

[88] B. Frankenhaeuser and A. F. Huxley. “The action potential in the myelinated nerve fibre of Xenopus laevis as computed on the basis of voltage clamp data”. In: *The Journal of Physiology* 171 (1964), pages 302–315.

[89] S. Y. Chiu, J. M. Ritchie, R. B. Rogart, and D. Stagg. “A quantitative description of membrane currents in rabbit myelinated nerve”. In: *The Journal of Physiology* 292 (1978), pages 149–166.

[90] C. C. McIntyre, A. G. Richardson, and W. M. Grill. “Modeling the excitability of mammalian nerve fibers: influence of afterpotentials on the recovery cycle”. In: *Journal of neurophysiology* 87 (2002), pages 995–1006.

[91] A. V. Hill. “The heat of shortening and the dynamic constants of muscle”. In: *Proceedings of the Royal Society of London B: Biological Sciences* 126 (1938), pages 136–195.

[92] C. Y. Scovil and J. L. Ronsky. “Sensitivity of a Hill-based muscle model to perturbations in model parameters”. In: *Journal of biomechanics* 39 (2006), pages 2055–2063.

[93] A. S. Wexler, J. Ding, and S. Binder-Macleod. “A mathematical model that predicts skeletal muscle force”. In: *IEEE Transactions on Biomedical Engineering* 44 (1997), pages 337–348.

[94] J. Ding, A. S. Wexler, and S. A. Binder-Macleod. “A mathematical model that predicts the force?frequency relationship of human skeletal muscle”. In: *Muscle & nerve* 26 (2002), pages 477–485.

[95] J. Bobet and R. B. Stein. “A simple model of force generation by skeletal muscle during dynamic isometric contractions”. In: *IEEE Transactions on Biomedical Engineering* 45 (1998), pages 1010–1016.

[96] J. Bobet, E. R. Gossen, and R. B. Stein. “A comparison of models of force production during stimulated isometric ankle dorsiflexion in humans”. In: *IEEE Transactions on Neural Systems and Rehabilitation Engineering* 13 (2005), pages 444–451.

[97] L. A. Frey Law and R. K. Shields. “Mathematical models use varying parameter strategies to represent paralyzed muscle force properties: a sensitivity analysis”. In: *Journal of neuroengineering and rehabilitation* 2 (2005), pages 12–29.

[98] L. A. Frey Law and R. K. Shields. “Mathematical models of human paralyzed muscle after long-term training”. In: *Journal of biomechanics* 40 (2007), pages 2587–2595.

[99] E. J. Perreault, C. J. Heckman, and T. G. Sandercock. “Hill muscle model errors during movement are greatest within the physiologically relevant range of motor unit firing rates”. In: *Journal of biomechanics* 36 (2003), pages 211–218.

[100] I. W. Hunter and M. J. Korenberg. “The identification of nonlinear biological systems: Wiener and Hammerstein cascade models”. In: *Biological cybernetics* 55 (1986), pages 135–144.

[101] K. J. Hunt, M. Munih, N. D. Donaldson, and F. Barr. “Investigation of the Hammerstein hypothesis in the modeling of electrically stimulated muscle”. In: *IEEE Transactions on Biomedical Engineering* 45 (1998), pages 998–1009.

[102] E. W. Bai, Z. Cai, S. Dudley-Javorosk, and R.K. Shields. “Identification of a modified Wiener-Hammerstein system and its application in electrically stimulated paralyzed skeletal muscle modeling”. In: *Automatica* 45 (2009), pages 736–743.

[103] G. Rau, C. Disselhorst-Klug, and R. Schmidt. “Movement biomechanics goes upwards: from the leg to the arm”. In: *Journal of biomechanics* 33 (2000), pages 1207–1216.

[104] R. Schmidt, C. Disselhorst-Klug, J. Silny, and G. Rau. “A marker-based measurement procedure for unconstrained wrist and elbow motions”. In: *Journal of Biomechanics* 32 (1999), pages 615–621.

[105] E. V. Biryukova, A. Roby-Brami, A. A. Frolov, and M. Mokhtari. “Kinematics of human arm reconstructed from spatial tracking system recordings”. In: *Journal of biomechanics* 33 (2000), pages 985–995.

[106] B. Hingtgen, J. R. McGuire, M. Wang, and G. F. Harris. “An upper extremity kinematic model for evaluation of hemiparetic stroke”. In: *Journal of biomechanics* 39 (2006), pages 681–688.

[107] B. A. Garner and M. G. Pandy. “Musculoskeletal model of the upper limb based on the visible human male dataset”. In: *Computer methods in biomechanics and biomedical engineering* 4 (2001), pages 93–126.

[108] A. A. Nikooyan, H. E. J. Veeger, E. K. J. Chadwick, and M. Praagman F. C. van der Helm. “Development of a comprehensive musculoskeletal model of the shoulder and elbow”. In: *Medical & biological engineering & computing* 49 (2011), pages 1425–1435.

[109] J. Ambrosio, C. Quental, B. Pilarczyk, J. Folgado, and J. Monteiro. “Multibody biomechanical models of the upper limb”. In: *2011 Symposium on Human Body Dynamics* 2 (2011), pages 4–17.

[110] K. R. Holzbaur, W. M. Murray, and S. L. Delp. “A model of the upper extremity for simulating musculoskeletal surgery and analyzing neuromuscular control”. In: *Annals of biomedical engineering* 33 (2005), pages 829–840.

[111] P. Cerveri et al. “Finger kinematic modeling and real-time hand motion estimation”. In: *Annals of biomedical engineering* 35 (2007), pages 1989–2002.

[112] P. Cerveri, N. Lopomo, A. Pedotti, and G. Ferrigno. “Derivation of centers and axes of rotation for wrist and fingers in a hand kinematic model: methods and reliability results”. In: *Annals of Biomedical Engineering* 33 (2005), pages 402–412.

[113] A. Gustus, G. Stillfried, J. Visser, H. Jorntell, and P. van der Smagt. “Human hand modelling: kinematics, dynamics, applications”. In: *Biological cybernetics* 106 (2012), pages 741–755.

[114] L. Vigouroux, F. Quaine, A. Labarre-Vila, and F. Moutet. “Estimation of finger muscle tendon tensions and pulley forces during specific sport-climbing grip techniques”. In: *Journal of biomechanics* 39 (2006), pages 2583–2592.

[115] I. Roloff, V. R. Schoffl, L. Vigouroux, and F. Quaine. “Biomechanical model for the determination of the forces acting on the finger pulley system”. In: *Journal of biomechanics* 39 (2006), pages 915–923.

[116] J. L. Sancho-Bru, A. Perez-Gonzalez, M. Vergara-Monedero, and D. Giurintano. “A 3-D dynamic model of human finger for studying free movements”. In: *Journal of Biomechanics* 34 (2001), pages 1491–1500.

[117] F. J. Valero-Cuevas, F.E. Zajac, and C. G. Burgar. “Large index-fingertip forces are produced by subject-independent patterns of muscle excitation”. In: *Journal of biomechanics* 31 (1998), pages 693–703.

[118] F. J. Valero-Cuevas, M. E. Johanson, and J. D. Towles. “Towards a realistic biomechanical model of the thumb: the choice of kinematic description may be more critical than the solution method or the variability/uncertainty of musculoskeletal parameters”. In: *Journal of biomechanics* 36 (2003), pages 1019–1030.

[119] F. J. Valero-Cuevas. “An integrative approach to the biomechanical function and neuromuscular control of the fingers”. In: *Journal of biomechanics* 38 (2005), pages 673–684.

[120] K. S. Fok and S. M. Chou. “Development of a finger biomechanical model and its considerations”. In: *Journal of biomechanics* 43 (2010), pages 701–713.

[121] J. L. Sancho-Bru, A. Perez-Gonzalez, M. Vergara, and D.J. Giurintano. “A 3D biomechanical model of the hand for power grip”. In: *Journal of biomechanical engineering* 125 (2003), pages 78–83.

[122] J. L. Sancho-Bru et al. “Theoretical Biomechanics”. In: edited by V. Klika. InTech, 2011. Chapter Towards a Realistic and Self-Contained Biomechanical Model of the Hand, pages 211–240. URL: http://www.intechopen.com/books/theoretical-biomechanics/towards-a-realistic-and-self-contained-biomechanical-model-of-the-hand.

[123] R. F. Kirsch and A. M. Acosta. “Model-based development of neuroprostheses for restoring proximal arm function”. In: *Journal of Rehabilitation Research and Development* 38 (2001), 619?626.

[124] D. Blana, J. G. Hincapie, E. K. Chadwick, and R. F. Kirsch. “A musculoskeletal model of the upper extremity for use in the development of neuroprosthetic systems”. In: *Journal of biomechanics* 41 (2008), pages 1714–1721.

[125] C. T. Freeman et al. “A model of the upper extremity using FES for stroke rehabilitation”. In: *Journal of biomechanical engineering* 131 (2009), page 031011.

[126] F. Le, I. Markovsky, C. T. Freeman, and E. Rogers. “Recursive identification of Hammerstein systems with application to electrically stimulated muscle”. In: *Control Engineering Practice* 20 (2012), pages 386–396.

[127] T. Keller, B. Hackl, M. Lawrence, and A. Kuhn. “Identification and control of hand grasp using multi-channel transcutaneous electrical stimulation”. In: *11th Annual Conference of the International Functional Electrical Stimulation Society*. Zao, Japan, 2006.

[128] A. J. Westerveld, A. C. Schouten, P.H. Veltink, and H. van der Kooij. “Control of thumb force using surface functional electrical stimulation and muscle load sharing”. In: *Journal of neuroengineering and rehabilitation* 10 (2013), pages 104–115.

[129] A. Soska, C. Freeman, and E. Rogers. “ILC for FES-based Stroke Rehabilitation of Hand and Wrist”. In: *IEEE International Symposium on Intelligent Control (ISIC)*. Dubrovnik, Croatia, 2012.

[130] C. T. Freeman. “Electrode array-based electrical stimulation using ILC with restricted input subspace”. In: *Control Engineering Practice* 23 (2014), pages 32–43.

[131] M. W. Coppieters and A. M. Alshami. “Longitudinal excursion and strain in the median nerve during novel nerve gliding exercises for carpal tunnel syndrome”. In: *Journal of orthopaedic Research* 25 (2007), pages 972–980.

[132] T. W. Wright, F. Glowczewskie, D. Cowin, and D. L. Wheeler. “Radial nerve excursion and strain at the elbow and wrist associated with upper-extremity motion”. In: *The Journal of hand surgery* 30 (2005), pages 990–996.

[133] N. Siddique and H. Adeli. *Computational intelligence: synergies of fuzzy logic, neural networks and evolutionary computing*. John Wiley & Sons, 2013.

[134] L. Rutkowski. *Computational intelligence: methods and techniques*. Springer, 2008.

[135] A. P. Engelbrecht. *Computational intelligence: an introduction*. 2nd ed. John Wiley & Sons, 2007.

[136] M. Gupta, L. Jin, and N. Homma. *Static and dynamic neural networks: from fundamentals to advanced theory*. John Wiley & Sons, 2003.

[137] J. S. R. Jang, C. T. Sun, and E. Mizutani. *Neuro-fuzzy and soft computing: a computational approach to learning and machine intelligence*. Prentice-Hall, 1997.

[138] K. A. De Jong. *Evolutionary computation: a unified approach*. MIT press, 2006.

[139] K. Price, R. M. Storn, and J. A. Lampinen. *Differential evolution: a practical approach to global optimization*. Springer, 2006.

[140] J. J. Abbas and H. J. Chizeck. “Neural network control of functional neuromuscular stimulation systems: computer simulation studies”. In: *IEEE Transactions on Biomedical Engineering* 42 (1995), pages 1117–1127.

[141] D. Graupe and H. Kordylewski. “Artificial neural network control of FES in paraplegics for patient responsive ambulation”. In: *IEEE Transactions on Biomedical Engineering* 42 (1995), pages 699–707.

[142] J. Riess and J. A. Abbas. “Adaptive control of cyclic movements as muscles fatigue using functional neuromuscular stimulation”. In: *IEEE Transactions on Neural Systems and Rehabilitation Engineering* 9 (2001), pages 326–330.

[143] A. Pedrocchi, S. Ferrante, E. De Momi, and G. Ferrigno. “Error mapping controller: a closed loop neuroprosthesis controlled by artificial neural networks”. In: *Journal of neuroengineering and rehabilitation* 3 (2006), pages 25–37.

[144] N. Lan, H. Q. Feng, and P. E. Crago. “Neural network generation of muscle stimulation patterns for control of arm movements”. In: *IEEE Transactions on Rehabilitation Engineering* 2 (1994), pages 213–224.

[145] J. P. Giuffrida and P. E. Crago. “Functional restoration of elbow extension after spinal-cord injury using a neural network-based synergistic FES controller”. In: *IEEE Transactions on Neural Systems and Rehabilitation Engineering* 13 (2005), pages 147–152.

[146] J. G. Hincapie and R. F. Kirsch. “Feasibility of EMG-based neural network controller for an upper extremity neuroprosthesis”. In: *IEEE Transactions on Neural Systems and Rehabilitation Engineering* 17 (2009), pages 80–90.

[147] D. Blana, R. F. Kirsch, and E. K. Chadwick. “Combined feedforward and feedback control of a redundant, nonlinear, dynamic musculoskeletal system”. In: *Medical & biological engineering & computing* 47 (2009), pages 533–542.

[148] N. Malesevic, L. Popovic . Bijelic, and G. Kvascev. “Classification of muscle twitch response using ANN: Application in multi-pad electrode optimization”. In: *10th Symposium on Neural Network Applications in Electrical Engineering (NEUREL)*. 2010.

[149] R. Davoodi and B. J. Andrews. “Fuzzy logic control of FES rowing exercise in paraplegia”. In: *IEEE Transactions on Biomedical Engineering* 51 (2004), pages 541–543.

[150] B. S. K. K. Ibrahim, M. O. Tokhi, M. S. Huq, and S. C. Gharooni. “Fuzzy logic based cycle-to-cycle control of FES-induced swinging motion”. In: *International Conference on Electrical, Control and Computer Engineering (INECCE)*. 2011.

[151] H. R. Kobravi and A. Erfanian. “A decentralized adaptive fuzzy robust strategy for control of upright standing posture in paraplegia using functional electrical stimulation”. In: *Medical engineering & physics* 34 (2012), pages 28–37.

[152] F. Sepulveda. “Simulating FES Gait: Radial Basis Function Networks vs. Neuro-Fuzzy Inference and Recurrent Neural Networks with Plant Wear Factors”. In: *5th Annual Conference of the International Functional Electrical Stimulation Society IFESS*. 2000.

[153] F. Sepulveda and J. B. Huber. “Descriptive vs. machine-learning models of vastus lateralis in FES-induced knee extension”. In: *2004 IEEE Conference on Cybernetics and Intelligent Systems*. 2004.

[154] A. Thrasher and F. Wang. “Self adaptive neuro-fuzzy control of neural prostheses using reinforcement learning”. In: *18th Annual International Conference of the IEEE Engineering in Medicine and Biology Society*. 1996.

[155] R. Hussain, R. Massoud, and M. Al-Mawaldi. “ANFIS-PID Control FES-Supported Sit-to-Stand in Paraplegics:(Simulation Study)”. In: *Journal of Biomedical Science and Engineering* 7 (2014), page 208.

[156] Z. Hussain, B. Zaidan, M. Arbayani, M. O. Tokhi, and R. Jailani. “The Adaptive Control of FES-assisted Indoor Rowing Exercise”. In: *CACS International Automatic Control Conference*. 2009.

[157] Z. Hussain, S. Z. Yahaya, R. Boudville, K. A. Ahmad, and M. M. Noor. “Self adaptive neuro-fuzzy control of FES-assisted paraplegics indoor rowing exercise”. In: *IEEE International Conference on Control System, Computing and Engineering (ICCSCE)*. 2011.

[158] R. Davoodi and G. E. Loeb. “A biomimetic strategy for control of fes reaching”. In: *Annual International Conference of the Engineering in Medicine and Biology Society*. 2003.

[159] J. Zhang and A. J. Morris. “Recurrent neuro-fuzzy networks for nonlinear process modeling”. In: *IEEE Transactions on Neural Networks* 10 (1999), pages 313–326.

[160] C. H. Lee and C. C. Teng. “Identification and control of dynamic systems using recurrent fuzzy neural networks”. In: *IEEE Transactions on Fuzzy Systems* 8 (2000), pages 349–366.

[161] R.A. Aliev, B. Fazlollahi, B.G. Guirimov, and R.R. Aliev. “Recurrent Neural Networks”. In: edited by X. Hu and P. Balasubramaniam. InTech, 2008. Chapter Recurrent Fuzzy Neural Networks and Their Performance Analysis, pages 107–126. URL: `http://www.intechopen.com/books/recurrent_neural_networks/recurrent_fuzzy_neural_networks_and_their_performance_analysis`.

[162] C.T. Chao, Y.J. Chen, and C.C. Teng. “Simplification of fuzzy-neural systems using similarity analysis”. In: *IEEE Transactions on Systems, Man, and Cybernetics* 26 (1996), pages 344–354.

[163] E. Imatz-Ojanguren, E. Irigoyen-Gordo, D.Valencia-Blanco, H. Zabaleta, and T. Keller. “Uso de redes neuro-borrosas RFNN para la aproximaci?n del comportamiento de una neuropr?tesis de antebrazo en pacientes con da?o cerebral”. In: *XXXVI Jornadas de Autom?tica*. 2015.

[164] E. Imatz, E. Irigoyen, D. Valencia, and T. Keller. “Feasibility of Using Neuro-Fuzzy Subject-Specific Models for Functional Electrical Stimulation Induced Hand Movements”. In: *9th IFAC Symposium on Biological and Medical Systems*. Volume 48. 2015, pages 321–326.

[165] C. Hager-Ross and M. H Schieber. “Quantifying the independence of human finger movements: comparisons of digits, hands, and movement frequencies”. In: *The Journal of neuroscience* 20 (2000), pages 8542–8550.

[166] R. A. Aliev, B. G. Guirimov, B. Fazlollahi, and R. R. Aliev. “Evolutionary algorithm-based learning of fuzzy neural networks. Part 2: Recurrent fuzzy neural networks”. In: *Fuzzy Sets and Systems* 160 (2009), pages 2553–2566.

[167] C. K. dos Santos, R. P. Espindola, V. F. Vieira, and A. G. Evsukoff. “Identification of dynamic systems using a differential evolution-based recurrent fuzzy system”. In: *IEEE International Conference on Fuzzy Systems (FUZZ-IEEE)*. 2014.

[168] Eukene Imatz-Ojanguren, Eloy Irigoyen, David Valencia-Blanco, and Thierry Keller. “Neuro-Fuzzy Models for Hand Movements Induced by Functional Electrical Stimulation in Able-Bodied and Hemiplegic Subjects”. Submitted to Medical Engineering & Physics.

[169] A. M. Wing, P. Haggard, and J. R. Flanagan, editors. *Hand and brain: the neurophysiology and psychology of hand movements*. Academic Press, 1996.

[170] R. L. Hart, K. L. Kilgore, and P. H. Peckham. “A comparison between control methods for implanted FES hand-grasp systems”. In: *IEEE Transactions on Rehabilitation Engineering* 6 (1998), pages 208–218.

[171] M. M. Adamczyk and P. E. Crago. “Simulated feedforward neural network coordination of hand grasp and wrist angle in a neuroprosthesis”. In: *IEEE Transactions on Rehabilitation Engineering* 8 (2000), pages 297–304.

[172] E. A. Pohlmeyer et al. “Toward the restoration of hand use to a paralyzed monkey: brain-controlled functional electrical stimulation of forearm muscles”. In: *PloS ONE* 4 (2009), page 5924.

[173] C. Ethier, E. R. Oby, and M. J. Bauman an L. E. Miller. “Restoration of grasp following paralysis through brain-controlled stimulation of muscles”. In: *Nature* 485 (2012), pages 368–371.

[174] M. B. Popovic. “Control of neural prostheses for grasping and reaching”. In: *Medical engineering & physics* 25 (2003), pages 41–50.

[175] A. Prochazka, M. Gauthier, M. Wieler, and Z. Kenwell. “The bionic glove: an electrical stimulator garment that provides controlled grasp and hand opening in quadriplegia”. In: *Archives of physical medicine and rehabilitation* 78 (1997), pages 608–614.

[176] C. Freeman, E. Rogers, J. H. Burridge, A. M. Hughes, and K. L. Meadmore. *Iterative Learning Control for Electrical Stimulation and Stroke Rehabilitation*. Springer, 2015.

[177] G. Gillen. *Stroke rehabilitation: a function-based approach*. Elsevier Health Sciences, 2015.

[178] R. S. Sutton and A. G. Barto. *Reinforcement learning: An introduction*. MIT press, 1998.

[179] P. Thomas, M. Branicky, A. van den Bogert, and K. Jagodnik. “Application of the actor-critic architecture to functional electrical stimulation control of a human arm”. In: *Procceedings of the Innovative Applications of Artificial Intelligence Conference*. 2009.

[180] J. Izawa, T. Kondo, and K. Ito. “Biological arm motion through reinforcement learning”. In: *Biological cybernetics* 91 (2004), pages 10–22.

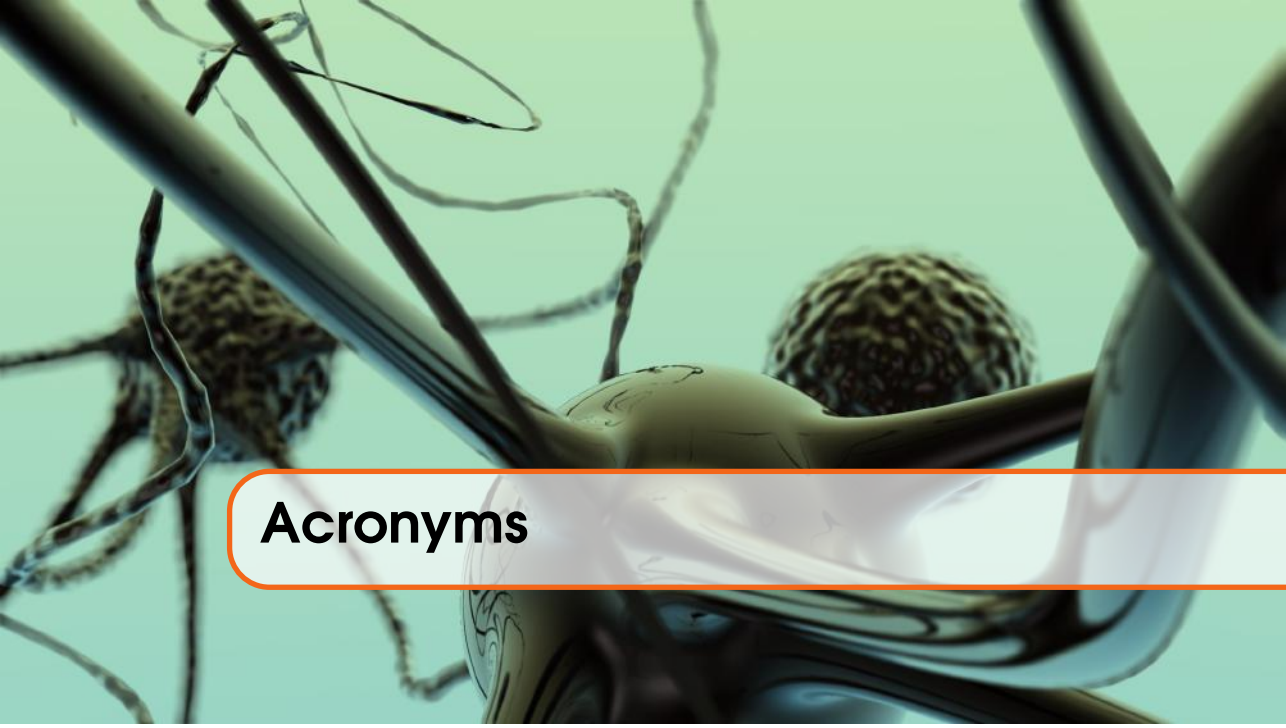

Acronyms

ANN Artificial Neural Network
AP Action Potential
AROM Active Range of Motion
BP BackPropagation
CI Computational Intelligence
CNS Central Nervous System
CP Cerebral Palsy
DE Differential Evolution
DOF Degrees Of Freedom
EMG ElectroMyoGraphy
FES Functional Electrical Stimulation
GUI Graphical User Interface
IRC Isometric Recruitment Curve
MIMO Multiple Input Multiple Output
MS Multiple Sclerosis
MSE Mean Square Error
MT Motor Threshold
NMES NeuroMuscular Electrical Stimulation
PID Proportional-Integral-Derivative
PNS Peripheral Nervous System
PROM Passive Range Of Motion
RFNN Recurrent Fuzzy Neural Network
RL Reinforcement Learning

RNN Recurrent Neural Network
SCI Spinal Cord Injury
USB Universal Serial Bus
VAS Visual Analog Scale